AD-A085 131 NEW MEXICO STATE UNIV LAS CRUCES PHYSICAL SCIENCE LAB F/G 17/9
ANALYSIS OF MONOPULSE TRACKER ANTENNA PERFORMANCE IN A MULTIPAT--ETC(U)
APR 80 K R CARVER, T F BUSH DAAD07-79-C-0008

UNCLASSIFIED ERADCOM/ASL -CR-80-0008-2 NL

1 - 2

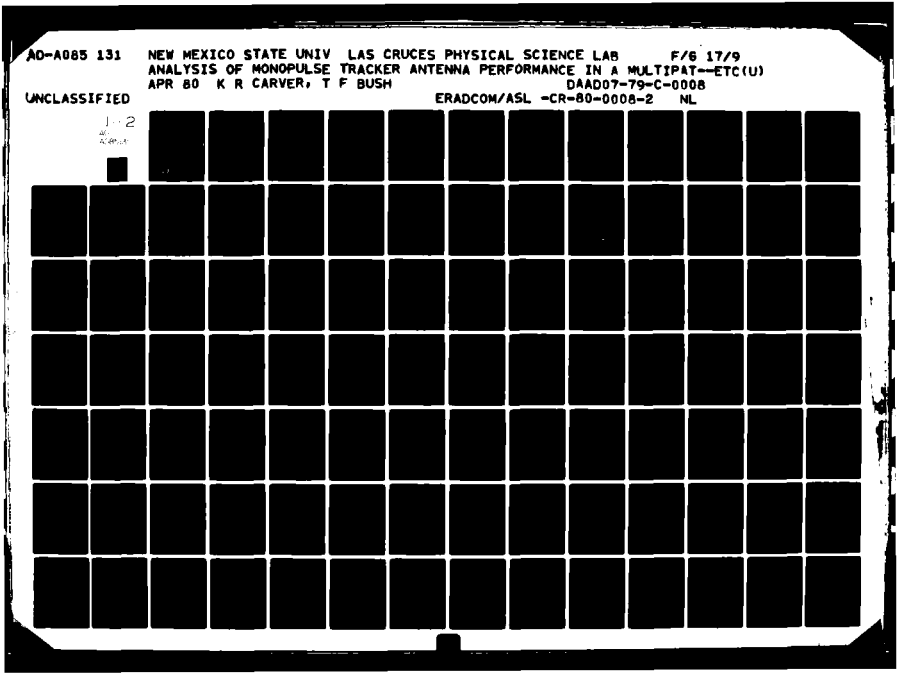

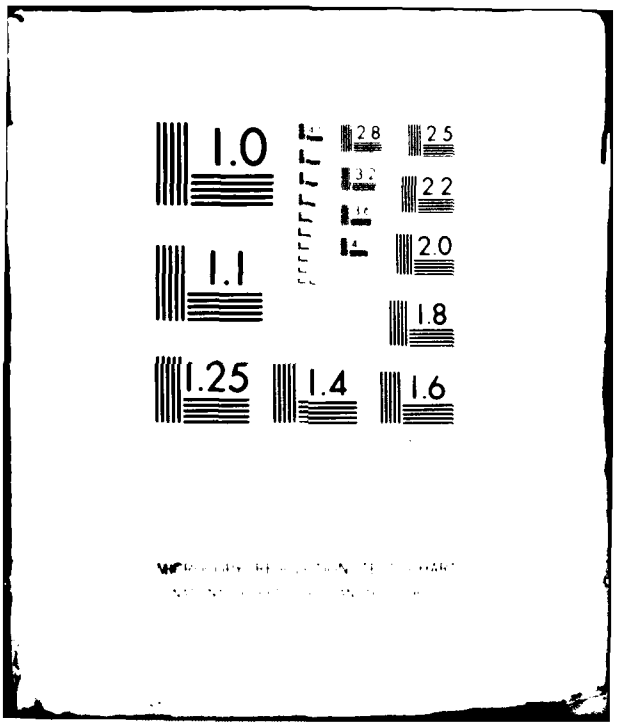
1.0
1.1
1.25
1.4
1.6
1.8
2.0
2.2
2.5
2.8

LEVEL II

12

AD

Reports Control Symbol
OSD-1366

ASL-CR-80-0008-2

ADA085131

ANALYSIS OF MONOPULSE TRACKER ANTENNA PERFORMANCE IN A MULTIPATH ENVIRONMENT

APRIL 1980

Prepared by

K. R. CARVER
T. F. BUSH

Physical Science Laboratory
New Mexico State University
Las Cruces, NM 88003

Under Contract: DAAD07-79-C-0008

Contract Monitor: W. J. VECHIONE

US Army Electronics Research and Development Command
ATMOSPHERIC SCIENCES LABORATORY
White Sands Missile Range, NM 88002

NOTICES

Disclaimers

The findings in this report are not to be construed as an official Department of the Army position, unless so designated by other authorized documents.

The citation of trade names and names of manufacturers in this report is not to be construed as official Government indorsement or approval of commercial products or services referenced herein.

Disposition

Destroy this report when it is no longer needed. Do not return it to the originator.

(18) ERADCOM/ASL

SECURITY CLASSIFICATION OF THIS PAGE (When Data Entered)

(19) **REPORT DOCUMENTATION PAGE**

READ INSTRUCTIONS BEFORE COMPLETING FORM

1. REPORT NUMBER	2. GOVT ACCESSION NO.	3. RECIPIENT'S CATALOG NUMBER
ASL-CR-80-0008-2	AD-A085 131	

(6) 4. TITLE (and Subtitle)

ANALYSIS OF MONOPULSE TRACKER ANTENNA PERFORMANCE IN A MULTIPATH ENVIRONMENT,

(9) 5. TYPE OF REPORT & PERIOD COVERED: Technical Report

6. PERFORMING ORG. REPORT NUMBER

(10) 7. AUTHOR(s): K. R. Carver [redacted] T. F. Bush

(15) 8. CONTRACT OR GRANT NUMBER(s): DAAD07-79-C-0008

9. PERFORMING ORGANIZATION NAME AND ADDRESS
Physical Science Laboratory
New Mexico State University
Las Cruces, NM 88003

(16) 10. PROGRAM ELEMENT, PROJECT, TASK AREA & WORK UNIT NUMBERS: 1L162111AH71-24 (17) 24

11. CONTROLLING OFFICE NAME AND ADDRESS
US Army Electronics Research and Development Command
Adelphi, MD 20783

(11) 12. REPORT DATE: April 1980

13. NUMBER OF PAGES: (12) 99

14. MONITORING AGENCY NAME & ADDRESS(if different from Controlling Office)
Atmospheric Sciences Laboratory
White Sands Missile Range, NM 88002

15. SECURITY CLASS. (of this report): UNCLASSIFIED

15a. DECLASSIFICATION/DOWNGRADING SCHEDULE

16. DISTRIBUTION STATEMENT (of this Report)

Approved for public release; distribution unlimited

17. DISTRIBUTION STATEMENT (of the abstract entered in Block 20, if different from Report)

18. SUPPLEMENTARY NOTES

Contract Monitor: W. J. Vechione

19. KEY WORDS (Continue on reverse side if necessary and identify by block number)

Monopulse	Planer array
Beamwidth	Multipath
Microstrip array	Specular

20. ABSTRACT (Continue on reverse side if necessary and identify by block number)

This report summarizes the results of a study of monopulse tracking antenna performance at low angles. The objectives of this study were two-fold:

(1) To investigate the multipath effects of surface roughness and soil moisture on the elevation accuracy of a monopulse tracker, particularly at low angles. This includes the antenna beam shape characteristics such as beamwidth, roll-off rate and sidelobe level,

DD FORM 1 JAN 73 1473 EDITION OF 1 NOV 65 IS OBSOLETE

SECURITY CLASSIFICATION OF THIS PAGE (When Data Entered)

282450

20. ABSTRACT (Cont)

(2) To determine which, if any, realizable antenna designs might yield a significant improvement in tracking accuracy down to about 5^0, keeping in mind logistics requirements for a light-weight portable antenna.

Although this study did not initially constrain itself to previous practical antenna sizes such as the GMD, PLUSS, etc., it was recognized that the optimum antenna selected would need to eventually consider size and weight factors. Therefore the previously measured performance characteristics of the GMD and PLUSS antennas were reviewed and included in a comparative performance evaluation.

There are two basic findings presented herein:

(1) In order to track in elevation down to 5^0, a sum-pattern 3 dB beamwidth of 5^0 and a -40 dB sidelobe level is required. This will require an aperture of approximately 9 feet in elevation by 4 feet in azimuth.

(2) This performance can be best obtained from a microstrip antenna array using graphite-epoxy struss technology. This should enable the antenna weight (not including positioner) to be reduced to between 95 and 155 lbs. Detailed analysis of wind stress resistance have not been performed.

TABLE OF CONTENTS

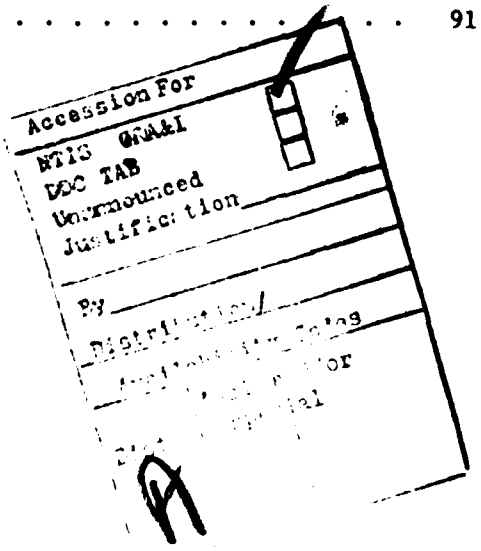

LIST OF FIGURES

LIST OF FIGURES (Cont'd)

LIST OF FIGURES (Cont'd)

LIST OF TABLES

1.1 Executive Summary

This report summarizes the results of a study of monopulse tracking antenna performance at low angles. The objectives of this study were two-fold:

1. To investigate the multipath effects of surface roughness and soil moisture on the elevation accuracy of a monopulse tracker, particularly at low angles. This includes the antenna beam shape characteristics such as beamwidth, roll-off rate and sidelobe level.

2. To determine which, if any, realizable antenna designs might yield a significant improvement in tracking accuracy down to about 5°, keeping in mind logistics requirements for a light-weight portable antenna. This includes the present pill-box antenna.

Although this study did not initially constrain itself to previous practical antenna sizes such as the GMD, PLUSS, etc., it was recognized that the optimum antenna selected would need to eventually consider size and weight factors. Therefore the previously measured performance characteristics of the GMD and PLUSS antennas were reviewed and included in a comparative performance evaluation.

There are two basic findings presented herein:

1. In order to track in elevation down to 5°, a sum-pattern 3 dB beamwidth of 5° and a -40 dB sidelobe level is required. This will require an aperture of approximately 9 feet in elevation by 4 feet in azimuth.

2. This performance can be best obtained from a foldable microstrip antenna array using graphite-epoxy struss technology. This should enable the antenna weight (not including positioner) to be reduced to between 95 and 155 lbs. The stowed folded antenna would be 3' X 4' X 0.5' in size. Detailed analysis of wind stress resistance have not been performed. It is not considered possible to modify the present PLUSS pillbox antenna to obtain a significant performance improvement at low angles.

1.2 Background

The events leading to this report form an interesting historical background to the present study, which began in July 1979. The central problem is to accurately track a radiosonde at low angles, say below 10°, in order to assess the range to the balloon and thereby measure wind speed; the balloon height is obtained from the hydrostatic equation for the atmosphere.

The AN/TMQ-19 radar used a 5' antenna and had a 9.8° beamwidth; it was abandoned in about 1976 because of excessive weight and the disadvantages of an active system. The workhorse AN/GMD 7' dish antenna uses conical scan and has a 6.5° beamwidth; although it performs satisfactorily, its large size and weight are a serious disadvantage in field logistics. In 1975, a report by Littell and Duff of WSMR/ASL investigated a feasibility of a Portable Lightweight Upper Air Sounding Sytem (PLUSS), including new antenna structures. In 1975-6, the first generation PLUSS antenna was developed as a 2.5' X 2.5' aperture of four short back-fire antennas. Its beamwidth of 27° was too large for accurate tracking so that the antenna was not satisfactory.

In 1976, a 2nd-generation PLUSS antenna was developed by Electromagnetic Processing Corporation (EMP) as a 2' X 2' co-planar array with an 18° beamwidth for use in tracking down to 17° elevation angle. Subsequently, the PLUSS performance specification was revised so that tracking down to 6.5° would be required, which meant that this 2nd-generation PLUSS could not meet the new requirement.

A 1976-7 Airborne Instruments Laboratory (AIL) analytical study for ASL of forward artillary meteorological antenna systems recommended that in order to meet the low-angle tracking requirement, a larger aperture antenna using the Redlien Fix technique be developed. The Redlien Fix technique modifies the sum and difference patterns to achieve a reduction in specular multipath signals which arise at low tracking angles [Redlien, 1969]. As a result of the AIL study, WSMR/ASL in 1977 requested EMP Corporation to develop a 3rd-generation 4' X 4' antenna having a 9° beamwidth, a weight of 80 lbs, and the incorporation of Redlien Fix circuitry. The delivered 3rd-generation EMP antenna was a pill-box antenna which weighed 240 lbs., and had a beamwidth of

13.5°, so that even with the Redlien Fix it failed to track accurately at low angles.

1.3 Rationale for this Study

The present study seeks to investigate more carefully the effects of multipath-induced tracking errors at low angles in relation to antenna pattern shape including beamwidth and sidelobe level. It was clear from the outset that the required antenna size for low angle tracking is governed by the immutable law of antenna physics that the beamwidth is given approximately by λ/D where D is the antenna aperture size. Thus, for tracking at 5° elevation angle, a beamwidth not exceeding 5° would be desired. At 1680 MHz, this corresponds to a 7' elevation aperture for -13 dB sidelobes. For lower sidelobe levels and the same beamwidth, the aperture size required would be larger.

The first phase of this study has concerned itself with modeling the response of a monopulse tracker in the presence of low-angle multipath signals. A mathematical model has been developed which has a predicted voltage error curve vs. angle as its output. As an input, the antenna sum and difference patterns are specified along with their beamwidths, sidelobe levels, squint angles, etc. Also, the multipath effect is an input by inclusion of surface roughness and reflection coefficients, both specular and diffuse. These coefficients are dependent, in turn, on the level of soil moisture in addition to angle(s) of incidence.

The second phase of the study addresses the problem of practical antenna designs which approximate idealized pattern performance from optimized antennas used in the first phase. Specifically, tracking to 5° requires a 5° beamwidth and -40 dB sidelobe level which in turn requires a 9' elevation aperture. Since this is much larger than any of the antennas used to date, is this required size compatible with other requirements for light weight, portability, durability, etc.? What generic antenna types might be used in such an antenna?

1.4 Organization of this Report

Chapter 2 of this report summarizes the results of the first phase of the study and models the interrelationship between the antenna pattern and multipath signals in determining tracking accuracy. Chapter 3 takes these results as an input for the necessary antenna beamwidth and sidelobe level in order to achieve low-angle tracking, and investigates practical antenna design approaches. Chapter 4 presents the principal conclusions and recommendations for further action on the part of ASL. The Appendix presents the FORTRAN computer program and instructions for its use.

2.1 Basics of Monopulse Tracking

Following the development of search radars during World War II, the need for tracking a target became apparent. Not only could a tracking system help in aiming anti-aircraft artillery but it could also aid friendly aircraft during operations in foul weather.

Perhaps the first such tracking system was the sequential lobing radar. This system relied on an antenna with the ability to sequentially switch its beam to four discrete positions squinted off the mechanical boresight axis of the antenna. By comparing the magnitude of the radar echo at each of the four beam positions, the operator was able to determine the location of the target in both the elevation and azimuth planes and thus track the target as it moved. While this was rather a cumbersome system it marked the beginnings of tracking radar.

A logical extension of the sequential lobing radar was the conical scan tracker. Instead of discretely switching an offset antenna beam to four positions, a squinted antenna beam was continuously rotated about the mechanical boresight axis of the antenna. If at least four pulses are transmitted (and thus received) during one rotation of the antenna beam, the return signal will be amplitude modulated at the beam rotation frequency. From the amplitude modulated signal, the information required to track the target could be extracted and used to direct the antenna (using servos) to the target.

It should be noted that both the sequential lobing and conical scan tracking scheme relied upon comparison of the amplitude of at least four echo pulses to extract the required tracking information from the echo. If target scintillation was extreme, the tracking accuracy was degraded since the radar could not distinguish scintillation from the modulation resulting from the change in beam or target movement. Thus the monopulse scheme was developed which, as its name implies, relies on only a single pulse for tracking and thus eliminates the troublesome scintillation problem. It can also be shown (1) that a monopulse system is somewhat more sensitive to target motion than either a conical scan system or a sequential lobing system.

While a monopulse radar tracking scheme is very popular for tracking airborne objects, tracking can be improved by placing a radio beacon on board the object being tracked. The principal effect is that of having a clean signal on reception with known characteristics as well as reducing the R^4 (R = range to target) to a R^2 power dependency. Moreover a rather cheap CW beacon can be used on board the tracked object so that a pulsed radar transmitter and duplexer are not required.

Figure 2.1 shows a simplified sketch of a single angular coordinate passive monopulse tracking system. Note that two receiver channels are shown. This is necessary because two antenna patterns are required for monopulse tracking. Because the two antenna patterns are the "heart" of monopulse tracking receiver, let us consider this aspect first assuming ideal operation conditions.

Shown in Figure 2.2, two overlapping beams are shown. The angle between 0° and the peak of each beam will be termed the squint angle. (It should be noted at this time that we are concerned with voltage rather than power antenna patterns.) In Figure 2.2 the squint angle is 20° and the half power beamwidth of the individual beams is 40°. The method for generating the two beams can be one of numerous methods, perhaps the simplest being the use of two offset feeds and a parabolic reflector. The hybrid junction shown in Figure 2.1 provides phasing so that both a "sum" and "difference" antenna pattern are produced. These are shown in Figures 2.3 and 2.4 respectively. It should be noted that the phase difference between the two lobes of the difference patterns is 180° and is so indicated in Figure 2.4 by a "+" and a "-" sign. The remainder of the receiver, Figure 2.1, is not unusual except that one arm of the receiver usually contains an adjustable phase shifter so that the phase shift of the signals as they propagate through the receiver retain their original relationship as when they entered the antenna.

The "dot-product" detector shown in Figure 2.1 is perhaps the only other oddity in the system. This type of detector produces the dot product of the sum and difference antenna patterns and forms the transfer function of the system. In Figure 2.5, the dot product pattern of the sum and difference patterns is shown. Note that since we cannot show a negative voltage pattern when plotted in polar coordinates we continue to use the "+" and "-" convention

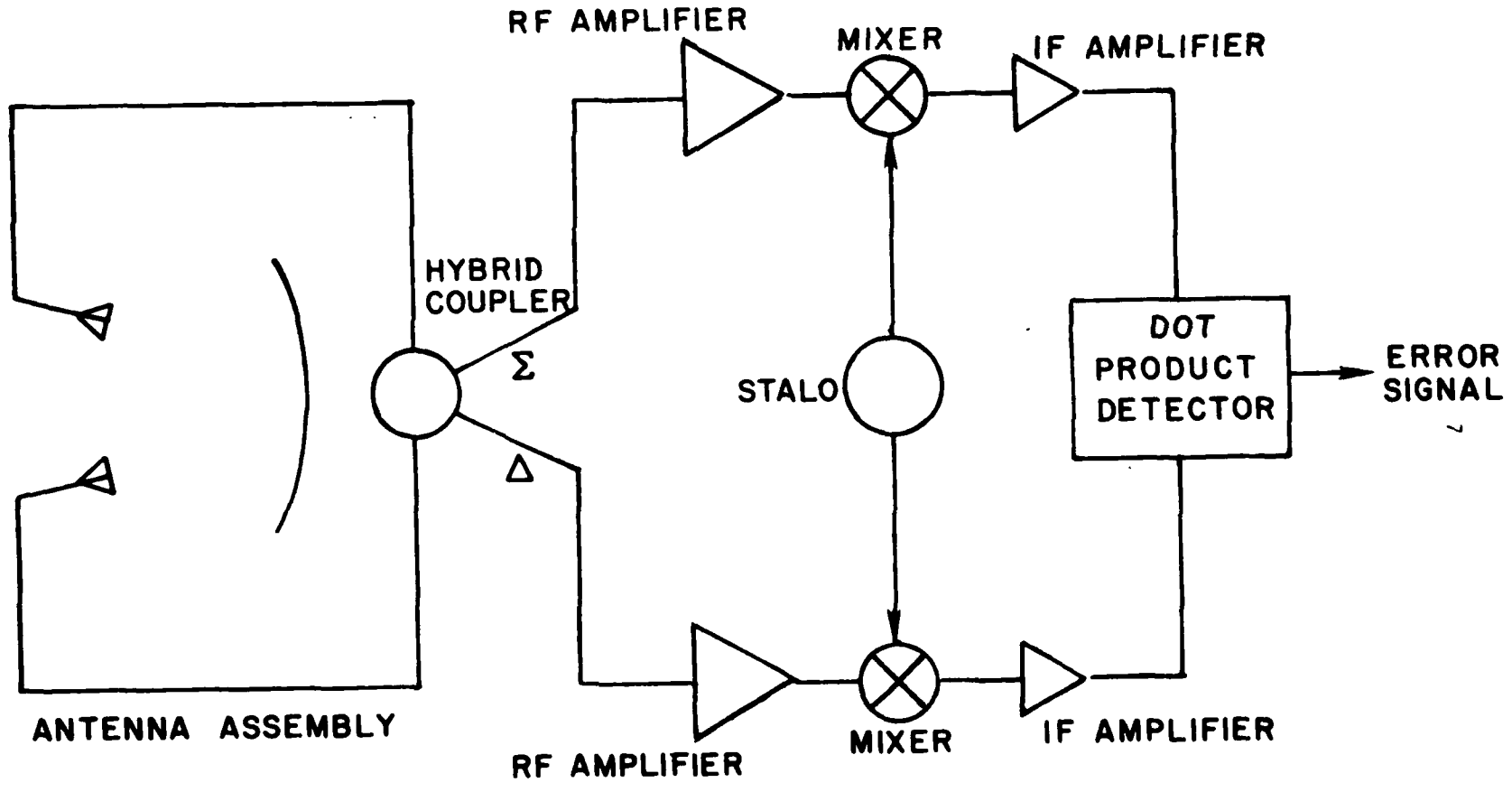

Figure 2.1 Basic Block Diagram of a Passive Monopulse Tracking Receiver (Elevation Plane Only)

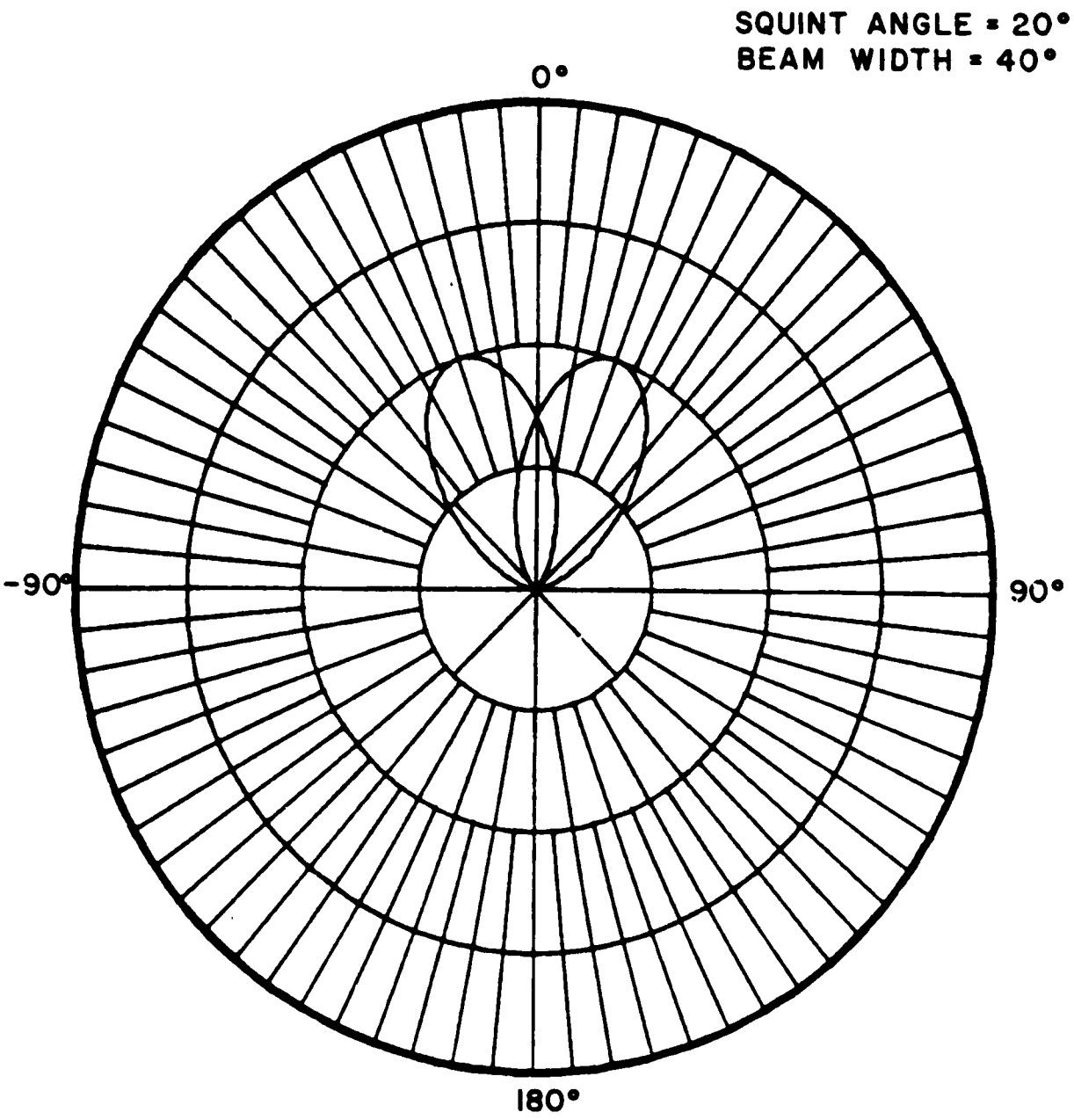

Figure 2.2
Polar Plot of Overlapping Antenna Beams

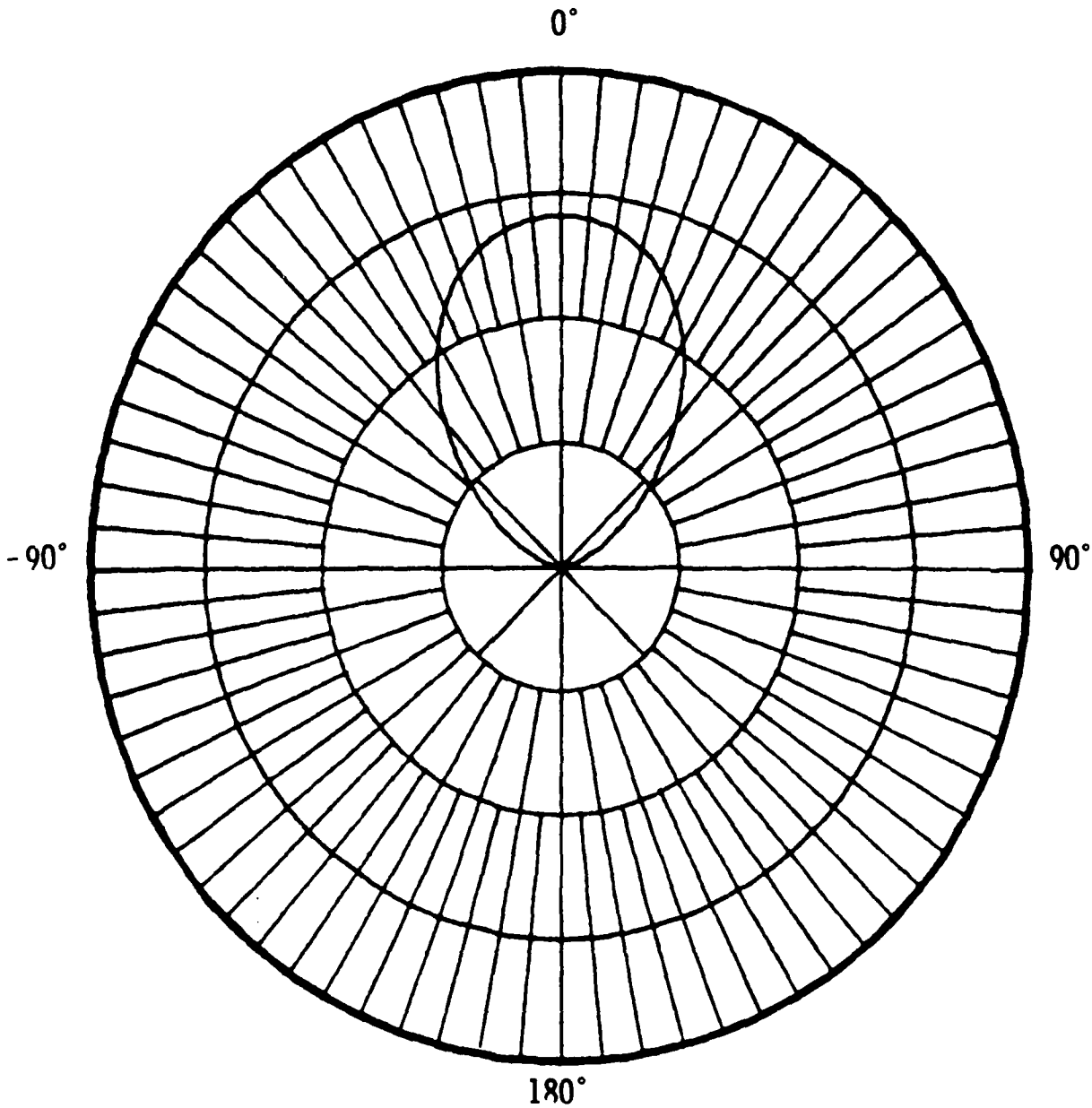

Figure 2.3
Sum Pattern of Beams Depicted
in Figure 2.2

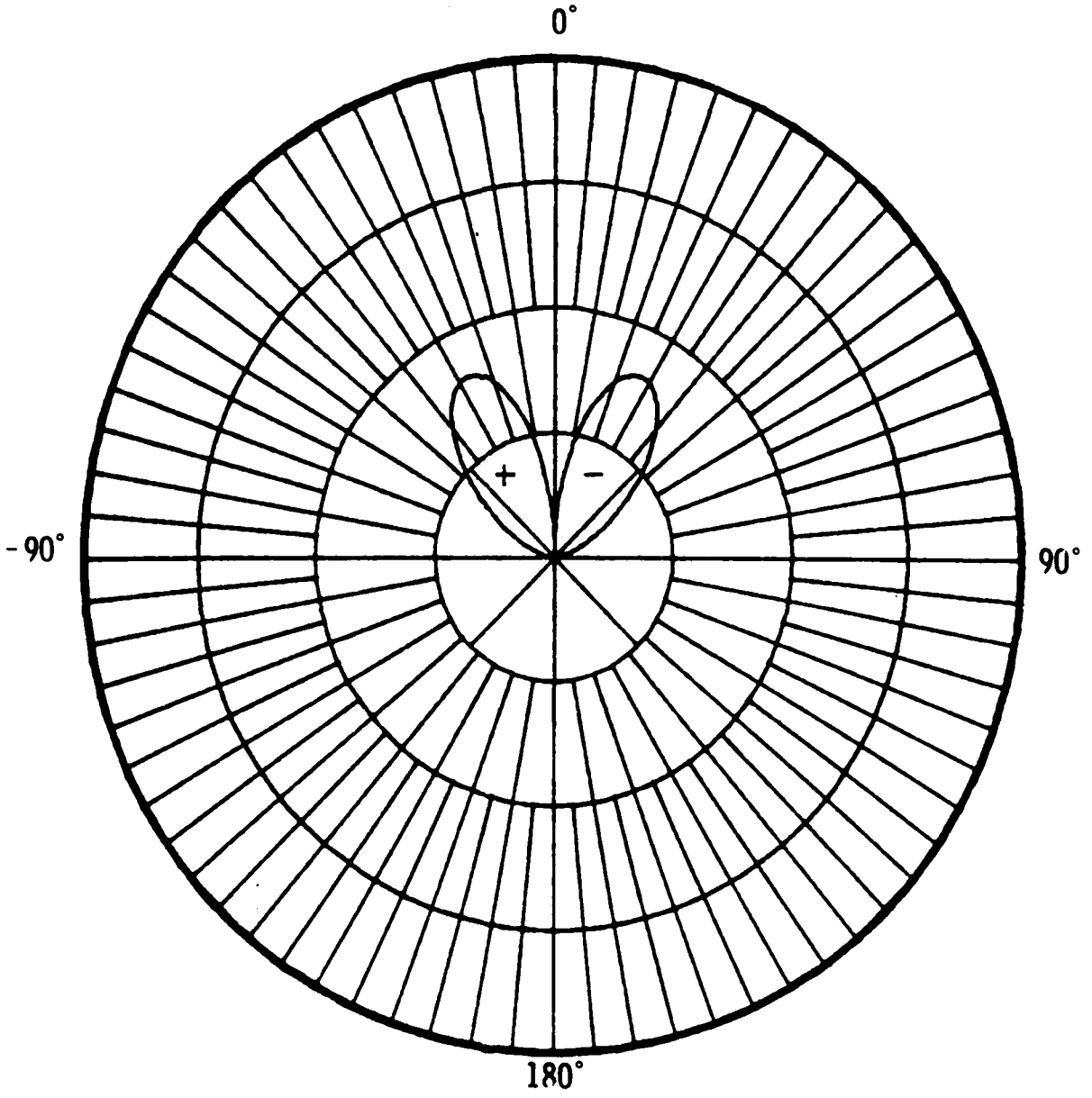

Figure 2.4
Difference Pattern Formed by
Beams Depicted in Figure 2.2

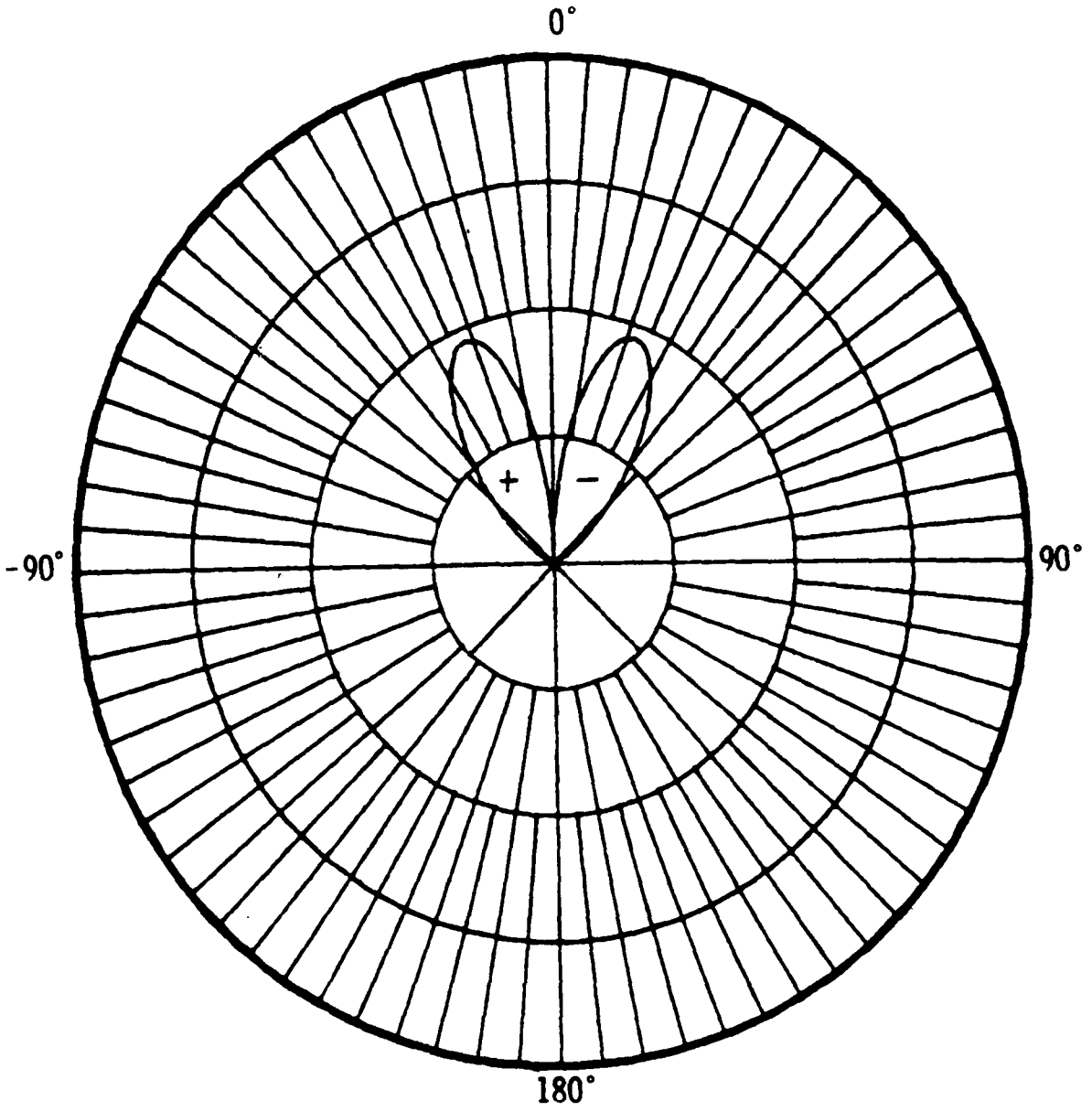

Figure 2.5
Dot Product of the Sum
and Difference Patterns

to show that the two lobes of the product pattern bear a 180° phase relationship. If we plot a hypothetical dot product pattern on rectangular coordinates, however, we can more clearly see the phase relatioship as in Figure 2.6.

Shown in Figure 2.7, a hypothetical situation is shown in which a signal enters the antenna at an angle θ off the boresight direction. After being weighted by the relative gains of the sum and difference antenna patterns the signal propagates through the (hopefully) identical sum and difference channels. Finally the dot product is formed by the detector. If we reconsider the hypothetical dot product pattern as shown in Figure 2.8 we can see the result of the signal which entered the antenna at an angle θ off the boresight direction. By noting the phase of the signal (0°) and the magnitude of the signal we can redirect the antenna to the boresight direction. Thus the S-curve transfer function "tells" the antenna pedestal the required direction to move as well as the number of degrees to move to place the signal in the null of the product pattern. Hopefully, once the tracker has locked onto the target beacon the signal should never be more than a few milliradians off boresight

2.2 The Effect of Multipath On a Monopulse Tracking Scheme

The effect of signal multipath on the performance of a monopulse tracking system can be quite severe. The problems become worse as the grazing angle of the arriving signal becomes small.

Let us consider the situation depicted in Figure 2.9. Note that since the direct signal is very nearly on axis, the sum pattern signal will be much higher in intensity than the difference signal. Now let us also suppose that a specularly reflected signal also enters the antenna through sidelobes (not shown). We can represent the received signals as phasors as shown in Figure 2.10. In Figure 2.10a the sum signal is depicted. $V_{\Sigma D}$ is the direct sum channel signal, V_r is the reflected signal with a phase angle relationship of ϕ. The resultant signal leaving the antenna terminals for processing is the vector sum of $V_{\Sigma D}$ and V_r and is shown as V_Σ.

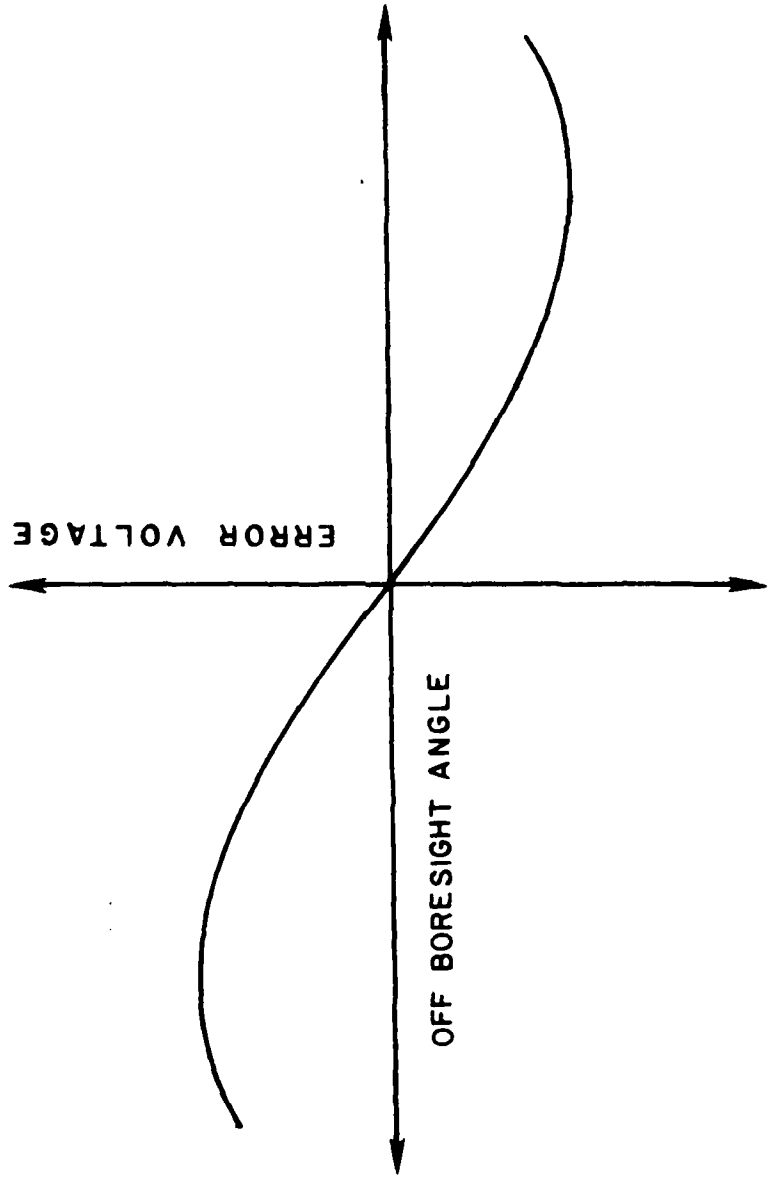

Figure 2.6
Typical Error Curve for a Monopulse Tracker

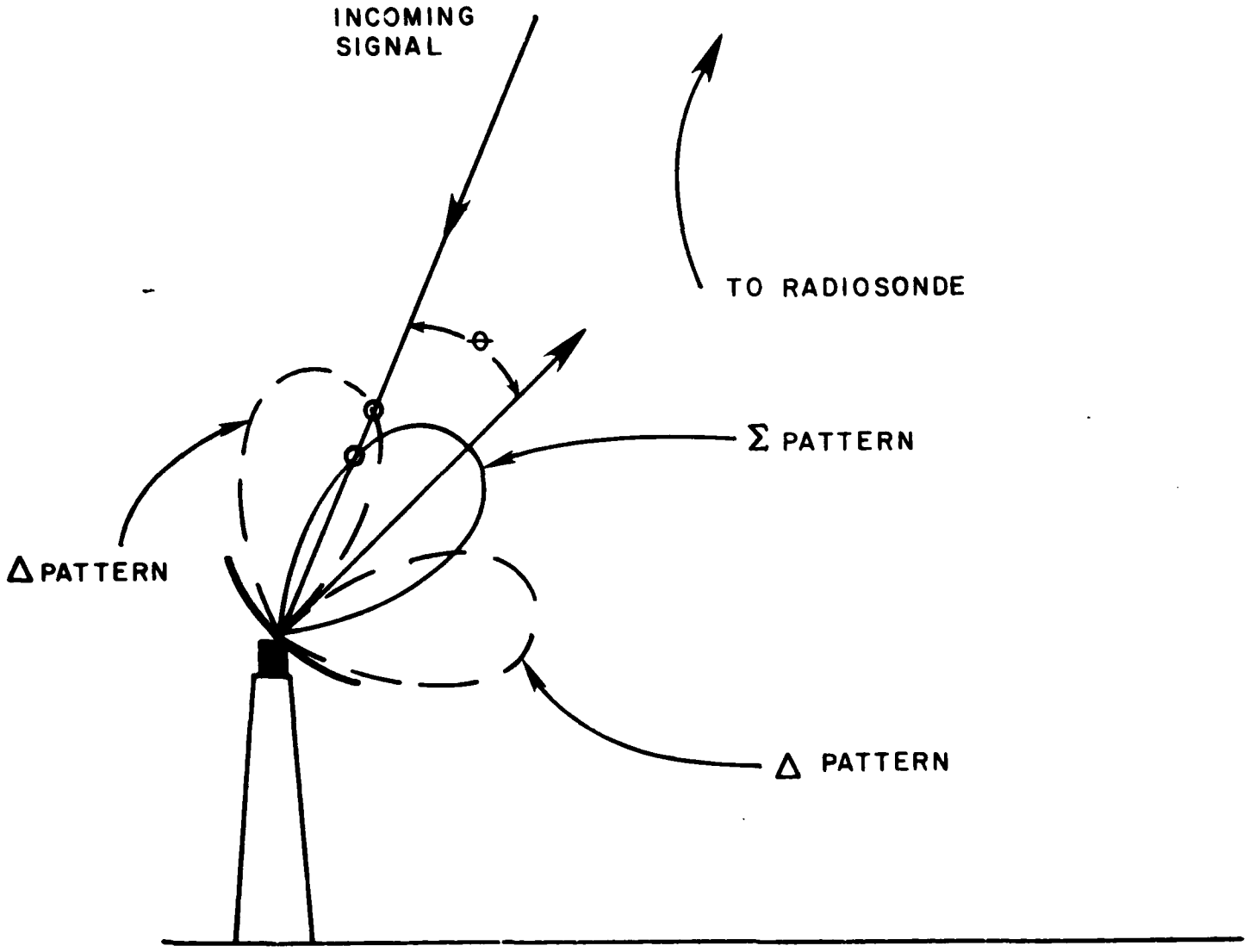

Figure 2.7 Free Space Antenna Patterns with an Incoming Signal at an off Boresight Angle at θ.

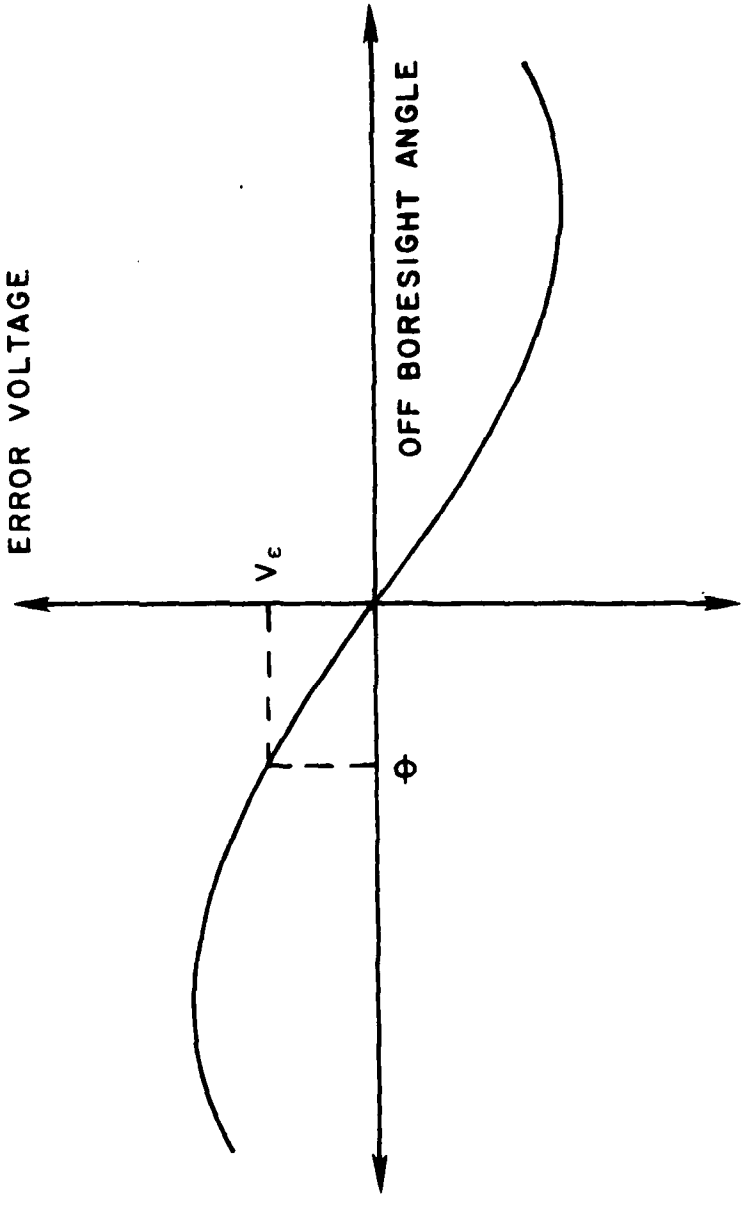

Figure 2.8 Error Voltage Response to the Tracked Target Signal Arriving at an Angle θ off the Boresight Axis.

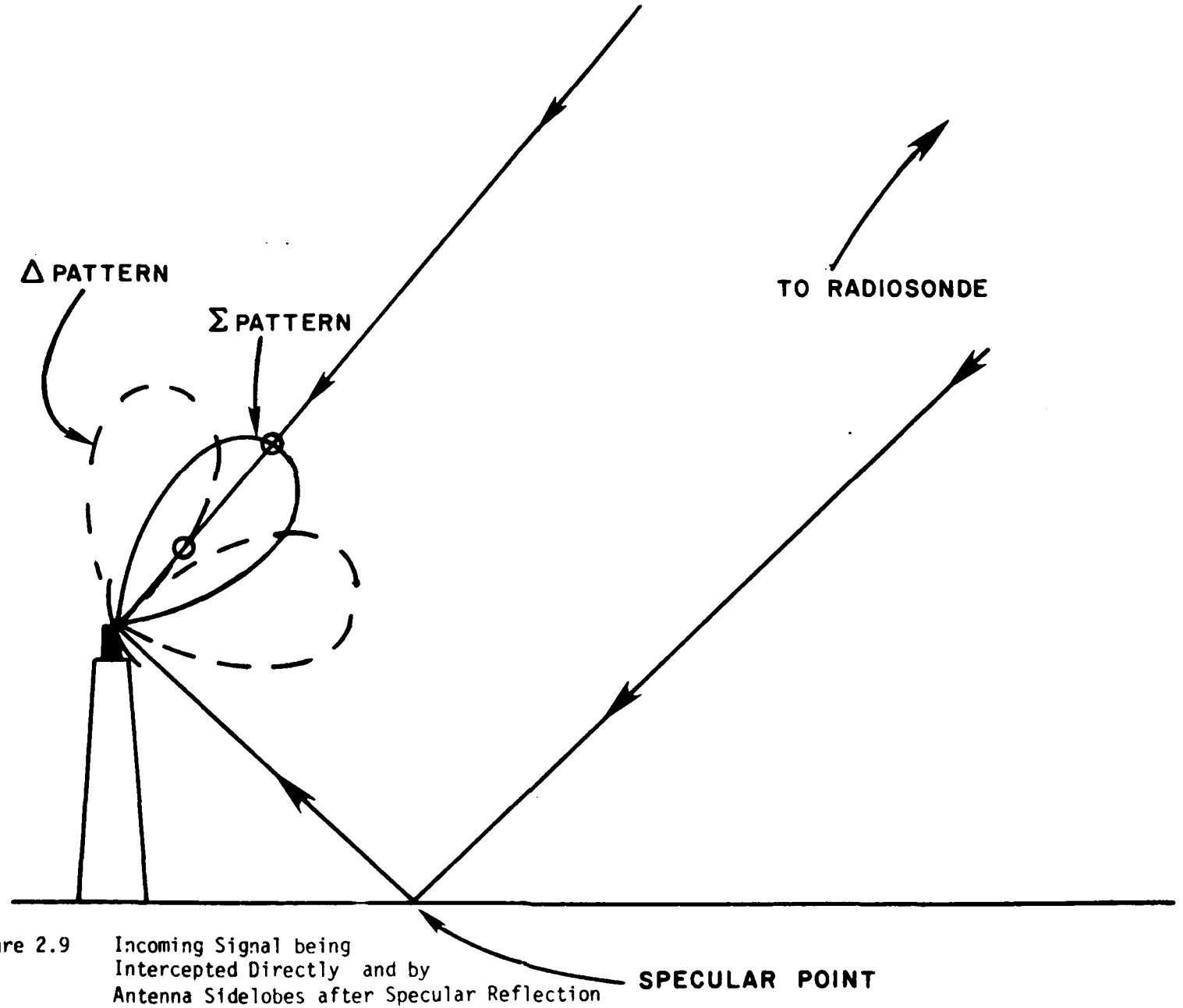

Figure 2.9 Incoming Signal being Intercepted Directly and by Antenna Sidelobes after Specular Reflection

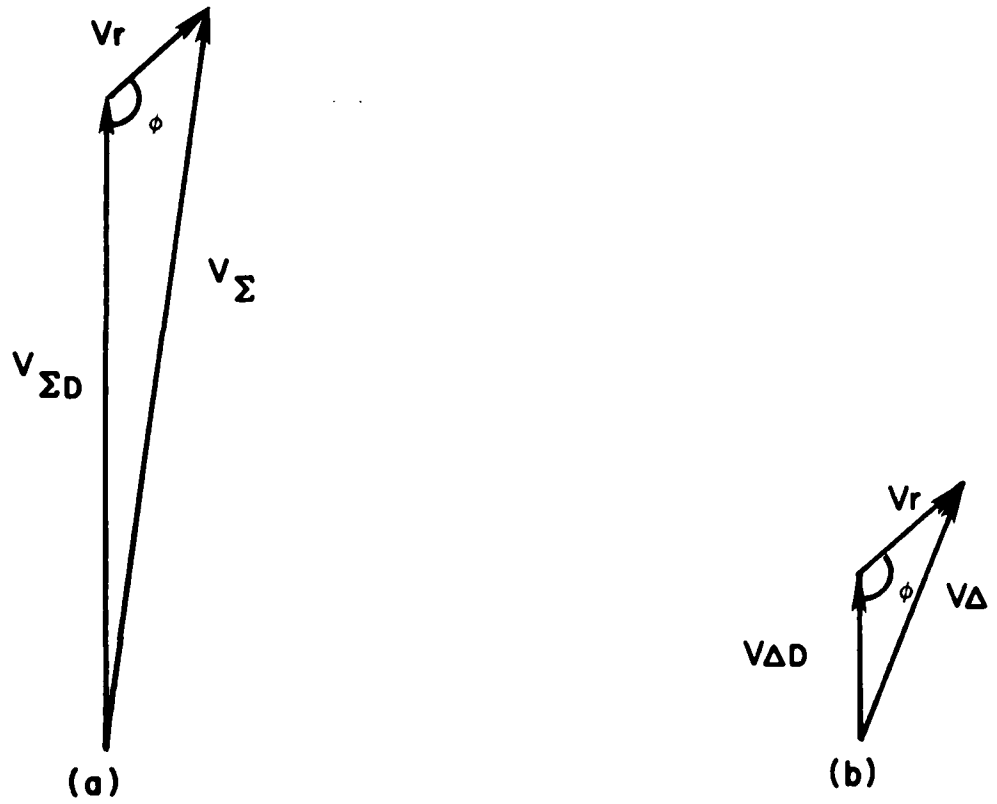

Figure 2.10 Phasor Relationship Between Direct and Multipath Specular Scatter for Both the Σ (a) and Δ(b) Channels

Using the law of cosines we can write

$$V_\Sigma = \sqrt{V_{\Sigma D}^2 + V_r^2 - 2V_{\Sigma D}V_r \cos \phi} \qquad 2.1$$

Now suppose

$$V_r = \alpha V_{\Sigma D} \qquad 2.2$$

where $0 \leq \alpha \leq 1$

Then

$$V_\Sigma = \sqrt{\frac{V_r^2}{\alpha^2} + V_r^2 - \frac{2V_r^2}{\alpha} \cos \phi} \qquad 2.3$$

$$= V_{\Sigma D} \sqrt{1 + \alpha^2 - 2\alpha \cos \phi}$$

Now suppose that the magnitude of the ground reflection coefficient is

$$R = 0.3$$

and the sidelobe through which the reflected signal enters the antenna is 30 dB below the peak gain of the sum pattern. In this case

$$\alpha = 9.5 \times 10^{-3} \qquad 2.5$$

so from Equation 2.3

$$V_\Sigma = V_{\Sigma D} \sqrt{1.0000922 - 0.0192 \cos \phi} \qquad 2.6$$

Thus in the worst cases ($\phi = 0°$ or $\phi = 180°$)

$$0.98V_{\Sigma D} \leq V_\Sigma \leq 1.02 V_{\Sigma D} \qquad 2.7$$

But now consider the error signal. If

$$V_{\Sigma D} = 50\ V_{\Delta D} \qquad 2.8$$

then $$49.0\ V_{\Delta D} \leqq V_{\Delta} \leqq 51.0\ V_{\Delta D} \qquad 2.9$$

It is apparent that while a reflected signal will cause errors during processing, the difference signal is generally much more sensitive to multipath errors than the sum signal.

To this point we have considered only a specularly reflected signal from the ground as interference. As shown in Figure 2.11 this is not generally the case unless the ground surface appears smooth to the radiosonde beacon signal. If the ground appears rough, signals from many points on the ground will enter the antenna resulting in poor tracking capabilities. This is particularly true when the signal grazing angle becomes small and the tracker antenna pattern illuminates the ground (vide Figure 2.12). In this case the term α (Equation 2.2) can approach unity resulting in loss of track.

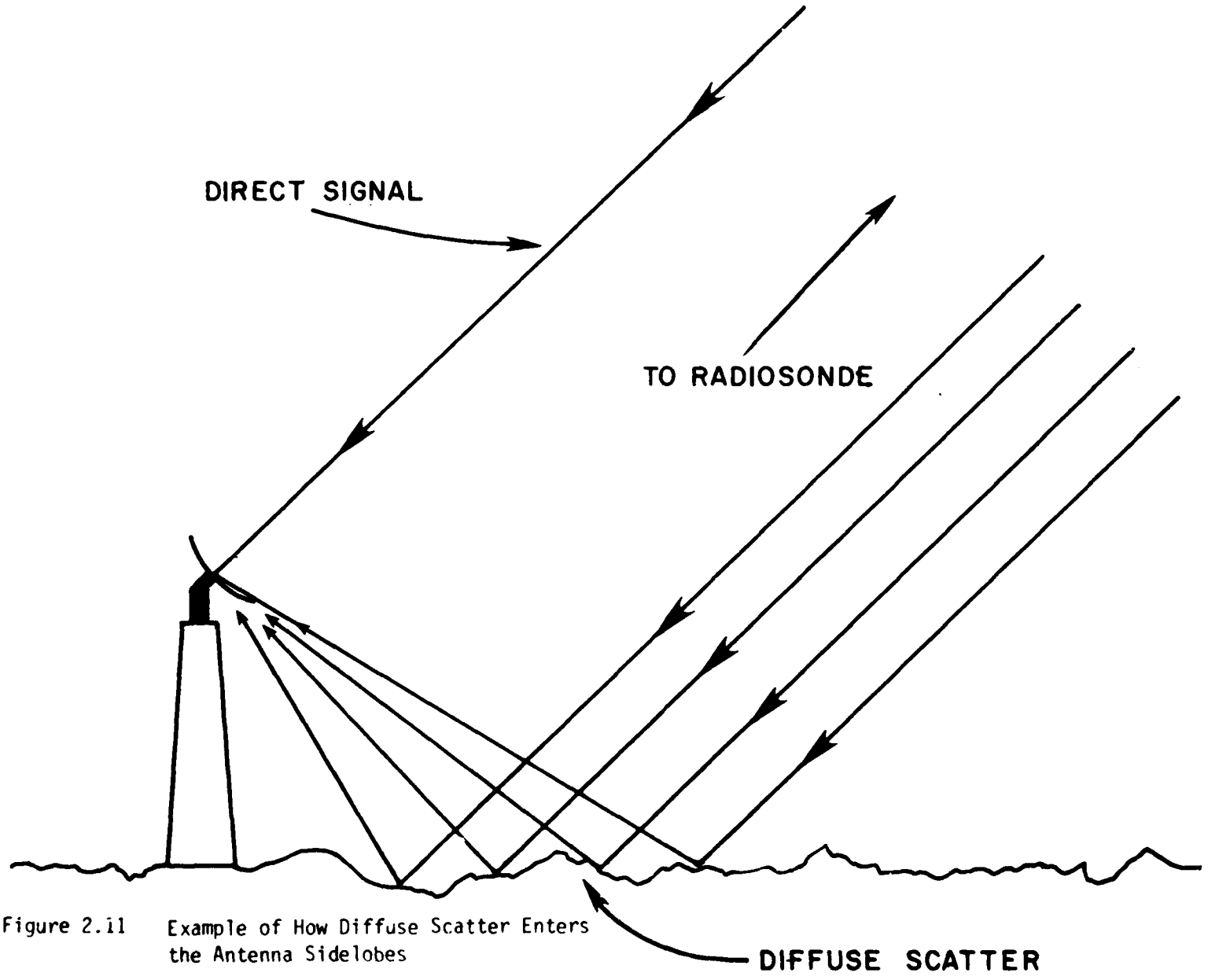

Figure 2.11 Example of How Diffuse Scatter Enters the Antenna Sidelobes

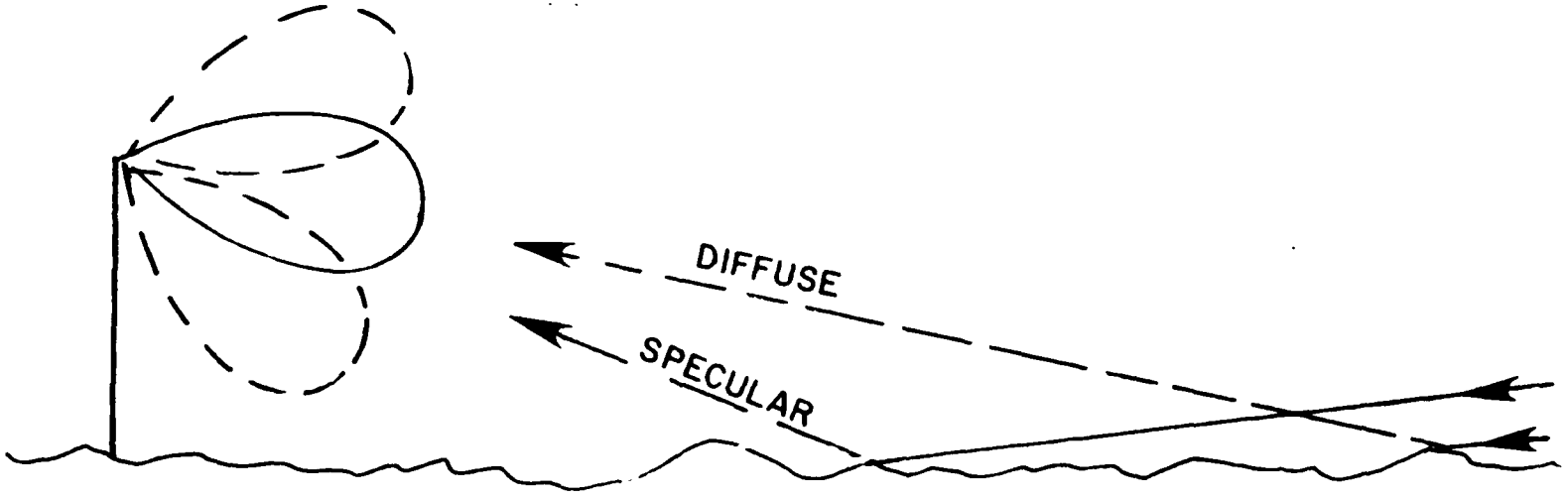

Figure 2.12 Example of How Both Specular and Diffuse Scatter can Enter the System through the Main Lobe at Low Grazing Angles.

2.3 Simulation of a Passive Monopulse Tracker

The intent of this section is not to simulate the entire passive tracking system. To do this would require knowledge of the entire system including servo bandwidth, antenna wind loading, system bias errors, etc. Furthermore this is beyond the scope of the contract which is to study the effect of antenna beam shape on tracker response to multipath induced errors.

2.3.1 Antenna Responses

As an initial attempt to simulate tracker response, gaussian shaped antenna beams will be used as in Figure 2.2. Thus the voltage antenna patterns which will be used to form the sum and difference patterns will be modeled as

$$G = \exp\left(\frac{-1.388\ \theta^2}{\theta_B{}^2}\right) \qquad 2.10$$

where θ_B is the half power beamwidth and θ is the off axis angle.

If we squint the antennas beam off the boresight axis, Equation 2.10 becomes

$$G = \exp\left(\frac{-1.388}{\theta_B{}^2}\ (\theta + \theta_S)^2\right) \qquad 2.11$$

or

$$G = \exp\left(\frac{-1.388}{\theta_B{}^2}\ (\theta - \theta_S)^2\right) \qquad 2.12$$

for two antenna beams squinted in opposite directions by θ_S degrees. The hybrid coupler shown in Figure 2.1 will form the sum and difference of Equations 2.11 and 2.12 so that

$$G_\Sigma = \exp\ [Z(\theta^2 + \theta_S{}^2)]\ \{\exp(2Z\theta\ \theta_S) + \exp(-2Z\theta\ \theta_S)\} \qquad 2.13$$

and

$$G_\Delta = \exp[Z(\theta^2 + \theta_S{}^2)]\ \{\exp(2Z\theta\ \theta_S) - \exp(-2Z\theta\ \theta_S)\} \qquad 2.14$$

where

$$Z = -\frac{1.388}{\theta_B^2}$$

It should be noted that for

$$G_{\Sigma,\Delta} < |SL| \qquad 2.15$$

where SL is a predescribed sidelobe level, a constant sidelobe level o. SL wili be assumed. However, the sidelobe of the voltage patterns may be positive or negative depending on the sign of a sin x/x antenna pattern having a beamwidth θ_B. As an example, Figure 2.13 shows an antenna pattern with a 25° half power beamwidth and $|SL| = 0.2$.

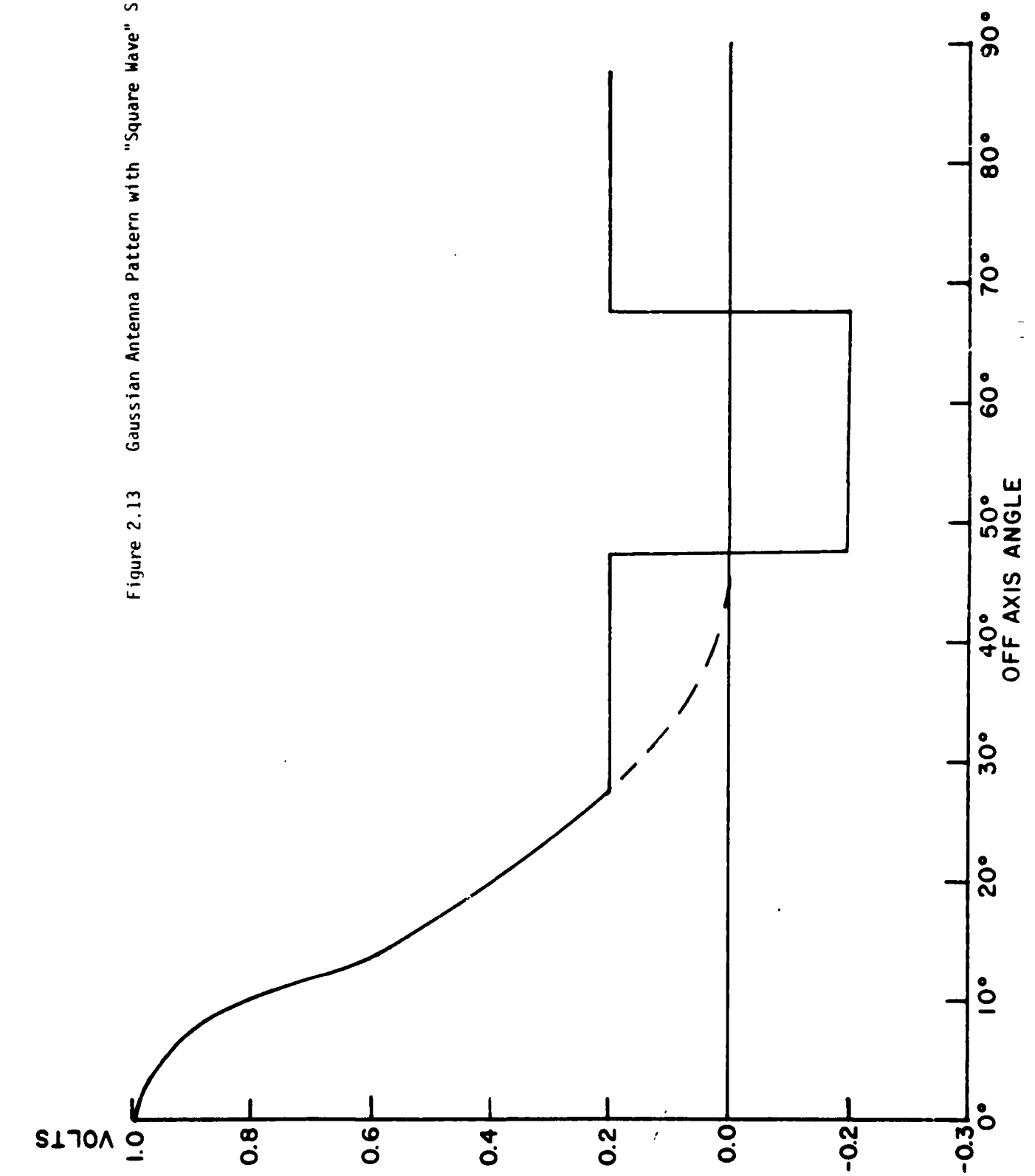

Figure 2.13 Gaussian Antenna Pattern with "Square Wave" Sidelobes

2.3.2 Simulation Geometry

Because the elevation plane response of the tracker suffers much more from multipath signals than the azimuth plane response, only the elevation plane tracker response will be considered. This is true even when the grazing angle is held constant and the azimuth angle of arrival changes. As the azimuth angle varies, the elevation multipath effects will vary as the antenna pattern "sees" different soil conditions such as moisture and roughness.

The tracker response will generally be dependent on three signals entering the antenna. First, of course, is the signal which propagates directly from the radiosonde to the tracker. Second, there will be a specular component of the signal as discussed in Section 2.2 (vide Figure 2.9). Finally, diffuse scatter (vide Figure 2.11) will also influence the tracker response. Because the intensity and phase of each of these three signals will vary with the grazing angle of the incoming signal, the simulation must account for this effect.

Figure 2.14 shows the geometry of the antenna and signal interaction. Because the influence of the direct, specular and diffuse signals will depend on the angle at which the enter the antenna, the antenna boresight angle will serve as a reference. This angle is shown as θ_H in Figure 2.14 and is merely the elevation angle of the antenna. The angle of arrival of the direct radiosonde signal is shown as θ and is measured as positive when the radiosonde signal enters the antennas below the boresight direction as shown in Figure 2.14. The angle of arrival of the specular component of the forward scatter is labelled θ_{sp} while θ_D will indicate the angle at which a particular component of the diffuse scatter enters the antenna pattern. In the simulation, ψ will represent the grazing angle of the incoming signal. Also shown in Figure 2.14 is h_a, the antenna height, f_c, the distance from the sub-antenna point to the center of the first Fresnel zone as well as f_ℓ, the length of the first Fresnel zone. Finally, X_{DN} indicates the point from which the Nth component of the diffuse signal is scattered.

FIGURE 2.14
Geometry of the Antenna and Signal Interaction

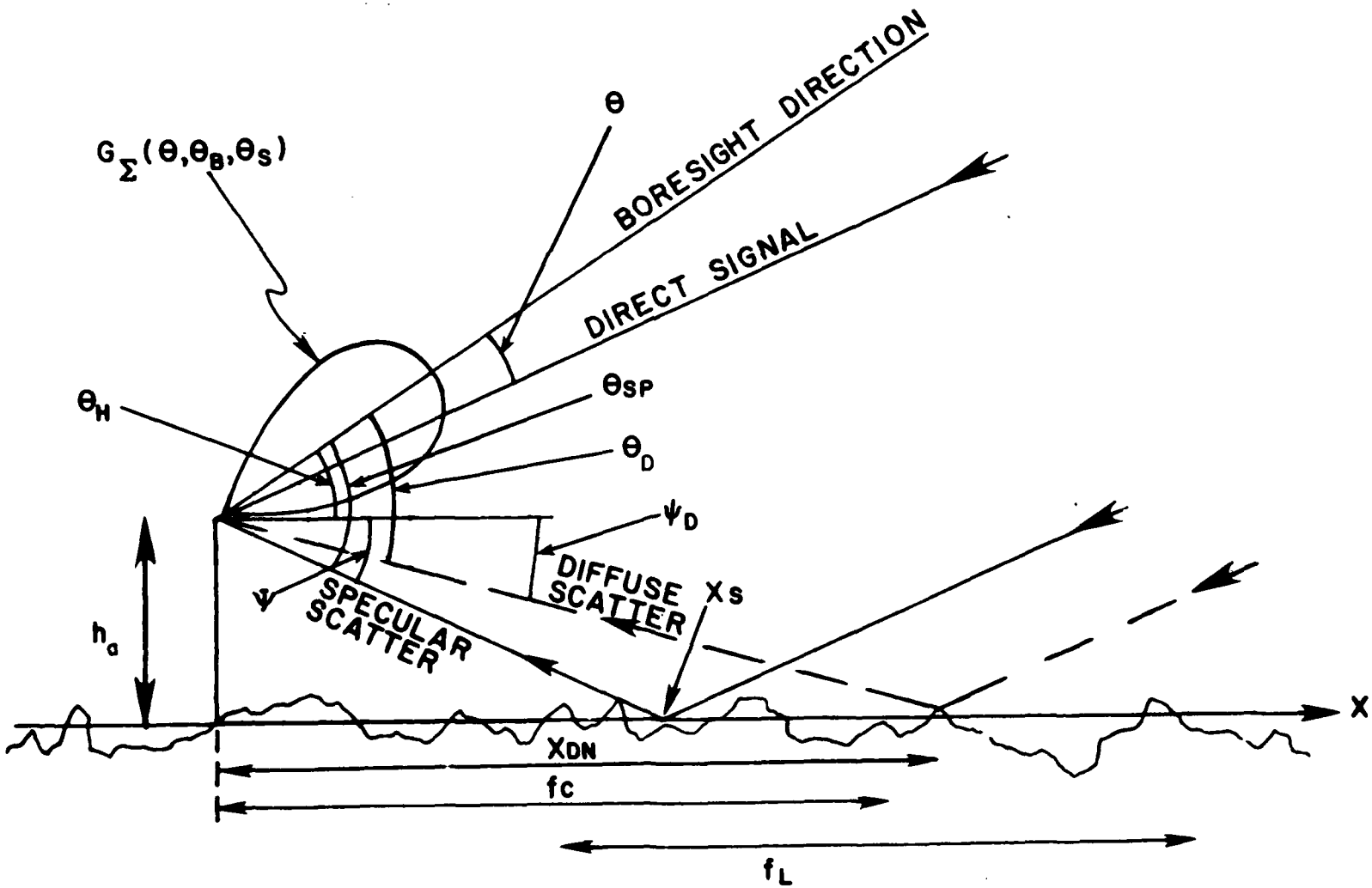

2.3.3 Simulation Implementation

The desired result of the simulation is the "S" curve (e.g., Figure 2.6) characteristic of a particular tracker operating under specified conditions. The resultant "S" curve can then be compared with that curve which is generated when the same tracker operates under ideal conditions.

If the point at which forward scatter occurs is smooth with respect to the signal wavelength, λ, the specular component of the forward scatter can be modeled as

$$E_{sp} = E_i \, R_{H,V} \qquad 2.15$$

where E_i is the incident electric field vector and $R_{H,V}$ is the Fresnel reflection coefficient associated with either a horizontally or vertically polarized field where

$$R_H = \frac{\sin\psi - \sqrt{\varepsilon_r - \cos^2\psi}}{\sin\psi + \sqrt{\varepsilon_r - \cos^2\psi}} \qquad 2.16$$

and

$$R_V = \frac{\varepsilon_r \sin\psi - \sqrt{\varepsilon_r - \cos^2\psi}}{\varepsilon_r \sin\psi + \sqrt{\varepsilon_r - \cos^2\psi}} \qquad 2.17$$

In Equations 2.16 and 2.17, ε_r is the complex relative dielectric constant of the reflection surface. Since ε_r for soil is a strong function of soil moisture we must include this effect in the simulation.

In general, the surface from which forward scatter occurs is not smooth. If we define the standard deviation of the surface from flat as σ_s, then the ratio σ_s/λ is a measure of surface roughness with respect to the signal wavelength. As the ratio σ_s/λ becomes small, specular scatter tends to dominate. As a qualitative example consider Figure 2.15 which shows a plane wave incident at a grazing angle ψ on a surface which is relatively smooth (e.g., $\sigma_s/\lambda = 0.125$). Note that while some diffuse scatter is shown, the specular term dominates. In Figures 2.16 and 2.17 the forward scatter becomes progressively more diffuse as σ_s/λ increases.

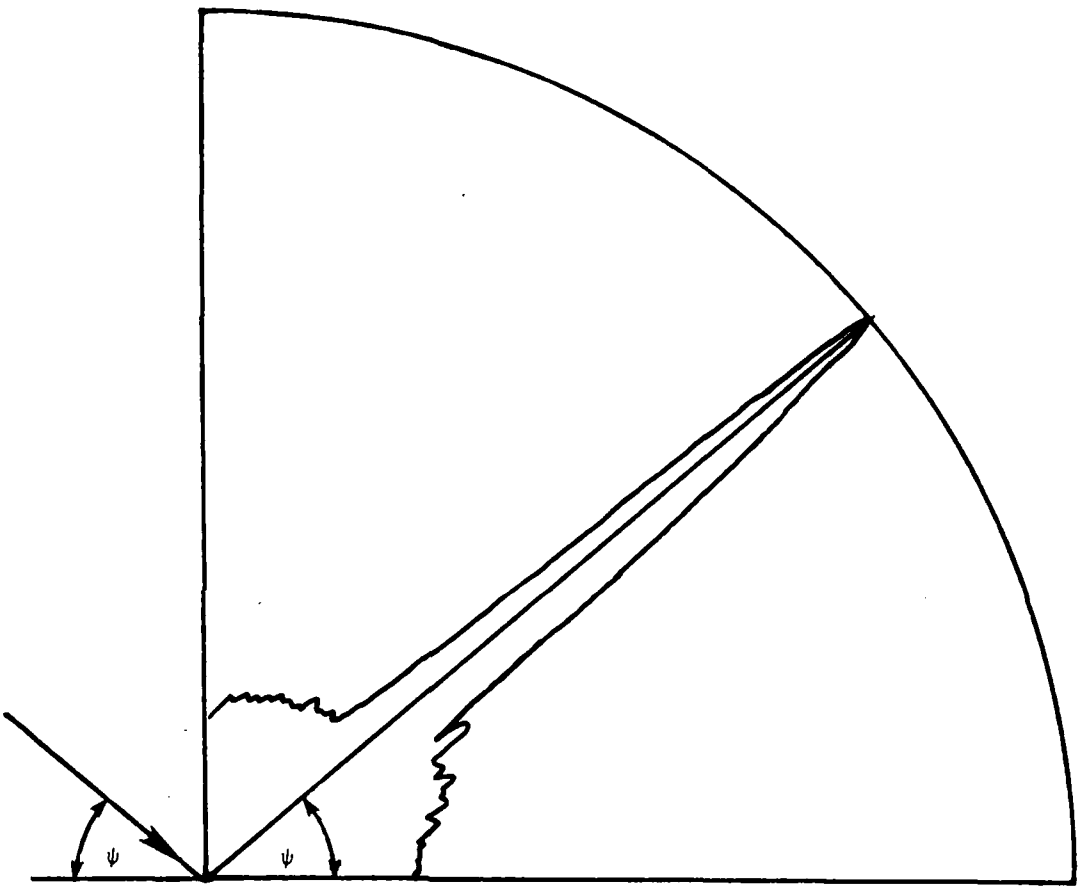

Figure 2.15
Qualitative Examples of a Surface Which is Smooth with Respect to a Wavelength.

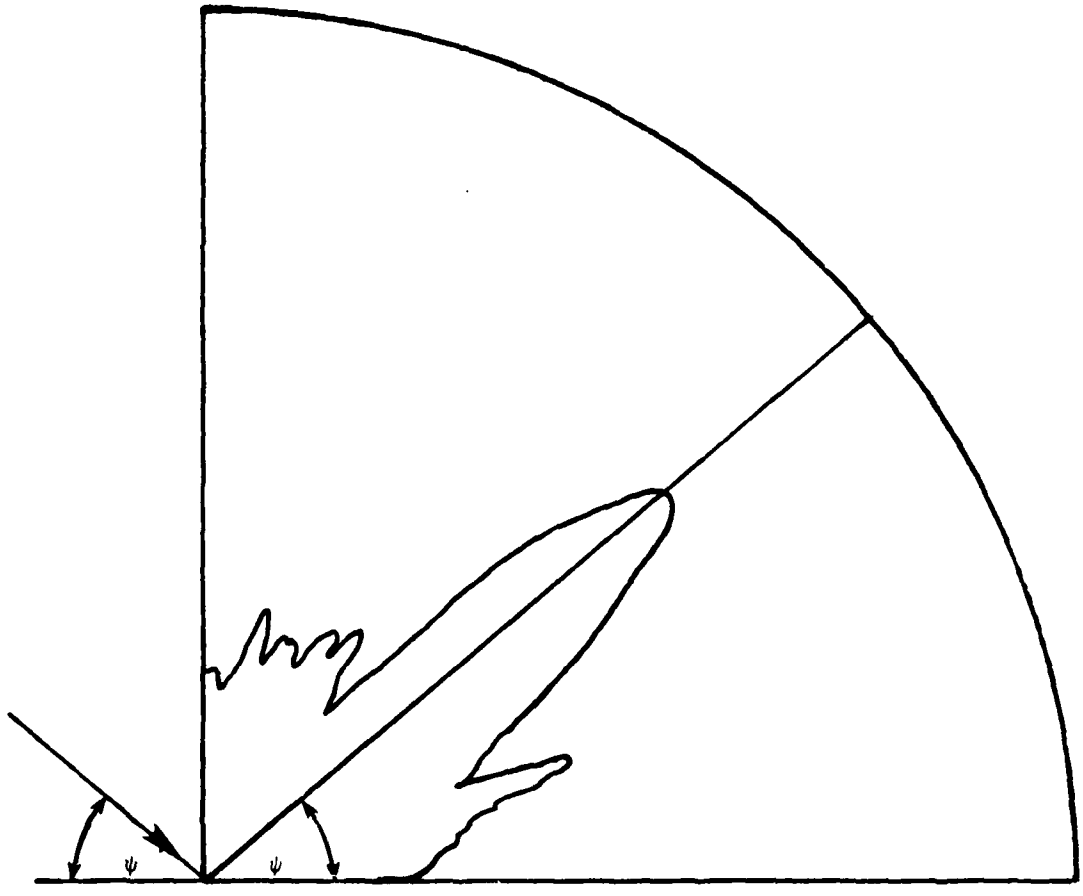

Figure 2.16

Qualitative Example of a Surface Which is Rough with Respect to a Wavelength

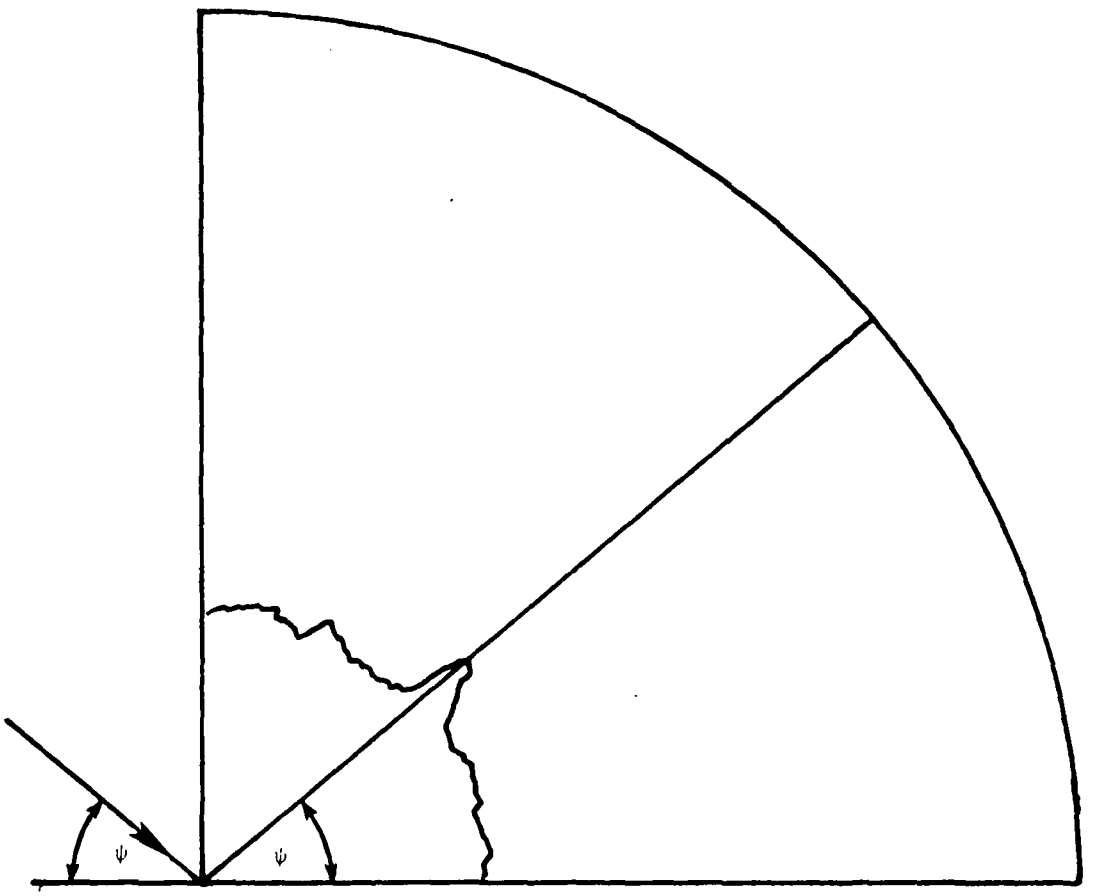

Figure 2.17
Qualitative Example of a Surface Which is Very Rough with Respect to a Wavelength

To account for these surface roughness effects, a model described by Beard, Katz and Spetner [2] is used. In this model the forward scattered signals are broken into two components. The first is the so-called "effective reflection coefficient" [3] R_e where

$$R_e = R\left\{\exp\left(-\frac{8\pi\sigma_s^2}{\lambda^2}\sin^2\psi + j\Delta\right)\right\} \qquad 2.18$$

where R is the Fresnel reflection coefficient and Δ is defined as

$$\Delta = \frac{4\pi\ h_a}{\lambda}\sin\psi \qquad 2.19$$

and simply represents the free space phase shift undergone while propagating to the antenna from the specular point. Inherent in the model is the assumption that the rough surface can be modeled as a stationary Gaussian random process with a mean of zero and standard deviation of σ_s. Moreover it is also assumed that the autocorrelation function of the surface is exponential [3]. Figure 2.18 depicts the behavior or Equation 2.18 as a function of σ_s/λ. (For purposes of simplication of plotting Equation 2.18, it was assumed that $\Delta = 0$.) Two examples are shown; the solid line depicts Equation 2.18 for $\psi = 20°$ and the dashed line represents $\psi = 10°$. The point of specular scatter can be shown to be (vide Figure 2.14)

$$X_s = \frac{h_a}{\tan\psi} \qquad 2.20$$

To quantify the intensity and phase of the diffuse forward scattered fields it was necessary to rely on experimental data which, while tenuous, are perhaps the best available at this time. These data are those reported by Beard, Spetner and Katz [3], and Beard [4,5]. All data reported in [3, 4 and 5] are derived from forward scatter from the ocean surface at frequencies somewhat higher (3.3, 5.7, 9.4 and 35 GHz) than the L-band data which are desirable. Moreover the data were acquired from a salt water surface rather than a terrain surface. This is also unfortunate but does represent a worst case than forward scatter from soil unless the soil has an electrical conductivity approaching that of ocean water. For a more complete discussion of these data the reader is referred to Carver [6] who proposed the following equation to best describe the RMS amplitude of those fields scattered from sea surfaces.

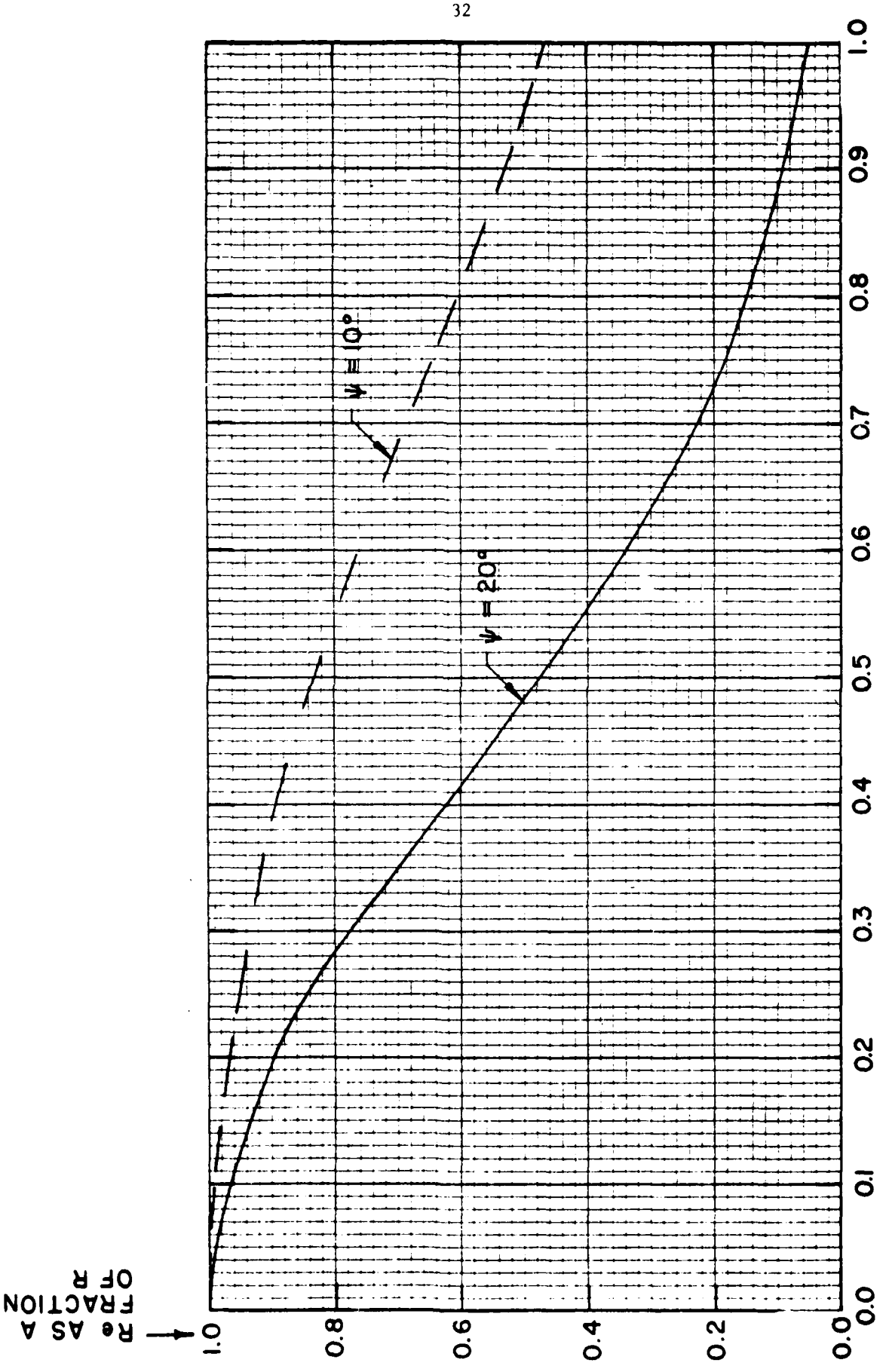

Figure 2.18 Behavior of R_e, the Effective Reflection Coefficient as Surface Roughness Varies

$$R_d \cong \left\{0.77[1-e^{-4\pi\delta}]e^{-4.73\delta}\right\} \left|R_{H,V}\right| \qquad 2.21$$

where $$\delta = \frac{\sigma_s}{\lambda} \sin \psi$$

and $R_{H,V}$ is the polarization dependent Fresnel reflection coefficient. Figure 2.19 presents Equation 2.21 for ψ 10° and ψ = 20° as a function of σ_s/λ. Note that both curves show a peak. For ψ = 10° the peak is broad and occurs for $\sigma_s/\lambda \cong 0.3$ for ψ = 20°. Since equation 2.21 is the RMS value of the forward scattered electric field, we must modify it to account for fading. This is done by changing Equation 2.21 to

$$R_d \cong \left\{0.77[1-e^{-4\pi\delta}]e^{-4.73\delta}\right\} \left|R_{H,V}\right| A\, e^{-j\eta} \qquad 2.22$$

where A is a random variable having a Rayleigh probability density function and η is uniformly distributed between 0 and 2π.

Unlike the specular component of the forward scatter, diffuse scatter occurs at an infinite number of points along the ground between the antenna and the sub-radiosonde point. Thus we should integrate 2.22 over all possible values of X_{DN} (vide Figure 2.14). This, however, would not be a judicious decision in terms of facilitating computational procedures.

As discussed by Kerr [7] the terrain between the sub-radiosonde and sub-antenna point can be divided into a series of ellipses call Fresnel zones. A qualitative example is shown in Figure 2.20. Forward scattered signals emanating from within a given Fresnel zone will vary by no more than π radians at the antenna. However, signals emanating from adjacent zones will arrive at the antenna in phase opposition. Thus, signals scattered from adjacent zones (other than the first zone) will, on the average, tend to cancel at the antenna, leaving signals scattered from within the first zone as the dominant signal. Thus, rather than integrating Equation 2.22 over all values of x, we can integrate over the first Fresnel zone and expect very reasonable results. According to Kerr [7] the center of the first Fresnel zone is given by

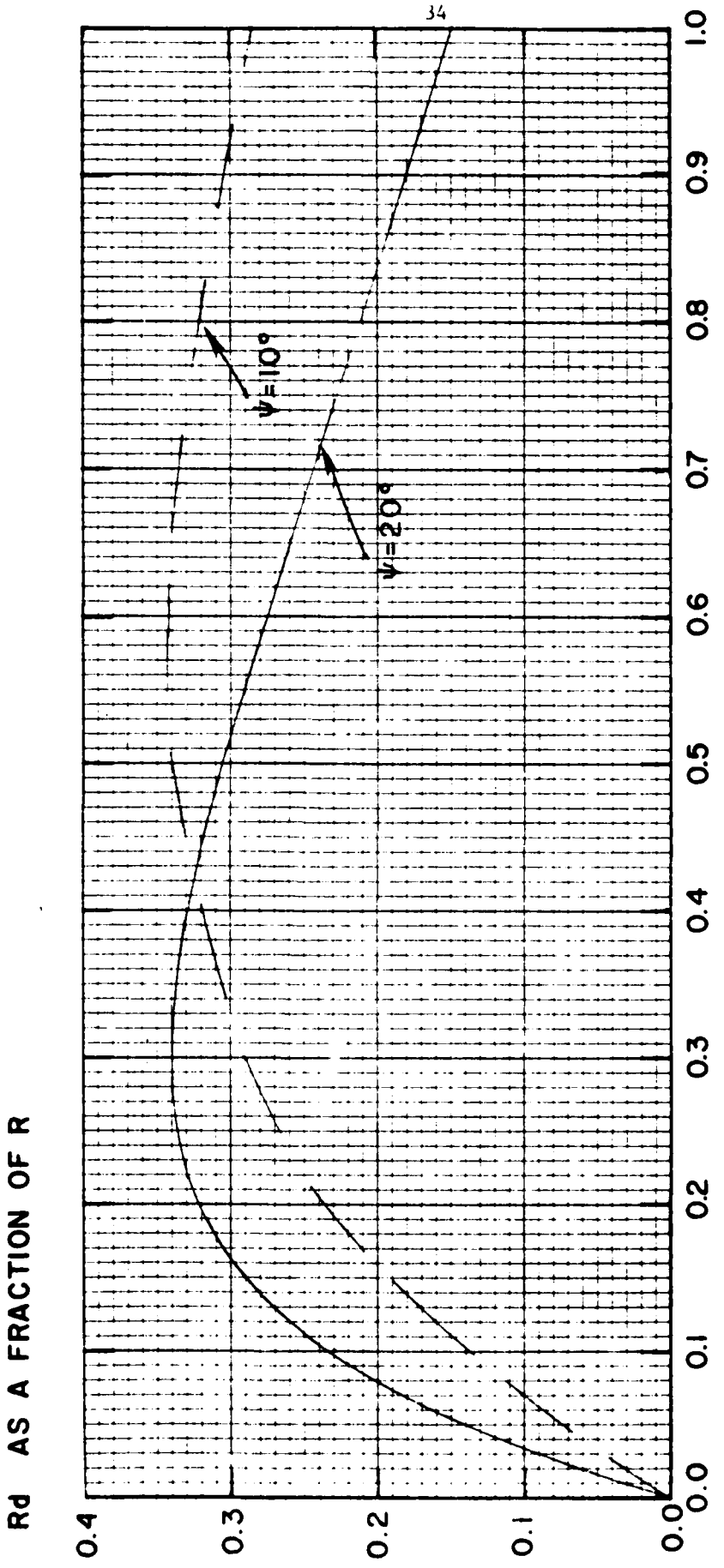

Figure 2.19 Behavior of R_d, the Diffuse Reflection Coefficient, as a Function of Surface Roughness.

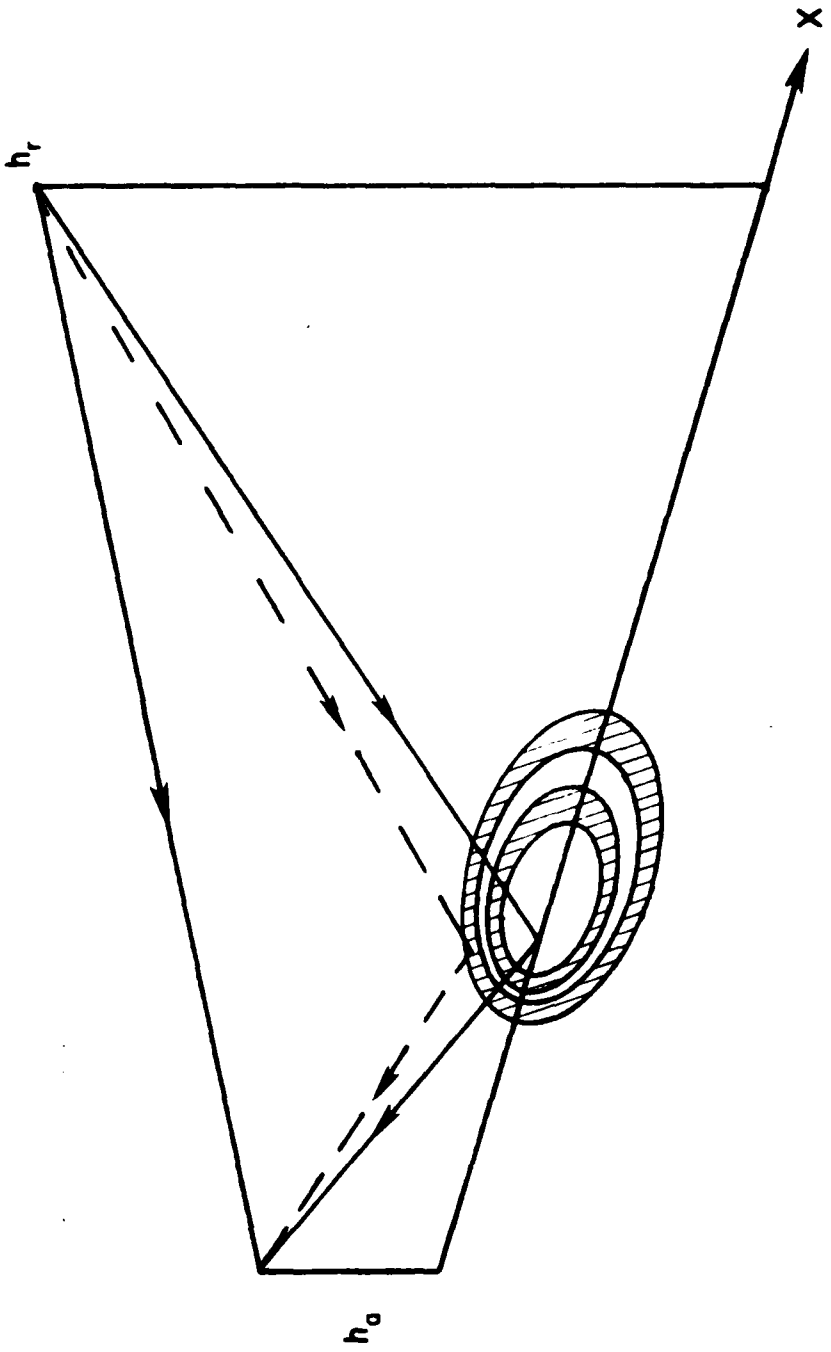

Figure 2.20
A Qualitative Example of Fresnel Zone Ellipses. The Center Ellipse is the First Fresnel Zone.

$$f_c = \frac{D}{2} \frac{1 + \frac{2h_a(h_a + h_r)}{\lambda D}}{1 + \frac{(h_a + h_r)^2}{\lambda D}} \qquad 2.23$$

where D is the distance from the sub-antenna point to the sub-radiosonde point and h_r is the height of the radiosonde. The length of the major axis of the first zone is

$$f_\ell = D \frac{\sqrt{1 + \frac{4h_a h_r}{\lambda D}}}{1 + \frac{(h_a + h_r)^2}{\lambda D}} \qquad 2.24$$

We are now in a position to determine the response of the tracker to the incident signal. It is assumed (without loss of generality) that the incident signal is a plane wave with an electric field intensity of one volt per meter and that the radiosonde transmits with an isotropic antenna. Thus, to satisfy the plane wave assumption the radiosonde must be far enough from the tracking antenna so that the phase taper across the receiving antenna is small.

Using the results obtained to this time we can write an expression for the field strength as integrated by the receiving antenna. For a given θ_s and θ_B, this is expressed as

$$E_{\Sigma,\Delta} = G_{\Sigma,\Delta}(\theta) + G_{\Sigma,\Delta}(\theta_{sp})R_e + \int_{f_c - \frac{f_\ell}{2}}^{f_c + \frac{f_\ell}{2}} G_{\Sigma,\Delta}(\theta)R_d \, dx \qquad 2.25$$

The first term in 2.25 accounts for the direct illumination while the second and third terms correspond to the coherent and incoherent ground scatter respectively. The subscripts Σ and Δ on E and G simply indicate that the expression for E_Σ or E_Δ is the same as long as the correct (G_Σ or G_Δ) gain pattern is used.

While Equation 2.25 represents the electric field as integrated by the tracking antenna, we can represent the open circuit voltage, V_{oc}, at the antenna terminal by the following equiation.

$$V_{oc} = \vec{E} \cdot \vec{h} \qquad 2.26$$

where E is the electric field vector and h is the vector effective height of the receiving antenna. If E and h are co-polarized, 2.26 becomes

$$V_{oc} = |E| \, |h| \qquad 2.27$$

If we now assume h = 1, we can, without loss of generality express 2.25 as

$$V_{\varepsilon} = V_{oc} = G_{\Sigma\Delta}(\theta) + G_{\Sigma\Delta}(\theta_{sp})R_e + \int_{f_c - \frac{\ell}{2}}^{f_c + \frac{\ell}{2}} G_{\Sigma\Delta}(\theta)R_d dx \qquad 2.28$$

where we have introduced V_{ε}, the tracking error voltage as shown in Figure 2.8.

As discussed earlier in Section 2.2.3, both R_e and R_d are functions of the Fresnel reflection coefficients. The soil Fresnel reflection coefficients are functions of the soil dielectric constant which is in turn a function of the soil moisture content. To account for this effect, second order polynomials were fitted to data published by Jedlicka [7] and are shown in Figure 2.21 along with the polynomials fitted to the data. Because the type of soil contributes to the variability of its dielectric constant, river sand was chosen to minimize the effects of soil variability. The reader is referred to [7] for a complete discussion of the effects of soil type on the dielectric constant of the soil.

Equation 2.28 was encoded using FORTRAN IV (see Appendix) and executed using an IBM 370 computer. The flow chart for the program can be found in Figure 2.22. Rather than numerically integrating the third term in Equation 2.28, the integral was replaced by a summation and evaluated at increments of λ so long as the point of diffuse scatter remained within the first Fresnel zone.

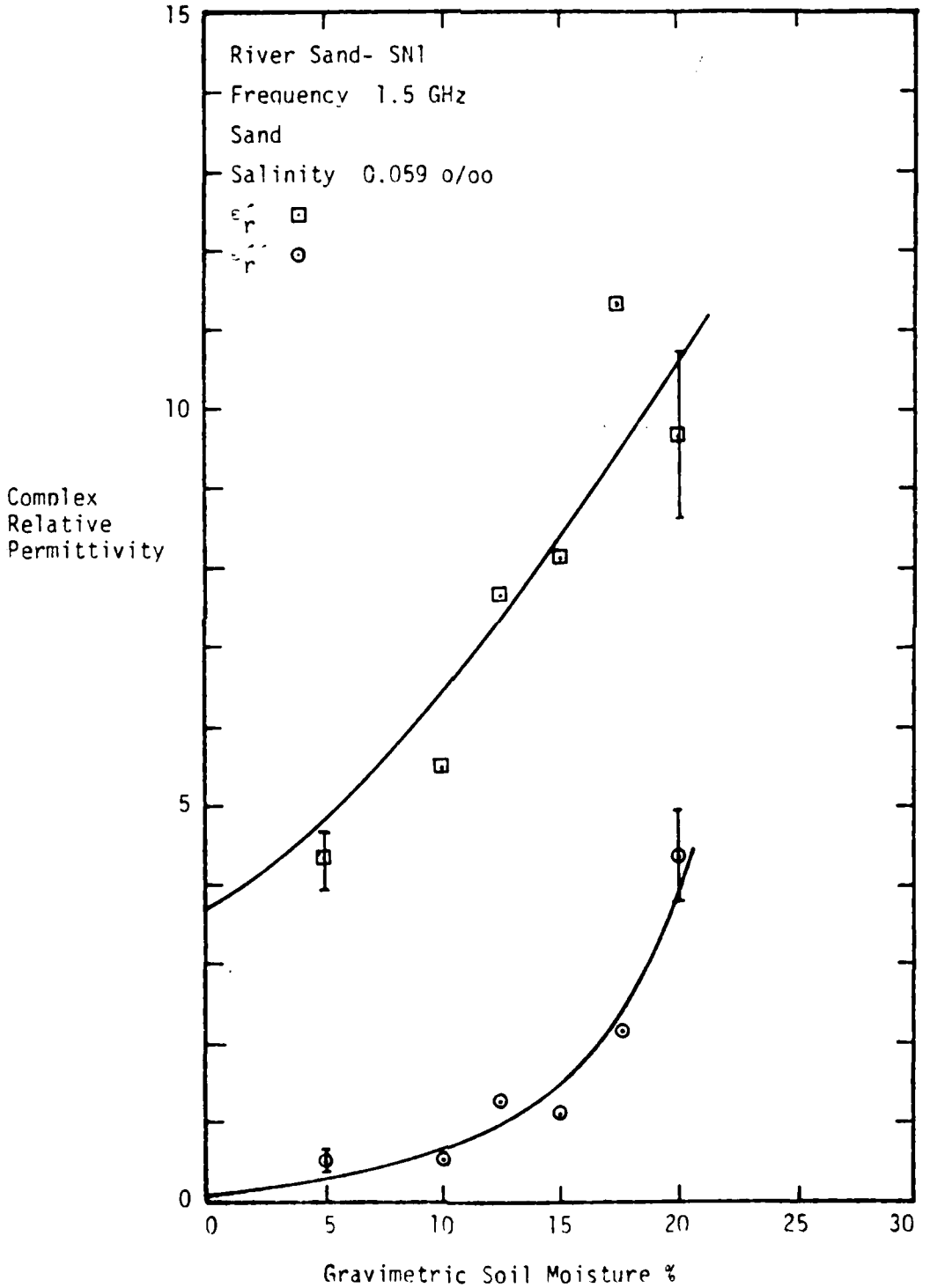

Figure 2.21 Soil Permittivity as a function of soil moisture

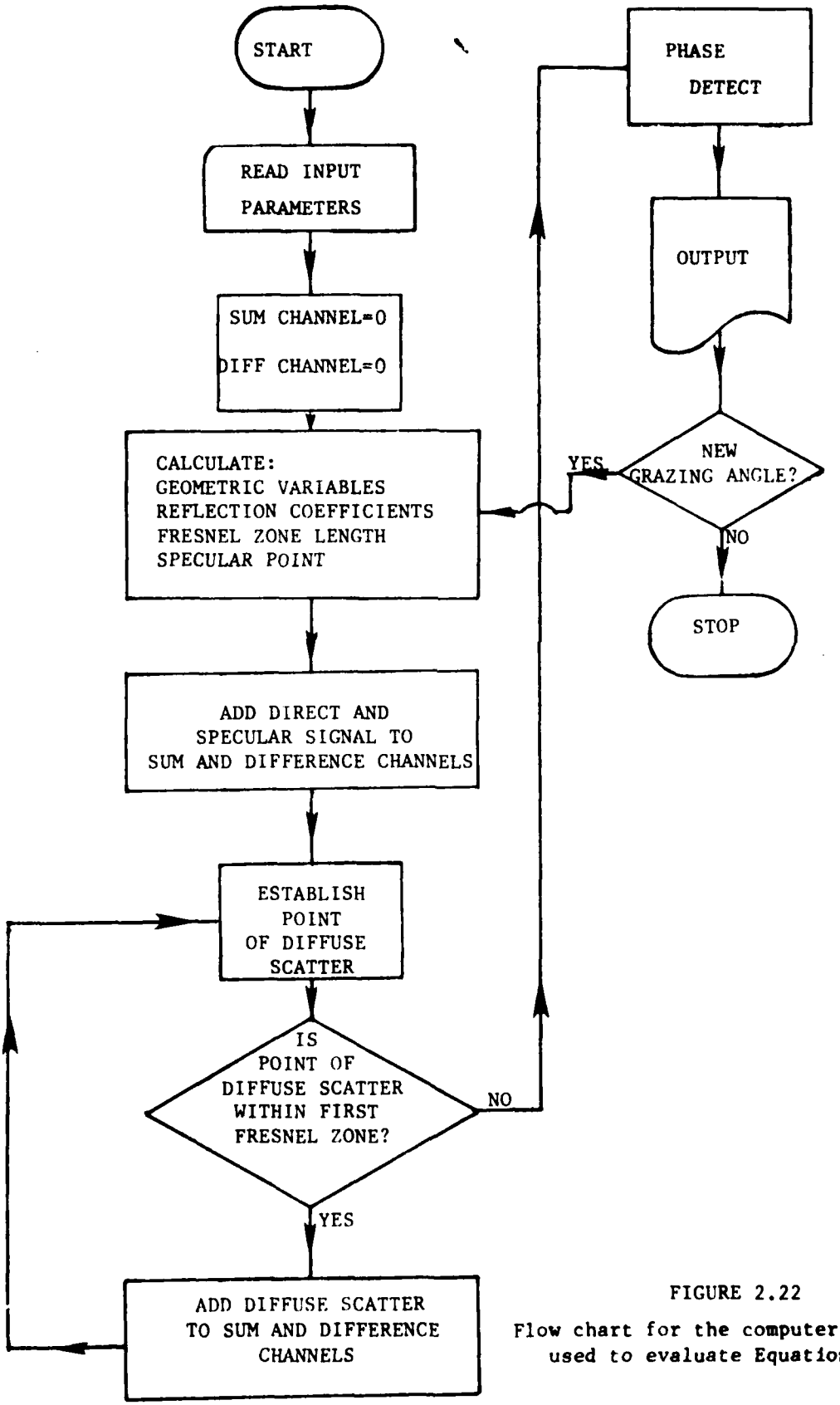

FIGURE 2.22

Flow chart for the computer program used to evaluate Equation 2.28

2.3.4 Simulation Results

The initial simulation was an attempt to simulate tracker response using the 2nd-generation PLUSS antenna pattern*. As shown in Figure 3.3 of [8], the 2' x 2' 2nd-generation PLUSS antenna has a Σ pattern beamwidth of approximately 18° with sidelobes approximately 30 dB below the Σ pattern. In an attempt to simulate the tracker response using the PLUSS antenna pattern, the antenna pattern shown in Figure 2.23 was used. While not identical with the PLUSS pattern, the pattern shown in Figure 2.23 does have a Σ pattern beamwidth of 18° and does have sidelobes 30 dB below the Σ pattern peak. It should also be noted that the points at which the pattern shown in 2.23 intercepts specular scatter are also shown. For example, for a grazing angle of $\psi = 5°$, the specular component will enter the Σ pattern at the -4 dB point and at the peak of the Δ pattern. This is interesting in light of the discussion of Section 2.2 in which the possible effects of specular scatter were addressed.

Figure 2.24 presents V_ε, the error voltage, as a function of θ, the off-boresight angle to the radiosonde. Notice that the antenna pointing angle is 30°, well above the horizon. The impact of choosing a large pointing angle is two-fold. First, because the pointing is large, no specular or diffuse scatter will enter the antenna through the main beam of either the Σ or Δ pattern; all scatter must enter through the -30 dB sidelobes. Second, the high pointing angle causes the length of the first Fresnel zone to be rather small. In this instance, the length of the first zone is 2.77 meters, centered 3.73 meters from the sub-antenna point. This has the effect of reducing the amount of diffuse scatter entering the antenna. Based on these two facts we should expect that the effects of soil moisture and surface roughness will be minimal. Studying Figure 2.24 indicates that this is indeed true. Note that V_ε appears very linear from $\theta = -2.5°$ to $\theta = 2.5°$ regardless of soil moisture.

In an attempt to quantify the nonlinearity present in the V_ε versus θ curves, the coefficient of non-determination will be used. To calculate the coefficient of non-determination, k, we must first propose a suitable relationship between V_ε and θ. In this case we will propose that for $-1° \leq \theta \leq 1°$, V_ε will vary linearly with θ. Any non-linearities will result from multipath effects. We can define k as

*See Section 2.3.5 for simulation of 3rd-generation PLUSS antenna.

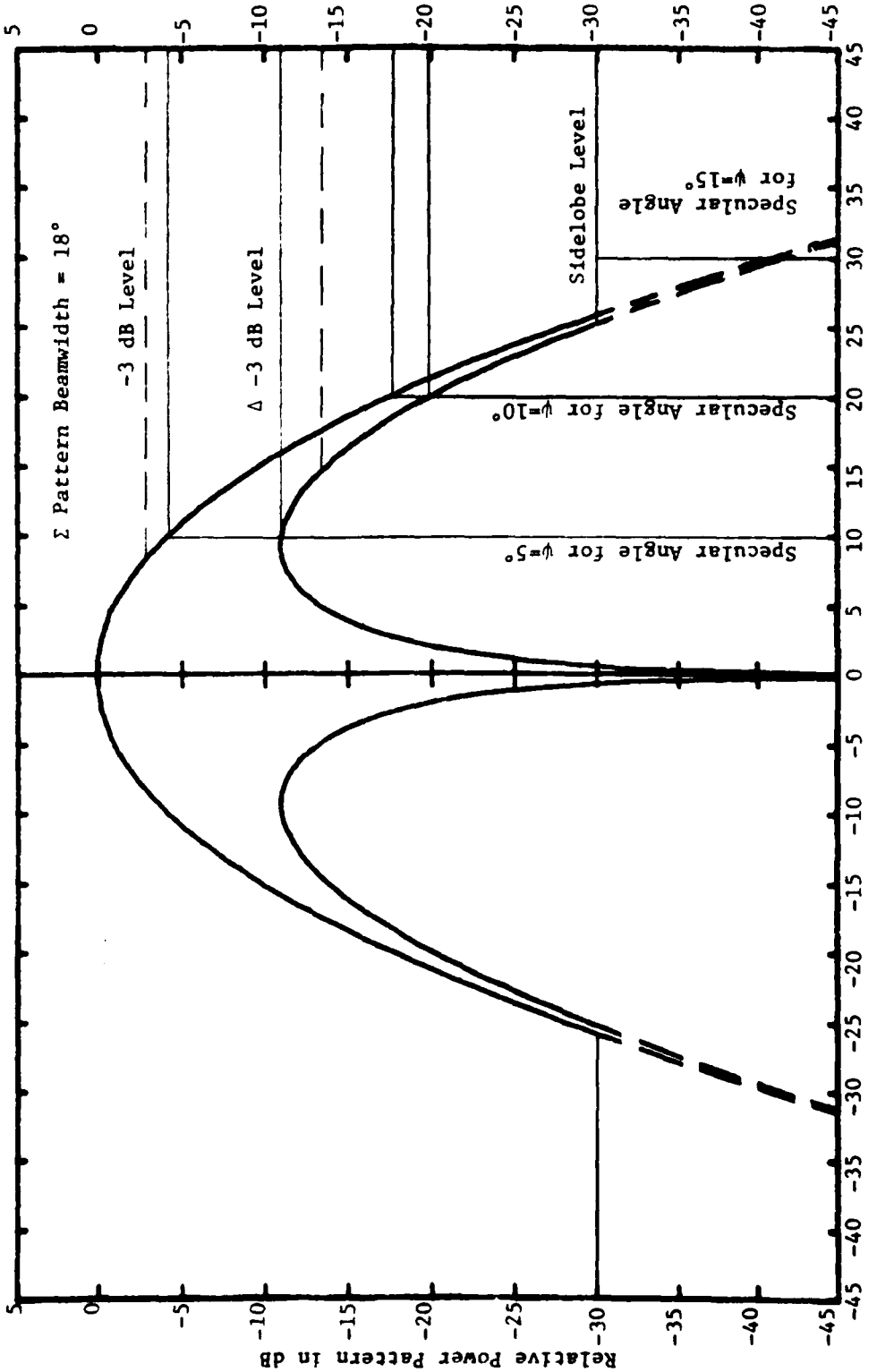

Figure 2.23 Simulated antenna pattern with a Σ beamwidth of 18°

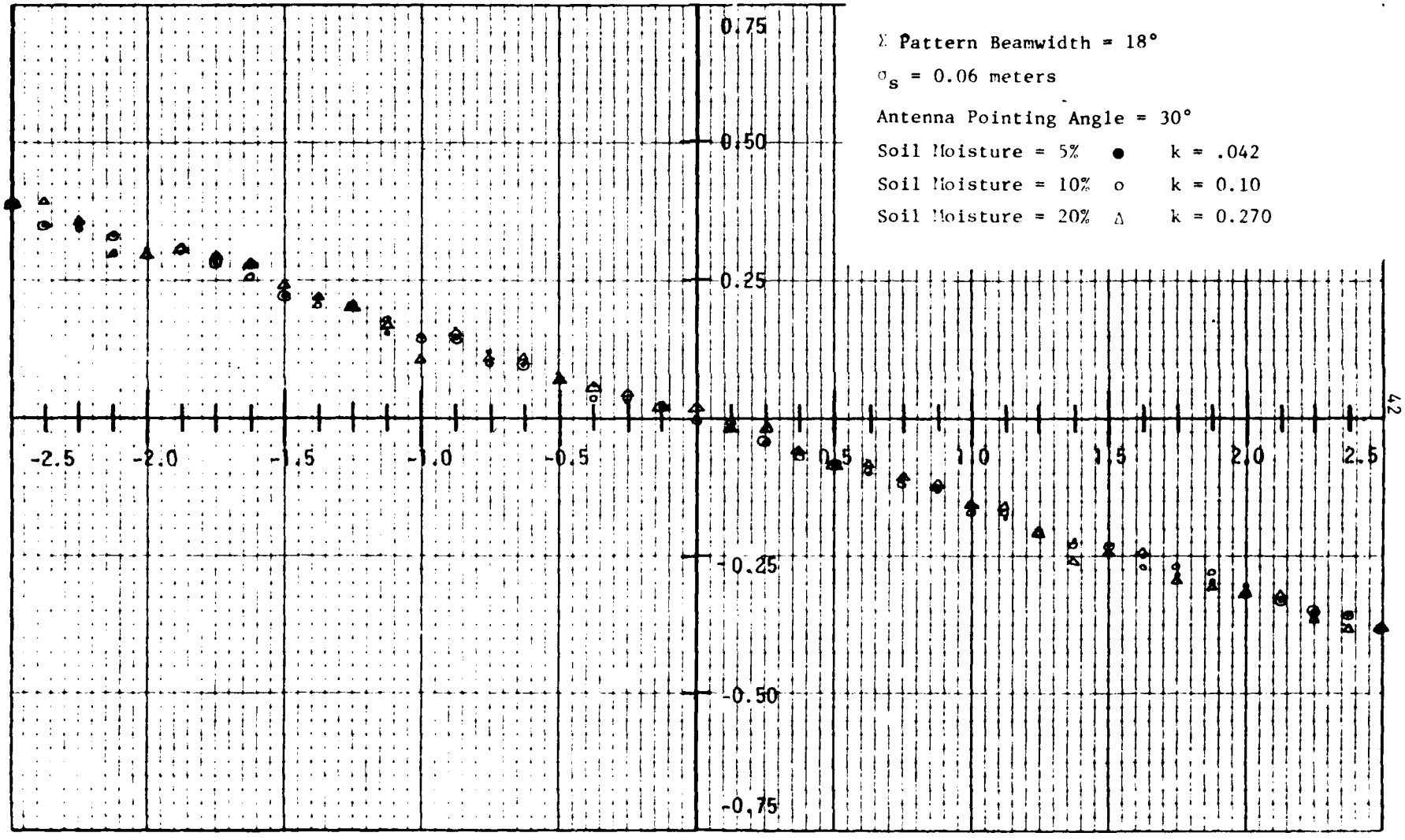

Figure 2.24

V_ϵ as a Function of Off-Boresight Angle for three values of soil moisture

$$k = \sqrt{\frac{\Sigma(V_\varepsilon - \hat{V}_\varepsilon)^2}{\Sigma(V_\varepsilon - \bar{V}_\varepsilon)^2}} \qquad 2.29$$

where

V_ε is the actual value of the error voltage

$\hat{V}_\varepsilon$ is an estimate of V_ε found using a linear regression model

$\bar{V}_\varepsilon$ is the arithmetic mean of V_ε

In all case, $0 \leq k \leq 1$. The interpretation of k is as follows. A value of $k = 1$ implies no relationship between V_ε and θ. As k tends toward $k = 0$, the linear relationship becomes more pronounced so that for $k = 0$, V_ε varies linearly with θ. In other words, k is a measure of the variation of V_ε about the linear regression line. In this case, the variance about the regression lines must be caused by signal multipath. Note that in Figure 2.24, the k values tend toward zero although the fact that k increases with soil moisture indicates that even with a 30° boresight angle, surface effects are noticeable.

Figure 2.25 presents V_ε versus θ for three values of soil moisture with σ_s, the surface standard deviation, held constant at $\sigma_s = 0.16$ meters. Note that for all three values of soil moisture, the k values are very small, particularly when compared to those shown in Figure 2.24. It is suggested that the large value of σ_s causes the multipath signals to be of a more incoherent nature so that the phasor sum of these signals tends toward zero. Figure 2.26 seems to support this conjecture. Note that for $\sigma_s = 0.16$ meters, $k = 0.070$ whereas $k = 0.100$ for $\sigma_s = 0.06$ meters.

Figure 2.27 presents V_ε versus θ for an antenna pointing angle of 15°. Note that again soil moisture has a large effect on V_ε with $k = 0.560$ for a soil moisture content of 5%. As soil moisture increases, however, k tends to become smaller. Again it may be that for a relatively smooth surface, ($\sigma_s = 0.06$ meters) specular scatter may dominate at lower moisture values whereas increasing soil moisture may cause incoherent scatter to dominate.

Figure 2.28 depicts V_ε versus θ for $\sigma_s = 0.06$ and $\sigma_s = 0.16$ meters with soil moisture fixed at 10%. The antenna pointing angle is 15°. Note that varying

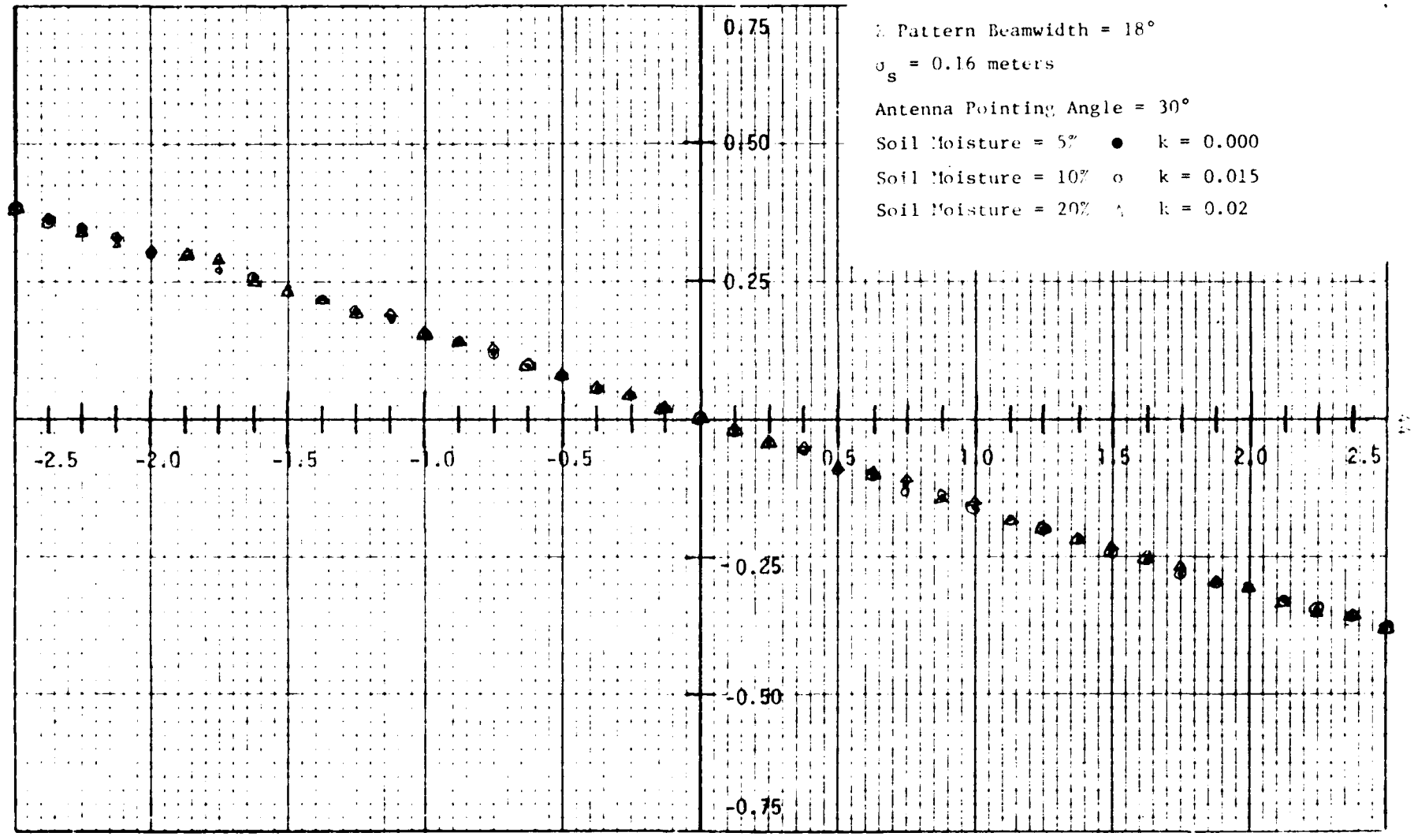

Figure 2.25
V_ε as a function of off boresight angle for three values of soil moisture.

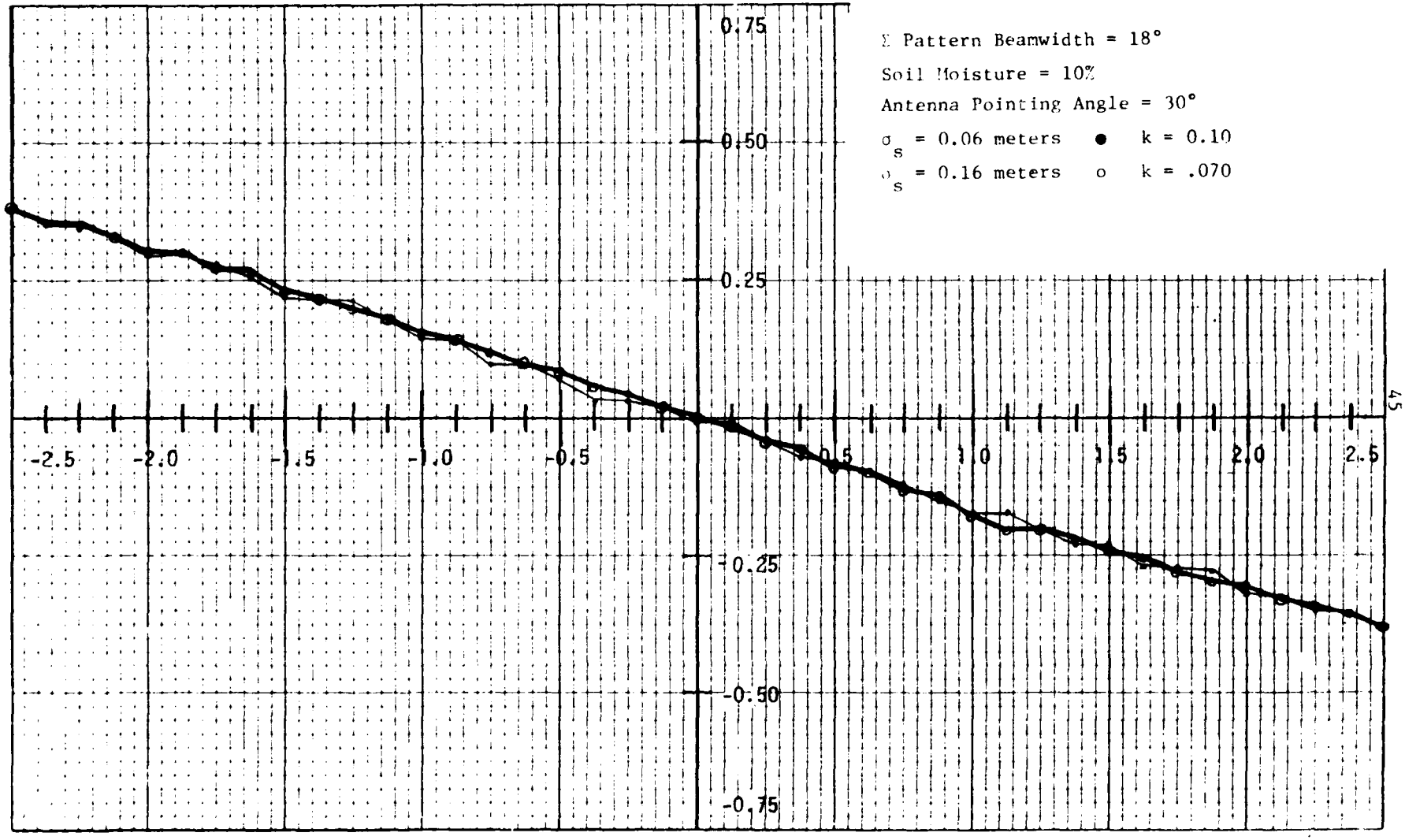

Figure 2.26

V_ε as a function of off-boresight angle for two values of surface roughness standard deviation.

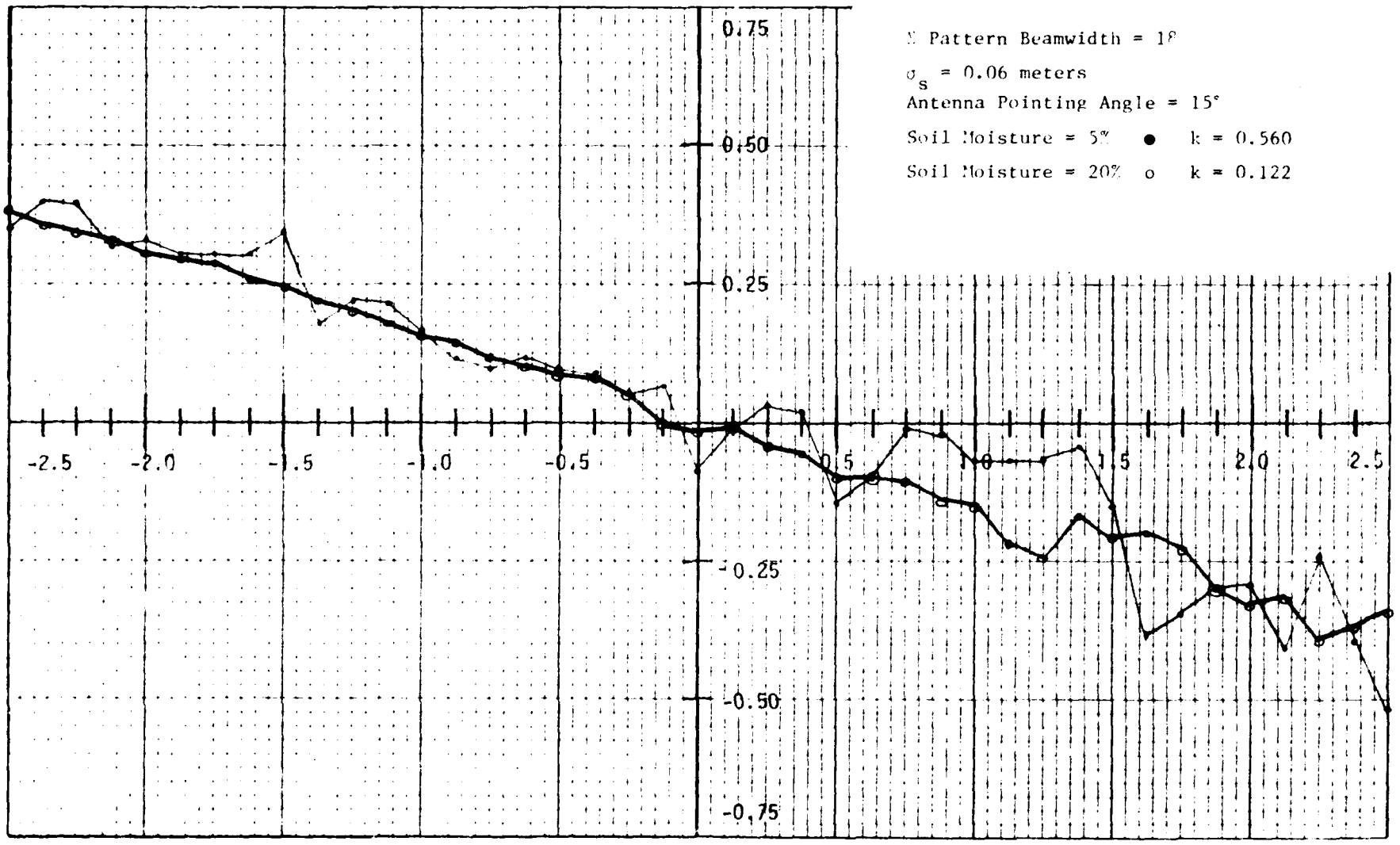

Figure 2.27
V_ε as a function of off-boresight angle for two values of soil moisture

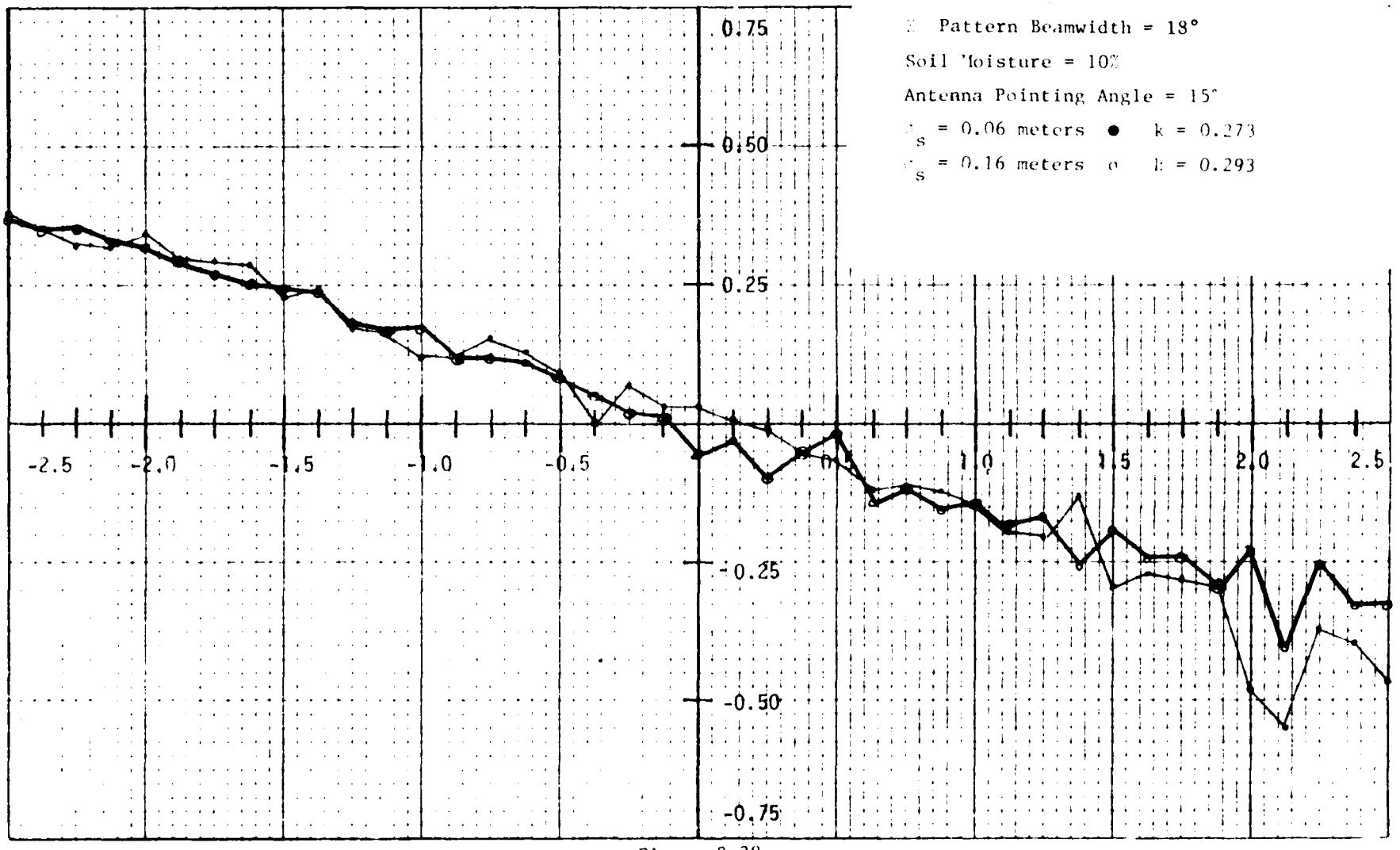

Figure 2.28

V_v as a function of off-boresight angle for two values of surface roughness standard deviation.

σ_s has little effect on V_ε. Decreasing the antenna pointing angle to either 10° or 5° caused V_ε to fluctuate an extreme amount as θ was varied. For example, for an antenna pointing angle of 5°, σ_s= 0.12 meters and a soil moisture content of 10%, the average value of V_ε over a range of $-2.5° \leq \theta \leq 2.5°$ was -16.0.

In an attempt to reduce forward scatter effects at lower grazing angles, V_ε versus θ curves were simulated using the antenna patterns shown in Figures 2.29 and 2.30. Note that the pattern shown in Figure 2.30 has been shaped on the side nearest the ground. By doing this it is hoped to further reduce multipath effects resulting from forward scatter entering the antenna pattern for off-boresight angles less than zero degrees.

Figure 2.31 shows the effect of decreasing the antenna pattern beamwidth to 8° (no pattern shaping). For the antenna pointing angle of 30° both V_ε curves are nearly perfectly linear functions of θ. However, reducing the antenna pointing angle to 15° (vide Figure 2.32) again results in non-linearities in the V_ε versus θ curve. By employing the shaped beam of Figure 2.30, some improvement is gained in V_ε versus θ linearity for the 20% soil moisture curve as shown in Figure 2.33. Note that k = 0.042 whereas k = 0.104 for the unshaped beam for the 20% soil moisture case. In both cases the sidelobe levels were -30 dB. Figure 2.34 depicts the effect of varying σ_s for a fixed soil moisture content. Note that the linearity in the $-1° \leq \theta \leq 1°$ is quite good, particularly when compared with that shown in Figure 2.28 which was generated with an 18° beamwidth antenna pattern.

Figures 2.35 and 2.36 show the result of decreasing the antenna pointing angle to 10° using the 8° unshaped and 8° shaped beams respectively. Note that the V_ε versus θ linearity becomes rather poor regardless of beam shape. This is particularly true for the 5% soil moisture cases. Referring to Figure 2.29 and 2.30 we can see that for an antenna pointing angle of 10°, neither the sum nor difference patterns illuminates the soil surface above the -3 dB point of the individual patterns. In fact, for an antenna pointing angle of 10°, the specular scatter enters the patterns through the -30 dB sidelobes. Figure 2.37 again indicates the nonlinearities present in the V_ε versus θ curves for an antenna pointing angle of 10°. Note that the k values are very close to one another regardless of σ_s.

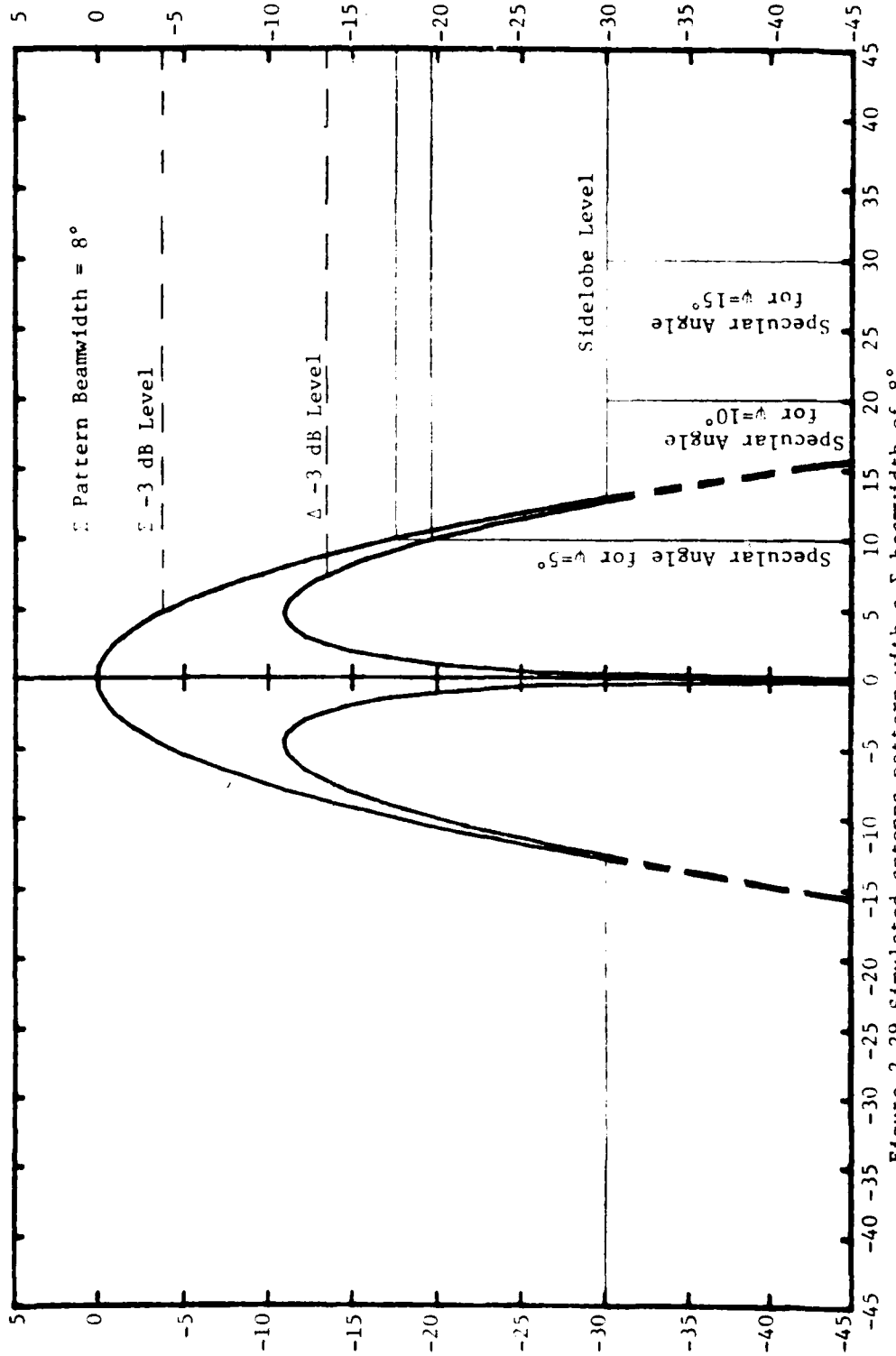

Figure 2.29 Simulated antenna pattern with a Σ beamwidth of 8°

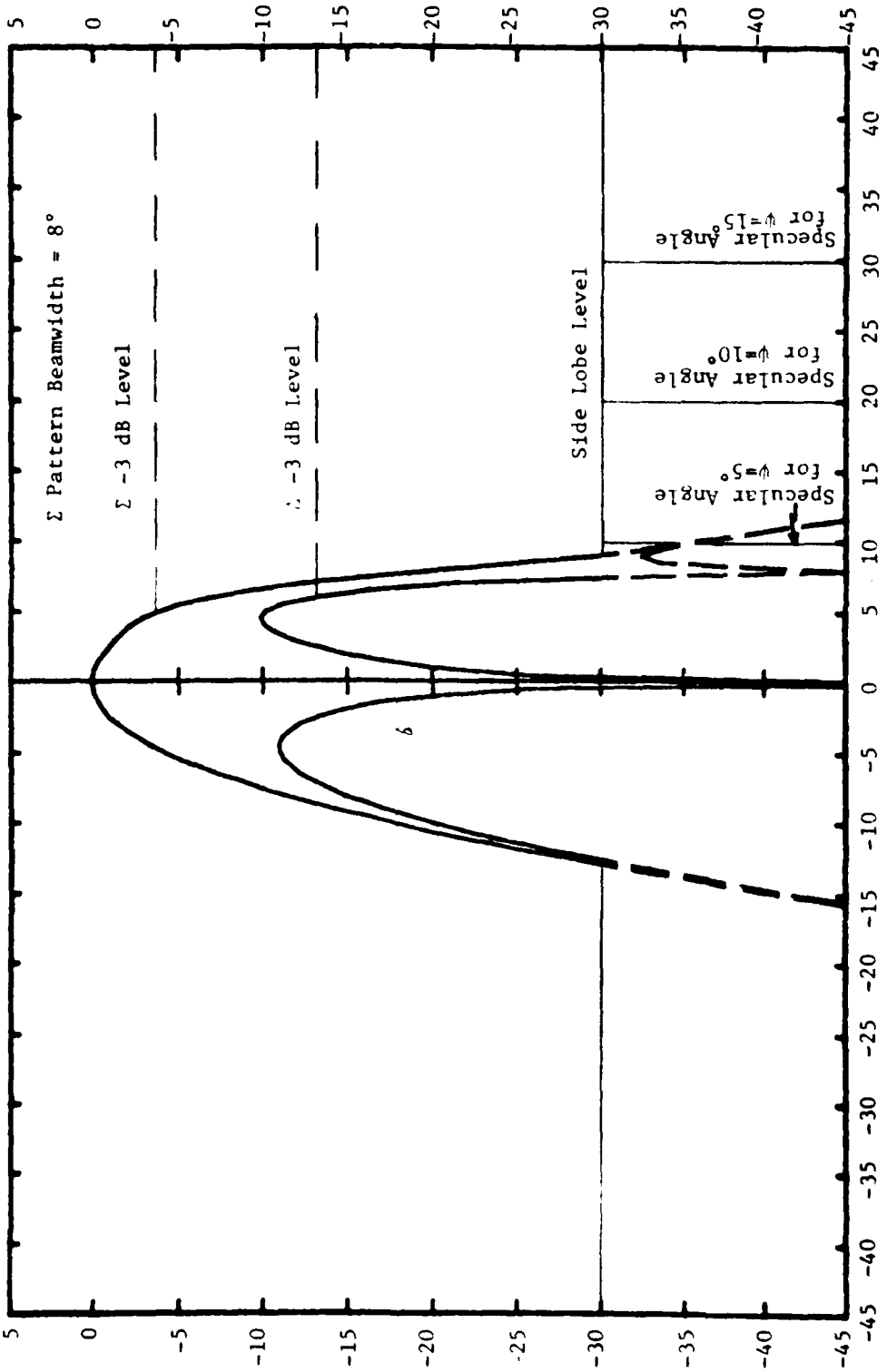

Figure 2.30
Simulated antenna pattern with a Σ beamwidth of 8°.
Note that this pattern is shaped to reduce forward scatter effects.

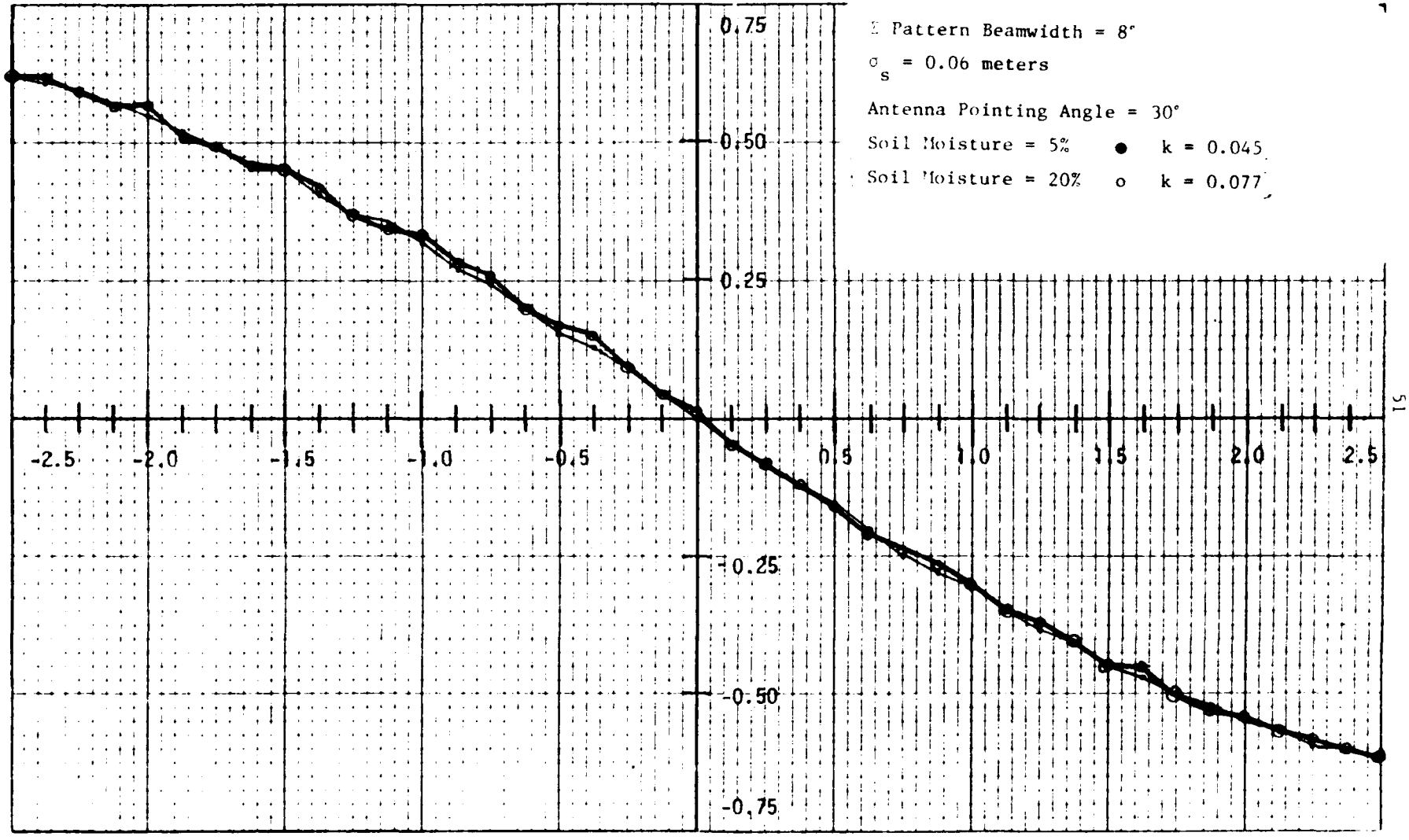

Figure 2.31
V_ε as a function of off-beamwidth angle for two values of soil moisture

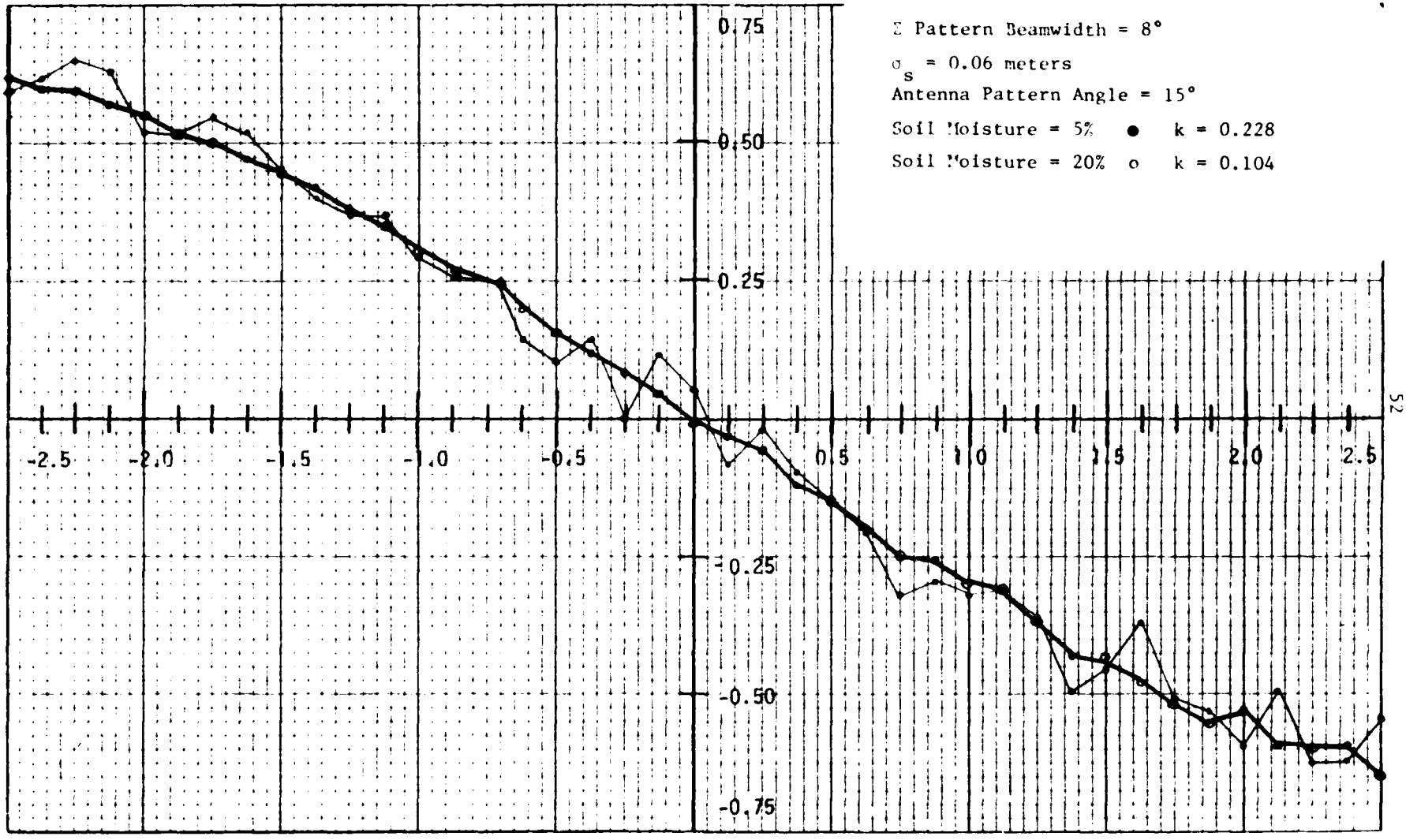

Figure 2.32

V_ε as a function of off-boresight angle for to values of soil moisture.

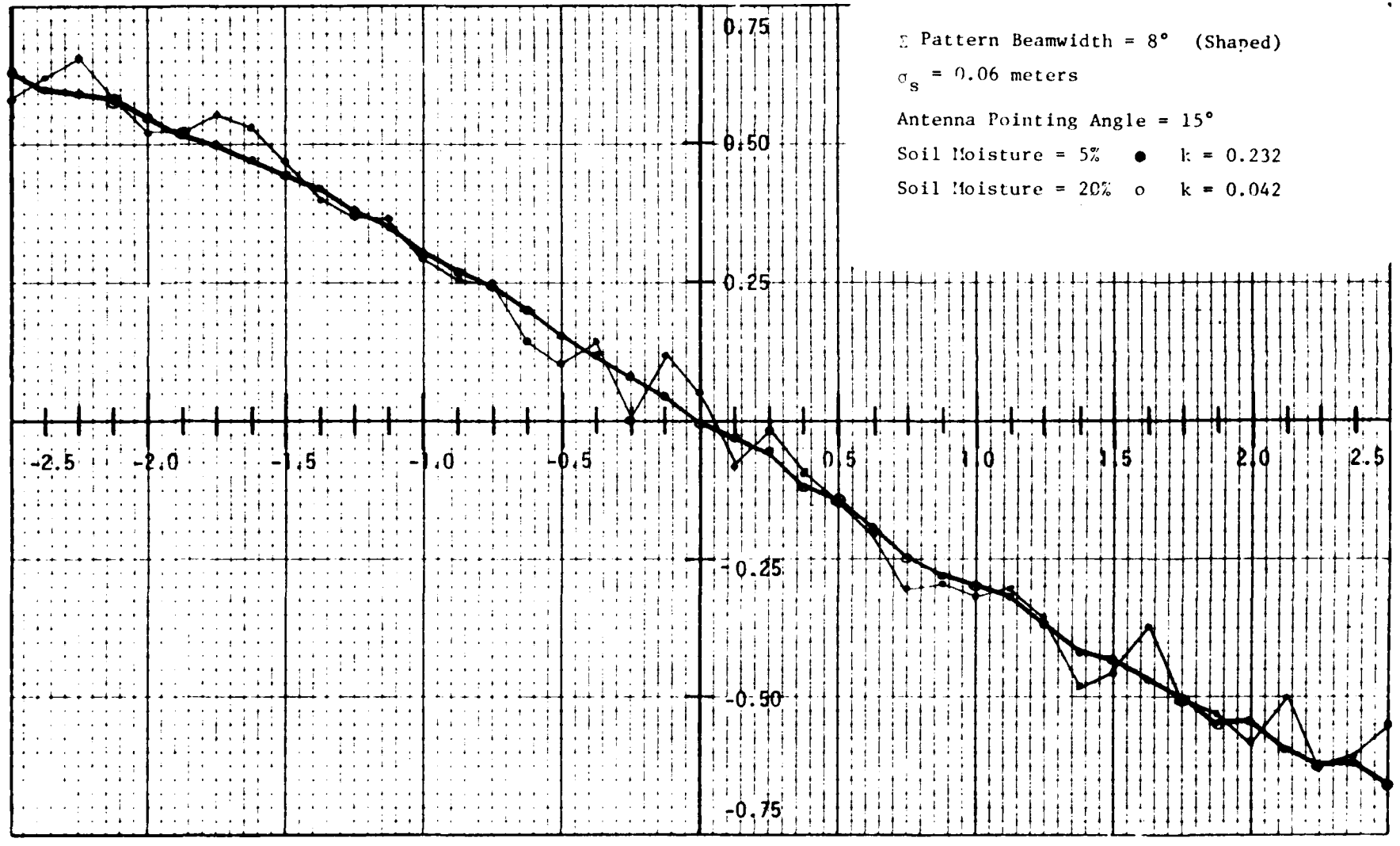

Figure 2.33

V_ε as a function of off-boresight angle for two values of soil moisture.

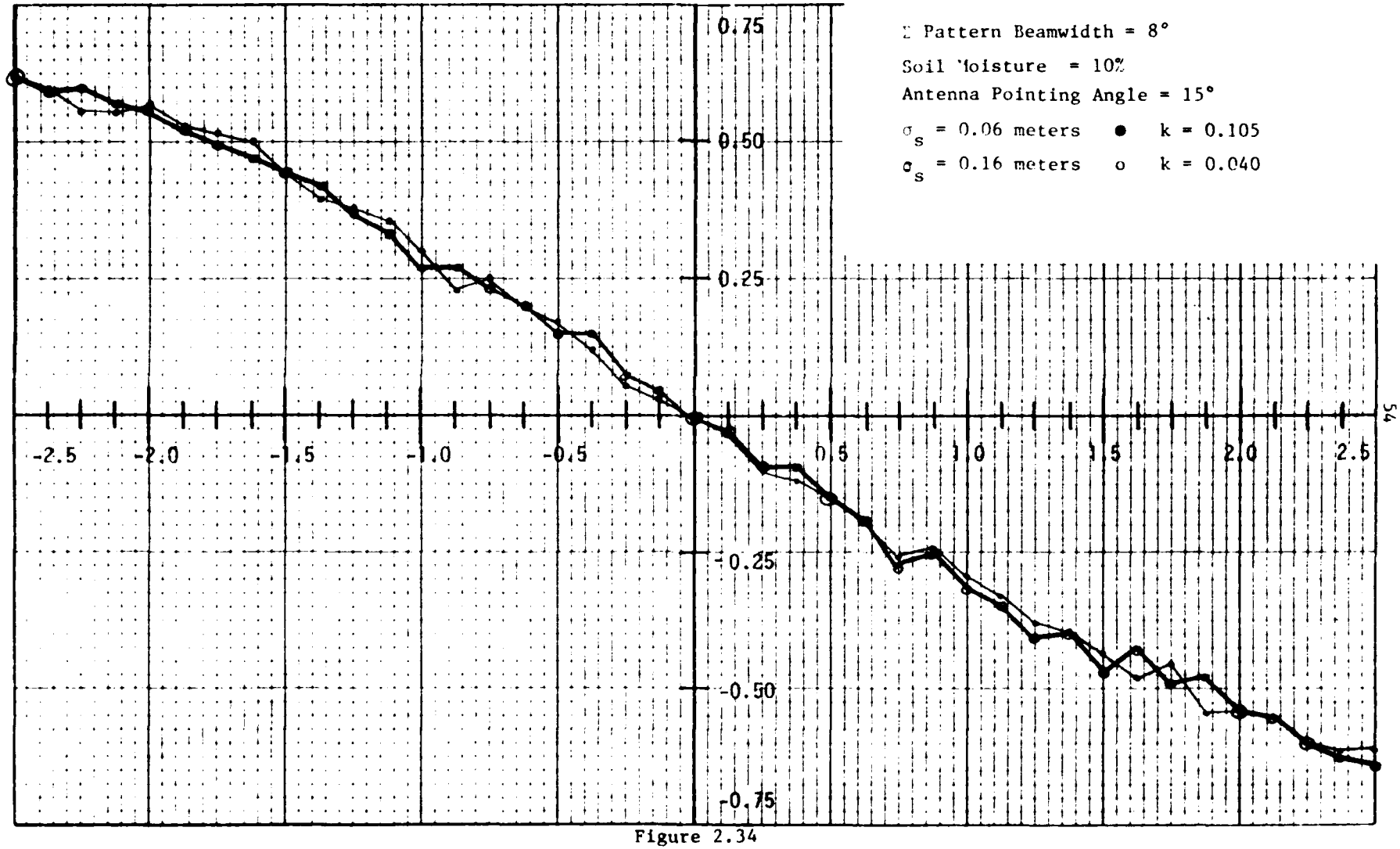

Figure 2.34

V_ε as a function of off-boresight angle for two values of surface roughness standard deviations.

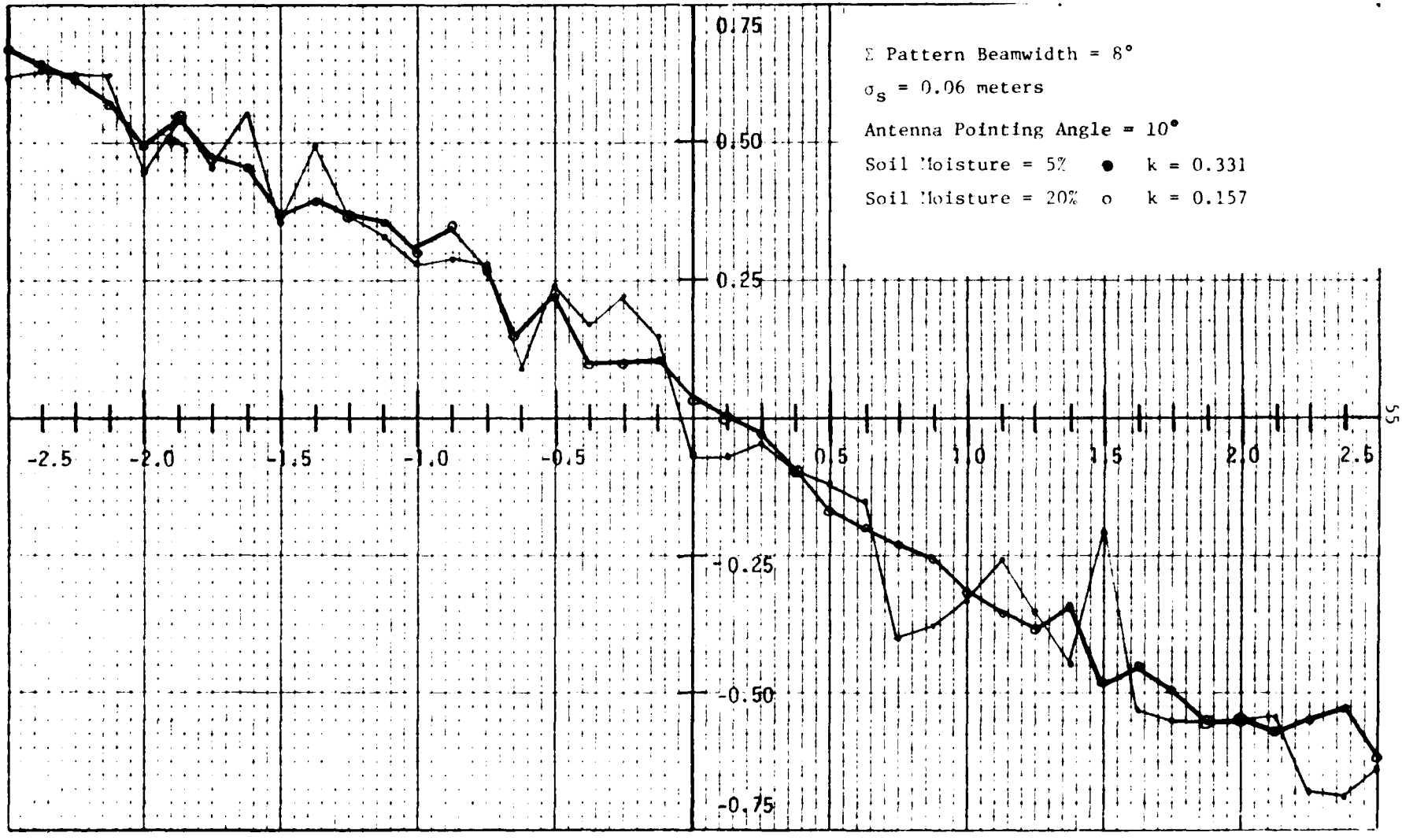

Figure 2.35
V_ε as a function of off-boresight angle for two values of soil moisture.

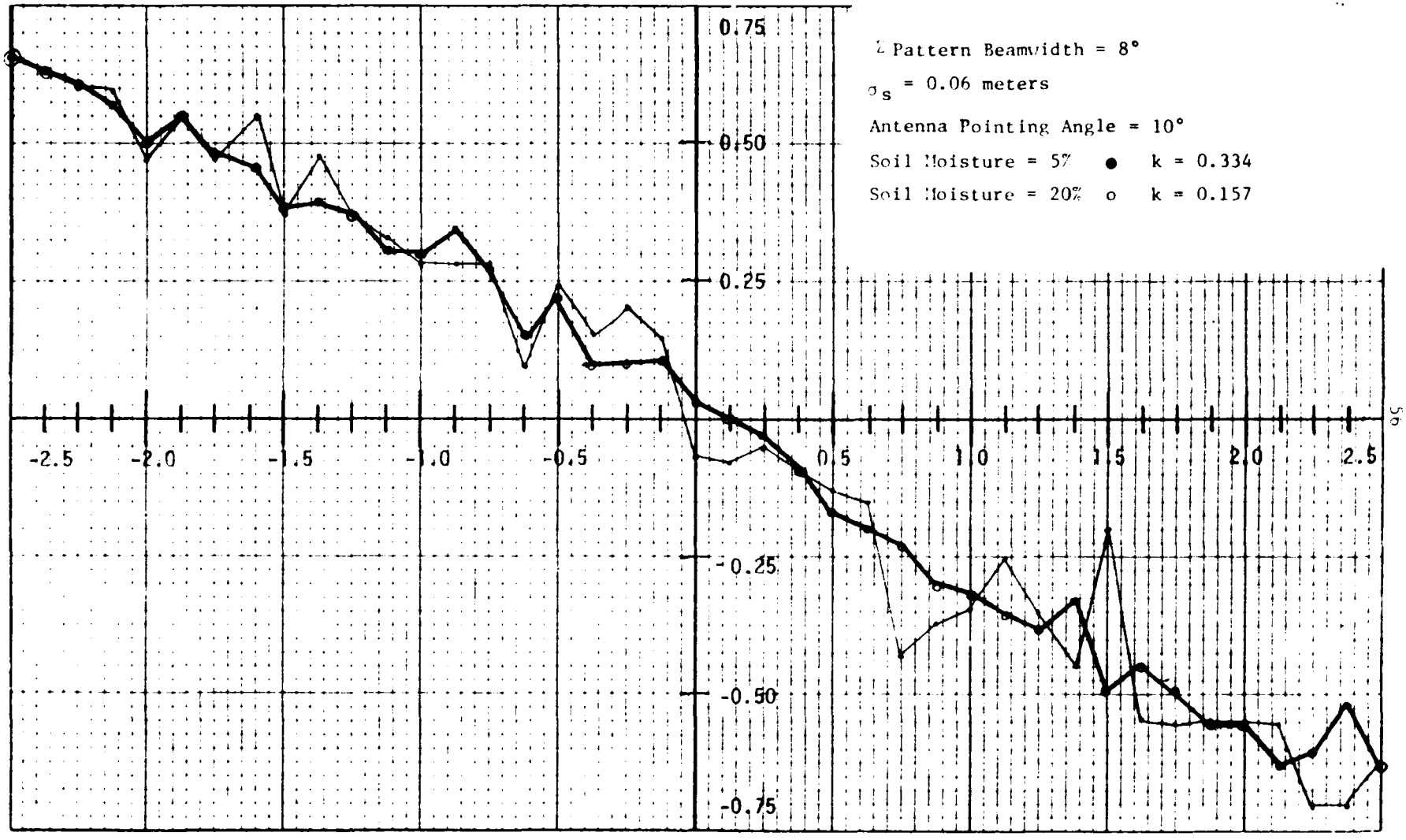

Figure 2.36
V_ϵ as a function of off-boresight angle for two values of soil moisture.

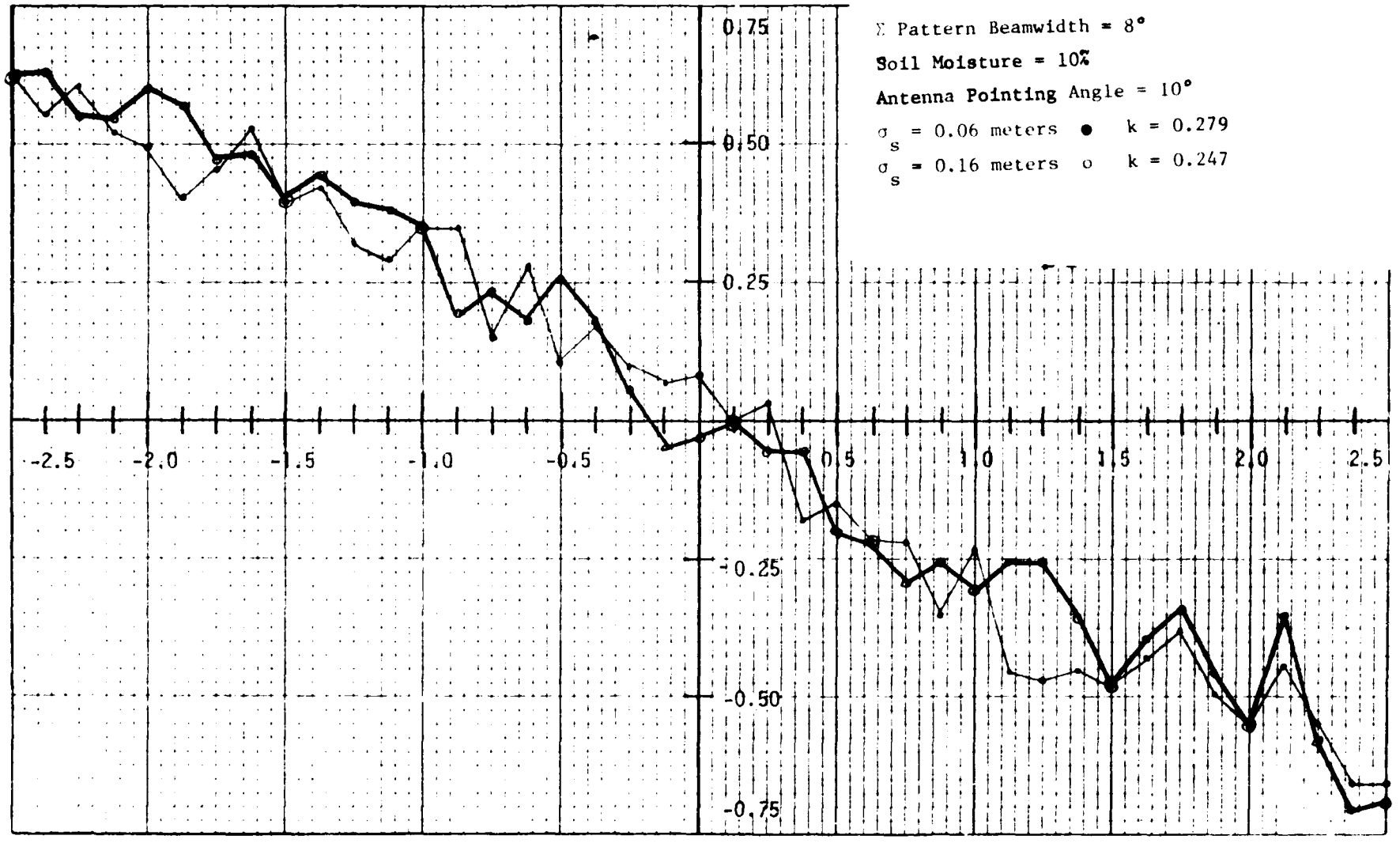

Figure 2.37

V_ε as a function of off-boresight angle for two values of surface roughness standard deviations.

While the above discussion indicates that a good percentage of the forward scatter enters the antenna through the sidelobes, it is obvious that some must also enter through the main beams of the antenna. If only specular scatter was considered this would not be true. However, because the rough surface scatters energy in many directions, we must consider the diffuse energy entering the antenna through paths other than the sidelobes.

In an attempt to reduce the amount of forward scatter entering the tracking antenna through the main beam, the antenna shape shown in Figure 2.38 was employed in the simulation. Note that even for an antenna pointing angle of 5°, the specular scatter enters the system through the sidelobes. Obviously this is also true for grazing angles greater than 5°.

The fact that diffuse scatter entering the pattern through the main beam is borne out by comparing Figures 2.35 (8° beamwidth) and 2.39 (5° beamwidth). Note the reduction in the k values which occur when a 5° rather than an 8° beamwidth is employed. This is also shown in Figures 2.37 and 2.40 which shows the advantage of the narrower beamwidth.

Figure 2.41 displays V_s versus θ for both -30 dB and -40 dB sidelobe levels. Notice that even at a pointing angle of 10°, a 10 dB reduction in sidelobe level results in k being reduced by a factor of 2. If, as shown in Figure 2.42, the sidelobes are further reduced to -50 dB, k is again halved.

Figures 2.43 through 2.46 depict V_s versus θ curves for various values of soil moisture and surface roughness. Each curve was generated with an antenna pointing angle of 5° and sidelobe levels of -40 dB. Note that while the values of k are not as good as those generated at an antenna pointing angle of 10°, using -40 dB sidelobes, they do compare favorably with the k values generated using -30 dB sidelobes at a 10° pointing angle. Moreover, all k values were generated using data between $\theta = -1°$ and $\theta = +1°$. Note that if we concern ourselves with the data between $\theta = -0.5°$ and $\theta = +0.5°$, the 5° data (Figures 2.43 through 2.46) shows good linearity.

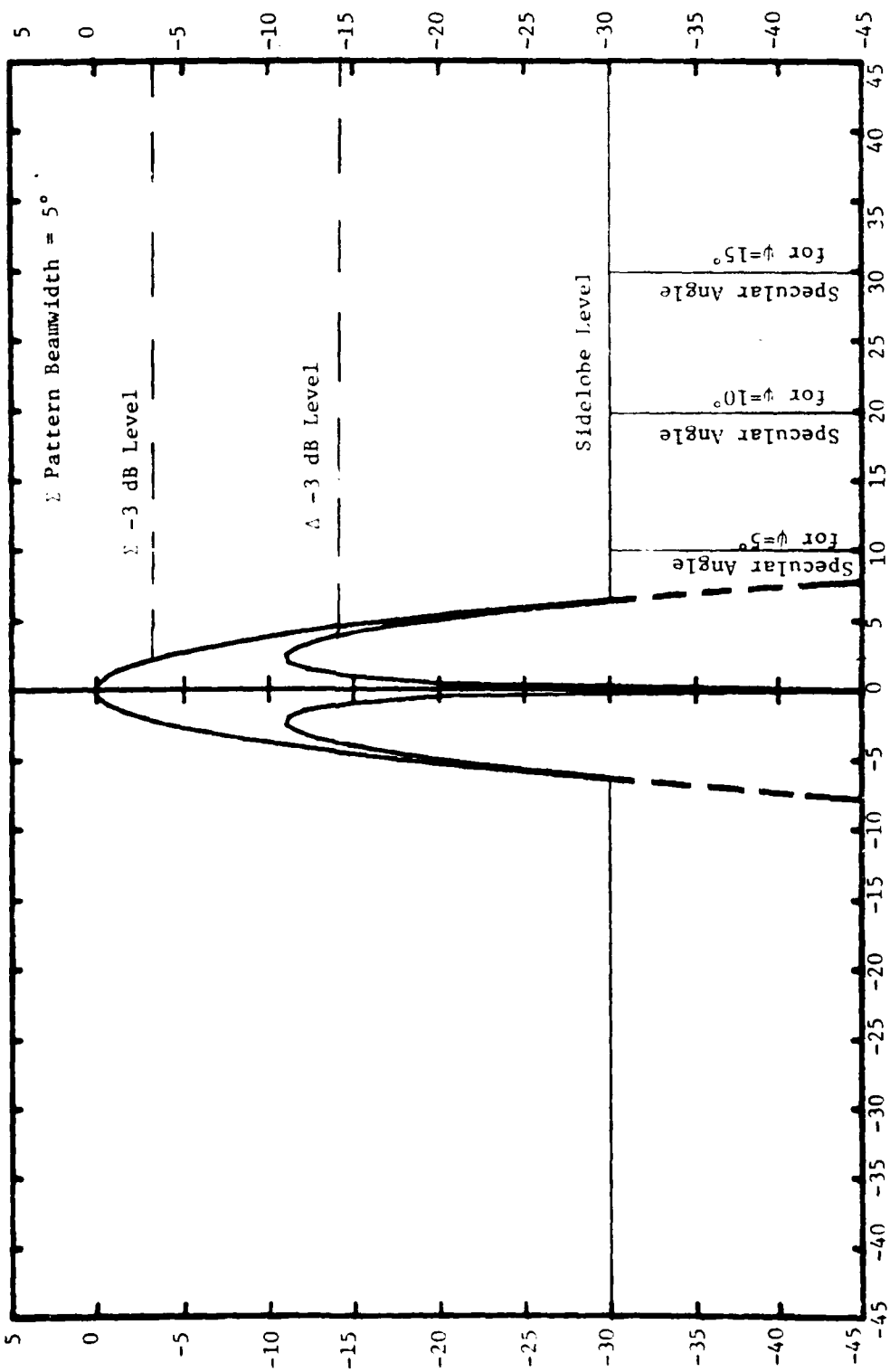

Figure 2.38
Simulated antenna pattern with a Σ beamwidth of 5°.

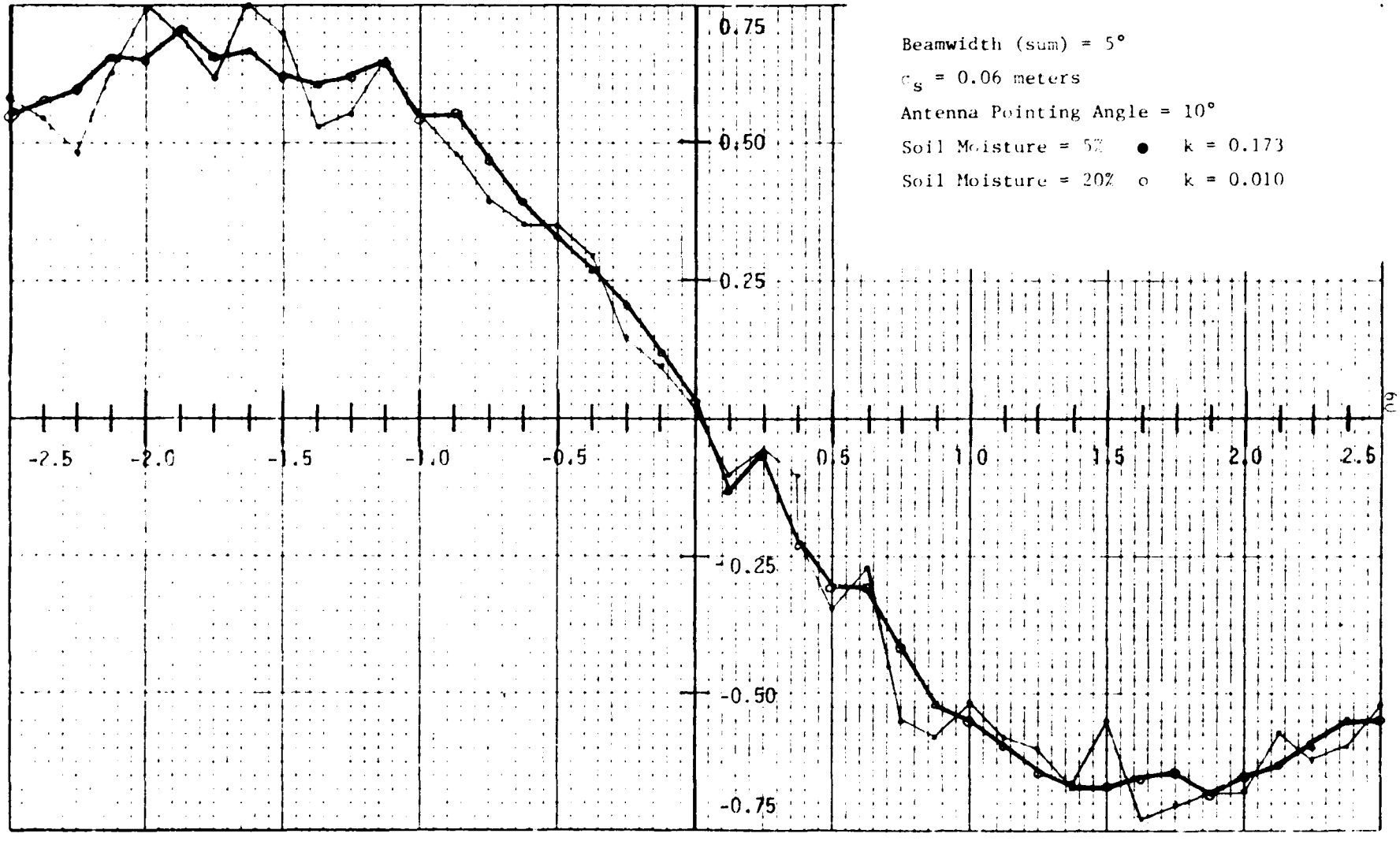

Figure 2.39
V_c as a function of off-boresight angle for two values of soil moisture.

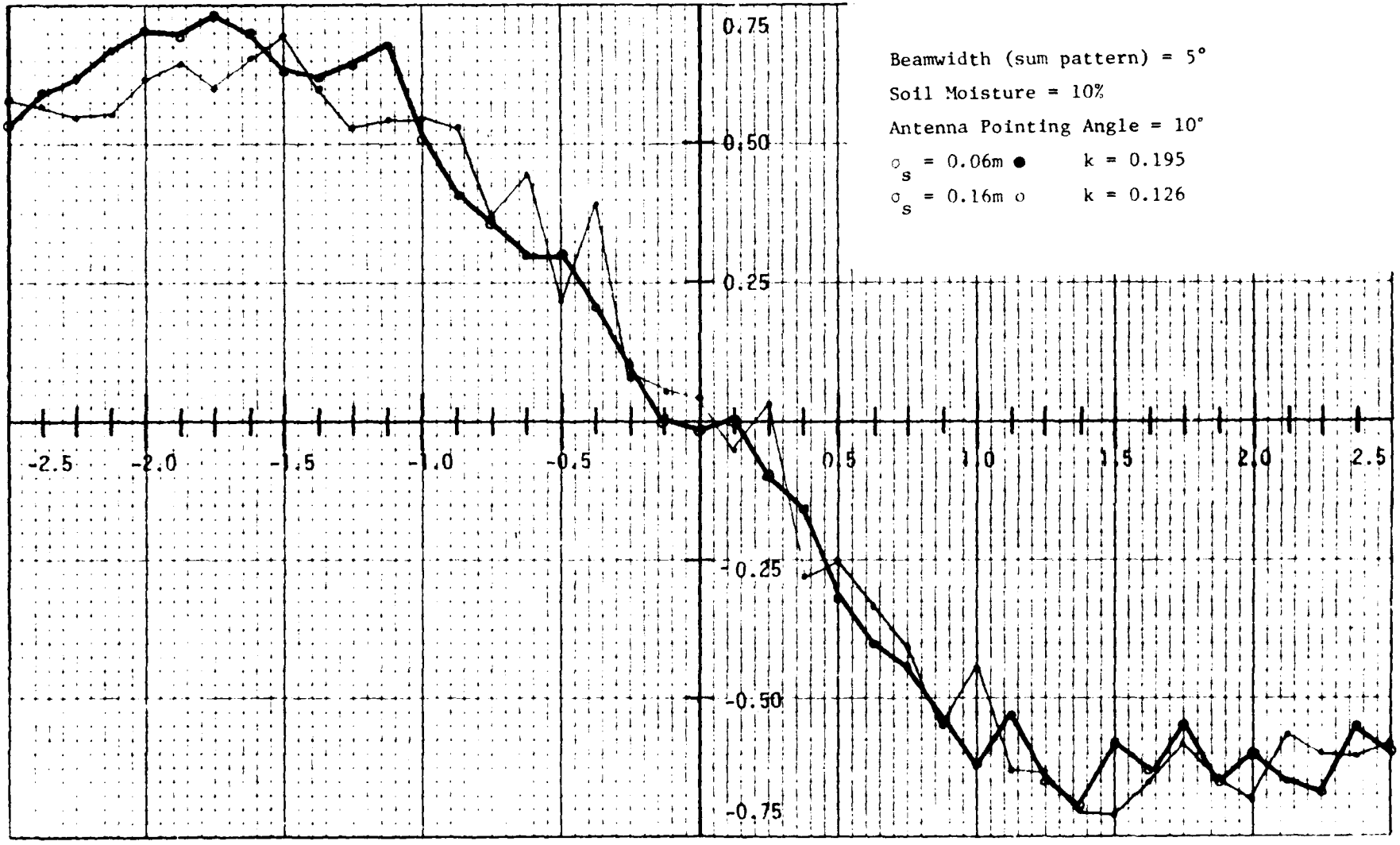

Figure 2.40

V_ε as a function of off-boresight angle for two values of surface roughness standard deviations.

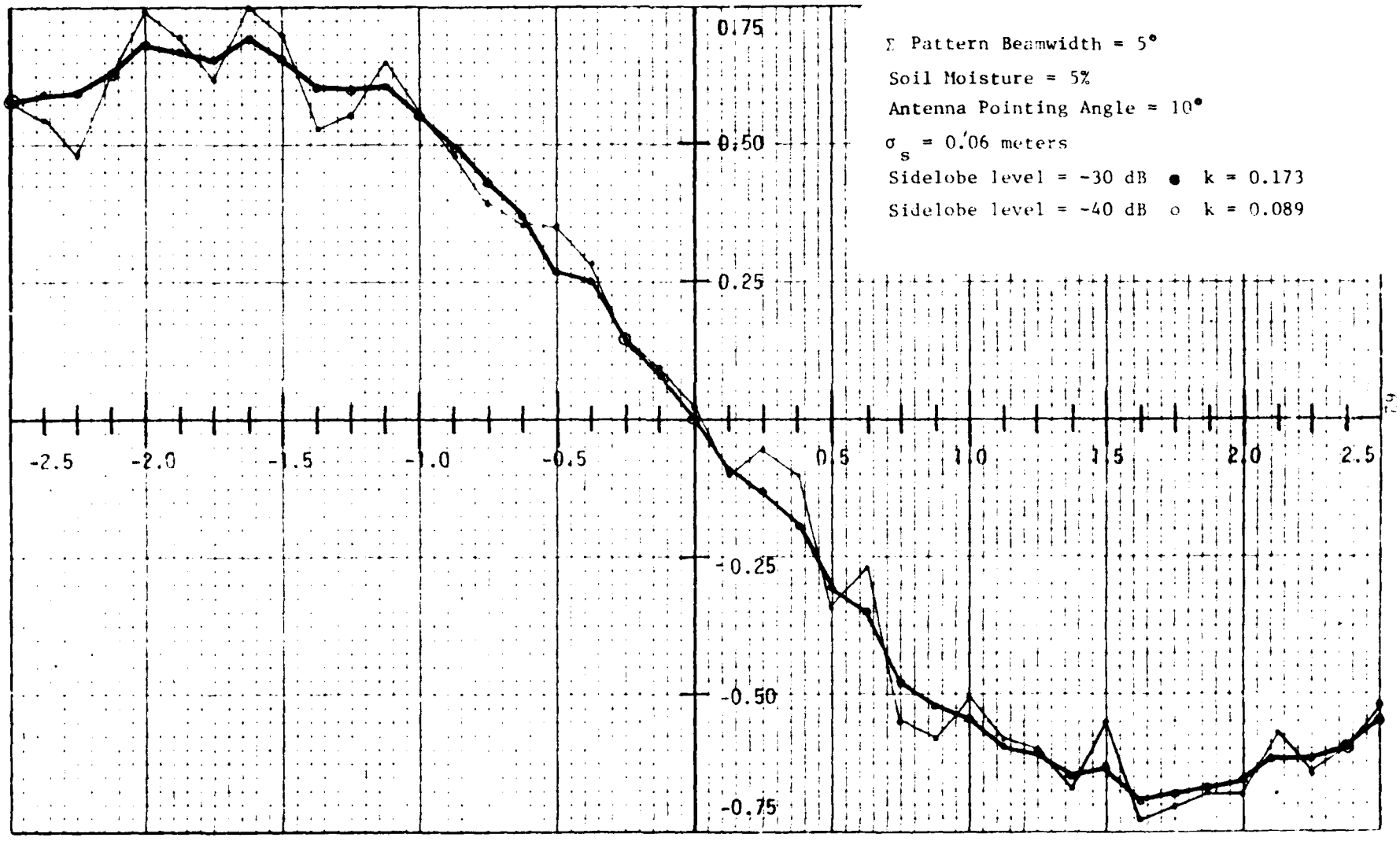

Figure 2.41
V_ε as a function of off-boresight angle for two values of sidelobe levels.

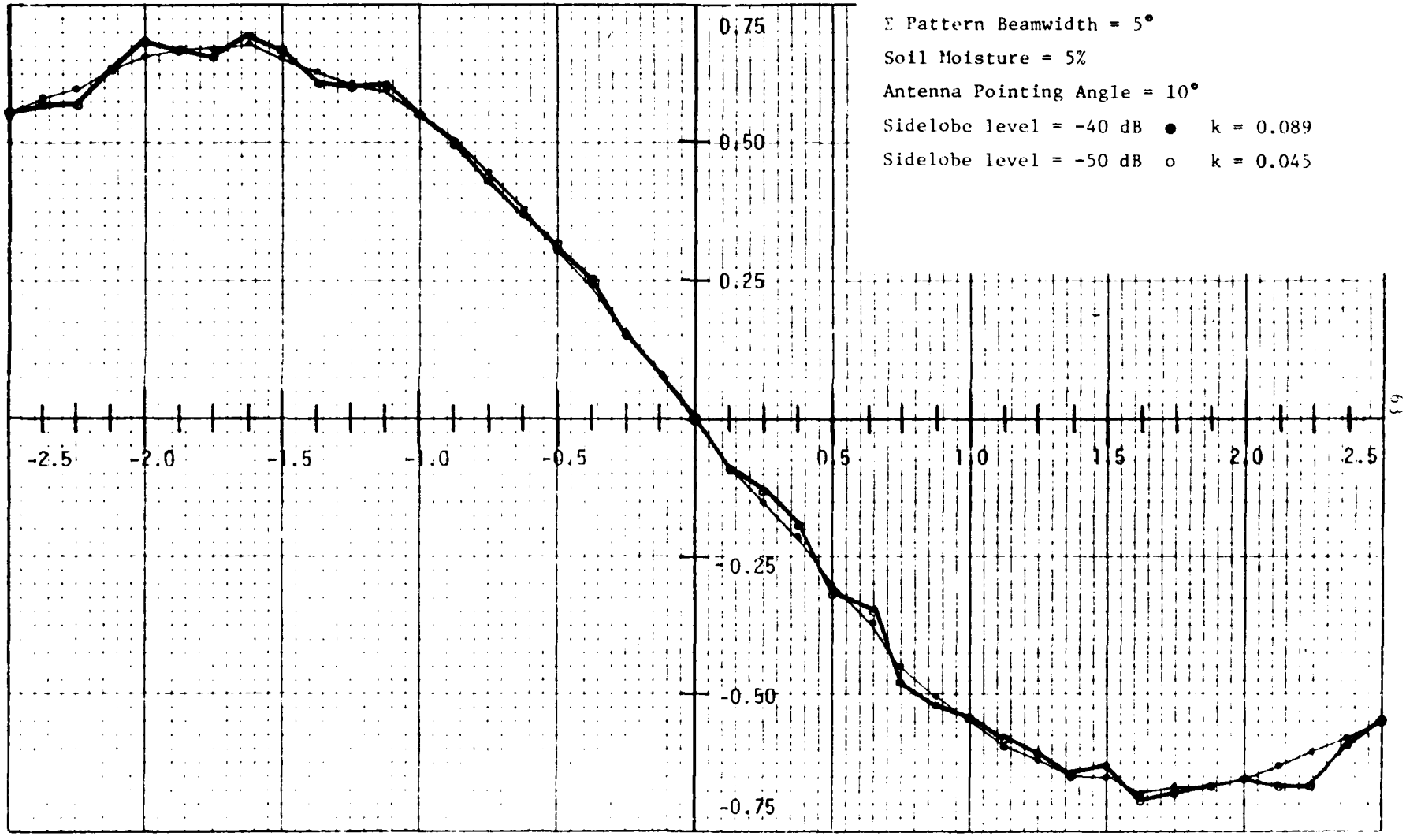

Figure 2.42

V_ε as a function of off-boresight angle for two values of sidelobe levels.

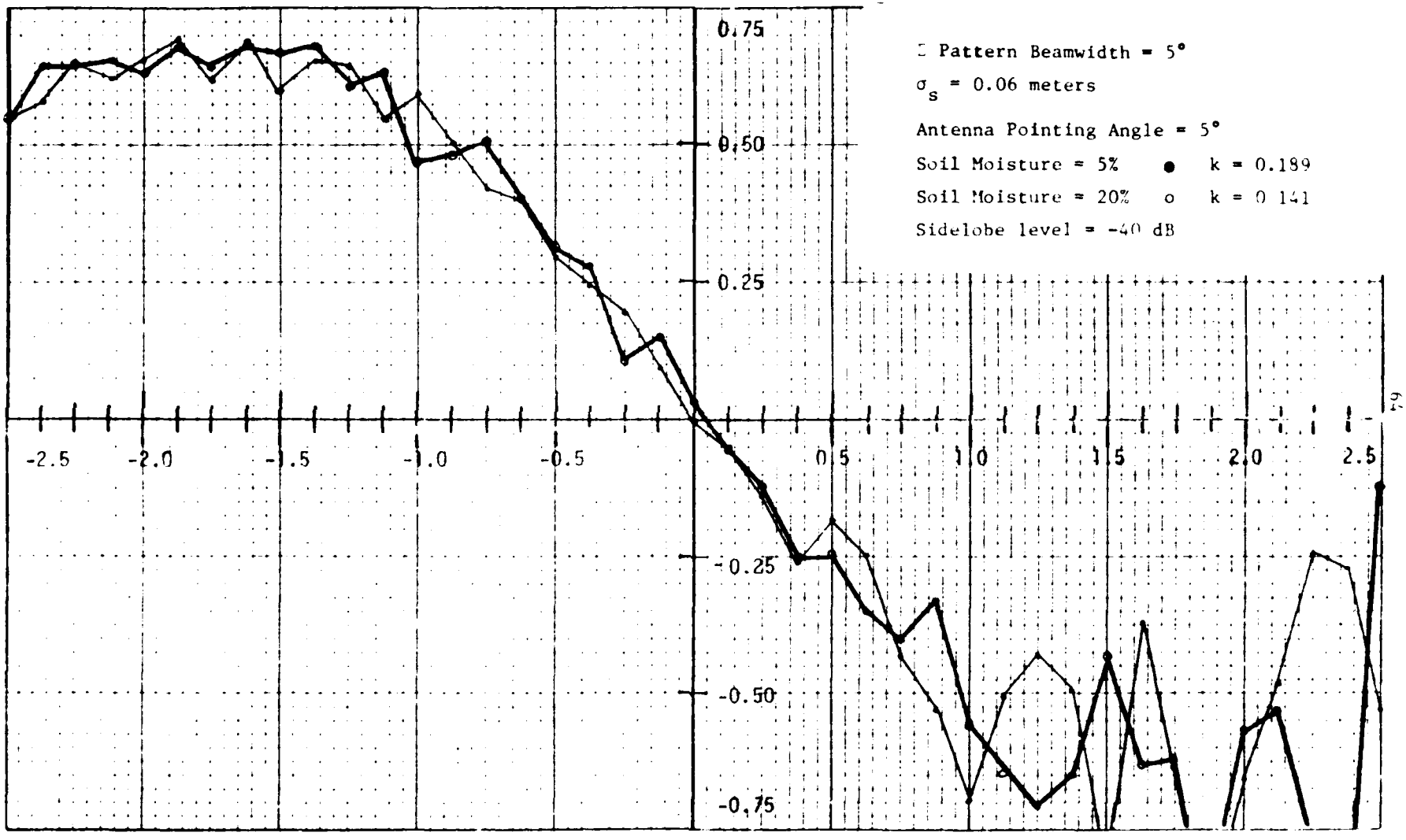

Figure 2.43
V_ϵ as a function of off-boresight angle for two values of soil moisture.

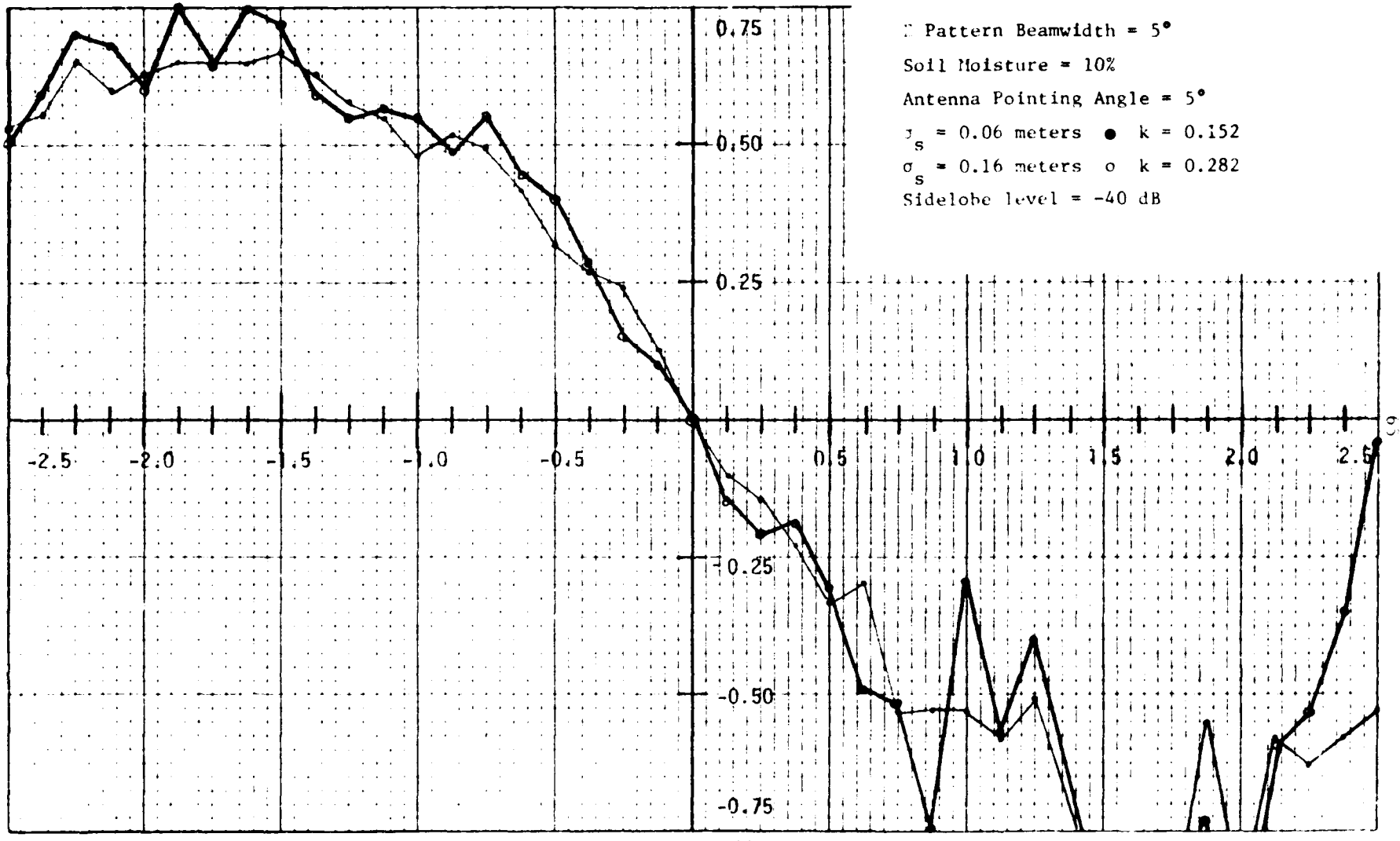

Figure 2.44

V_ε as a function of off-boresight angle for two values of surface roughness standard deviation

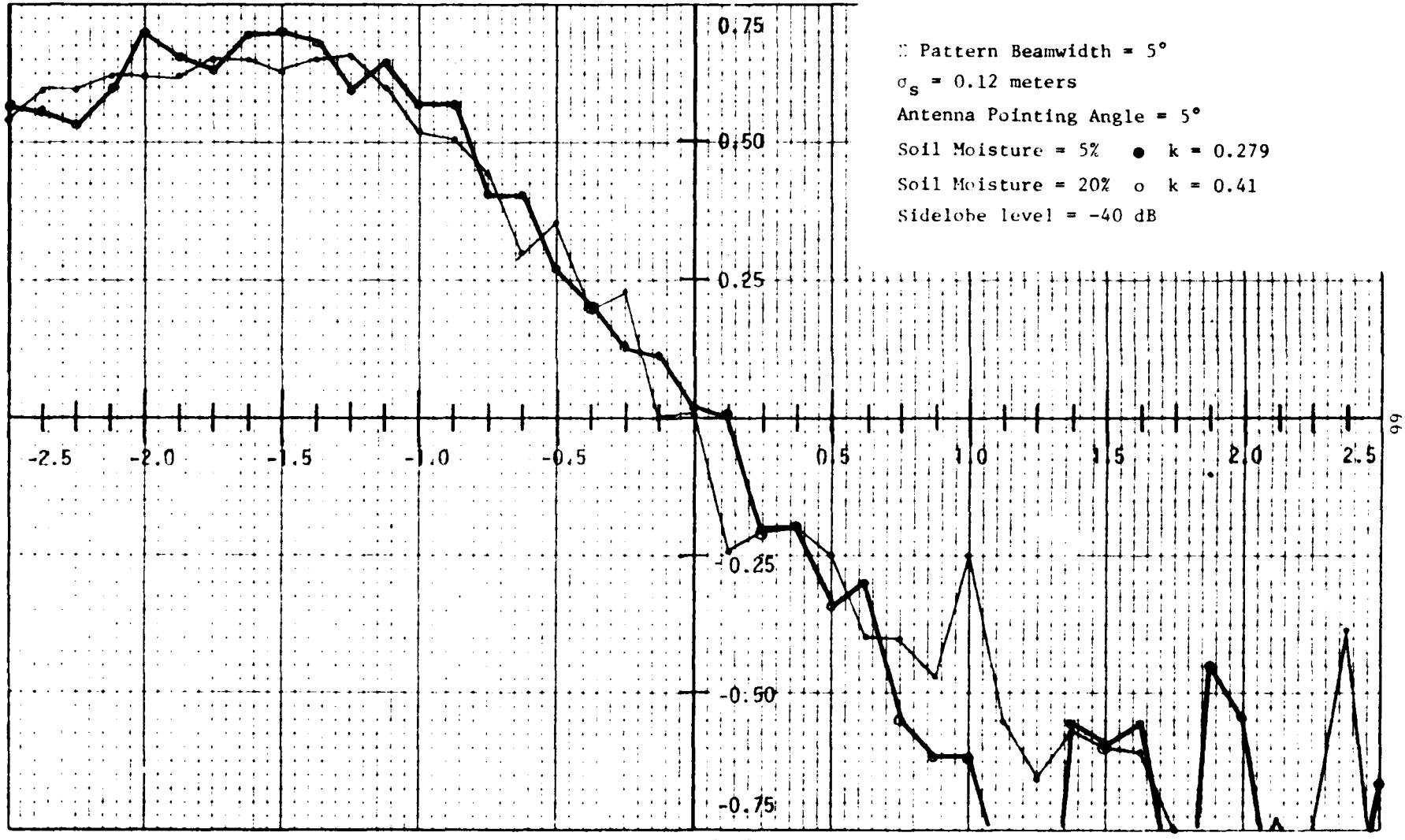

Figure 2.45
V_ε as a function of off-boresight angle for two values of soil moisture.

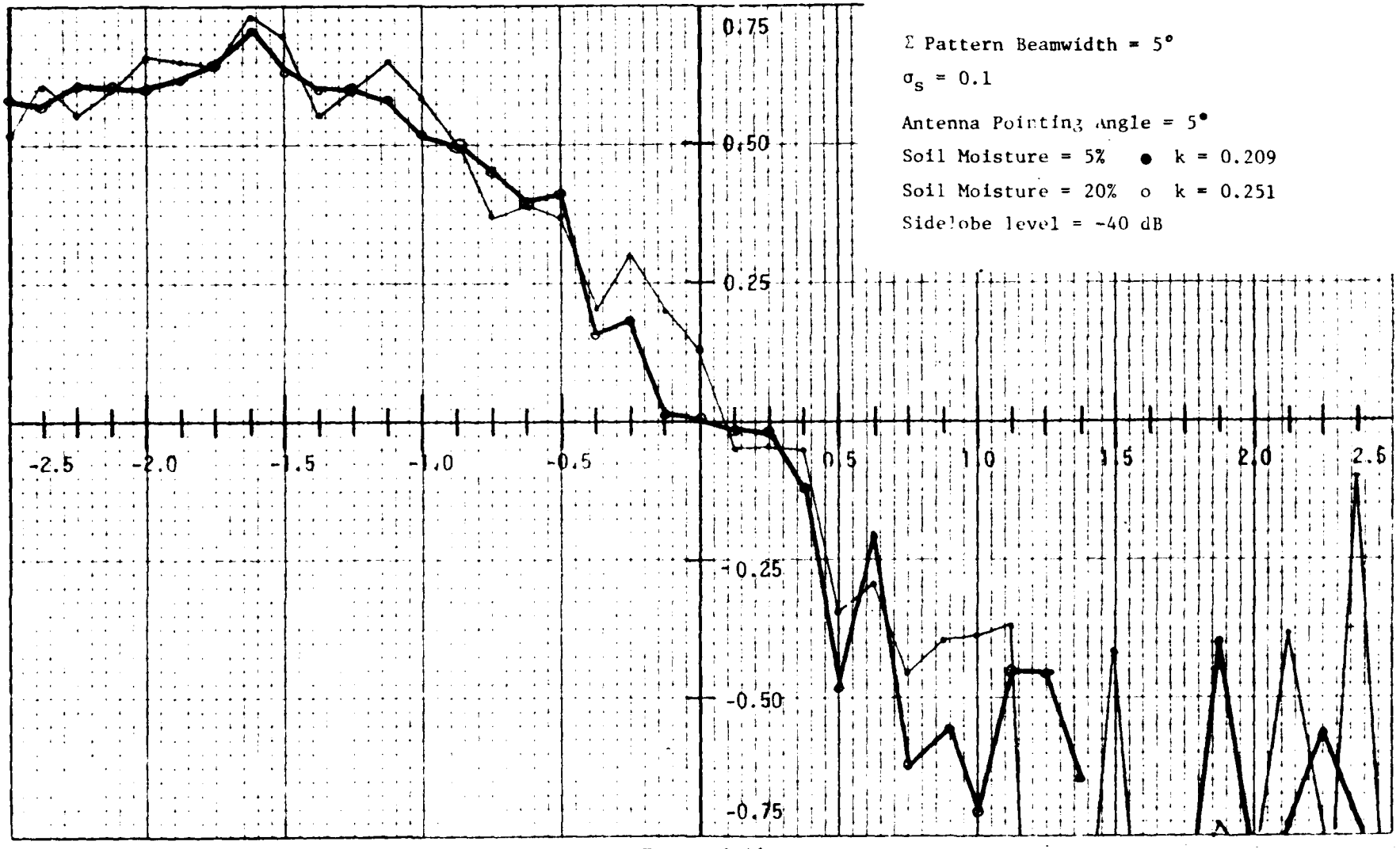

Figure 2.46

V_ε as a function of off-boresight angle for two values of soil moisture. . .

2.3.5 Simulation of 3rd-generation PLUSS Pillbox Antenna

One of the objectives of this study was to determine if the present 3rd generation PLUSS antenna (a 4' x 4' pillbox structure with metal-plate lens) could be modified in such a way as to achieve a significant improvement in low-angle tracking. This antenna has an elevation sum pattern beamwidth of 13.5° and a nominal sidelobe level of -30 dB.

A designer-specific question would ask what effect lowering the level from -30 dB to -40 dB would have on tracking accuracy. In order to answer this, a computer scenario was first created with a $\sum$ pattern beamwidth of 13.5°, a sidelobe level of -30 dB, a range of 75 km, an rms surface roughness of 16 cm and a soil moisture of 10%. The error-voltage curve vs. off-boresight angle was then computed for three elevation boresight angles: 20°, 15°, and 10°. The results are shown in Figure 2.47, where it is seen that tracking is good at 20° and 15°, but is very poor at 10° where k = 0.927. Now what happens if the sidelobe level is lowered to -40 dB? This is shown in Figure 2.48 where again the tracking is good at 20° and 15°, but is still very poor at 10°. The reduced sidelobe level gives k = .882 at 10°, which again indicates unstable tracking.

The reason for this only marginal improvement at 10° is that most of the ground scatter which causes a lack of tracking enters through the main lobe, not through the sidelobes. Therefore for the pillbox antenna, the only significant improvement which can be made is to reduce the beamwidth, which means that the antenna aperture size must be increased in an inverse ratio.

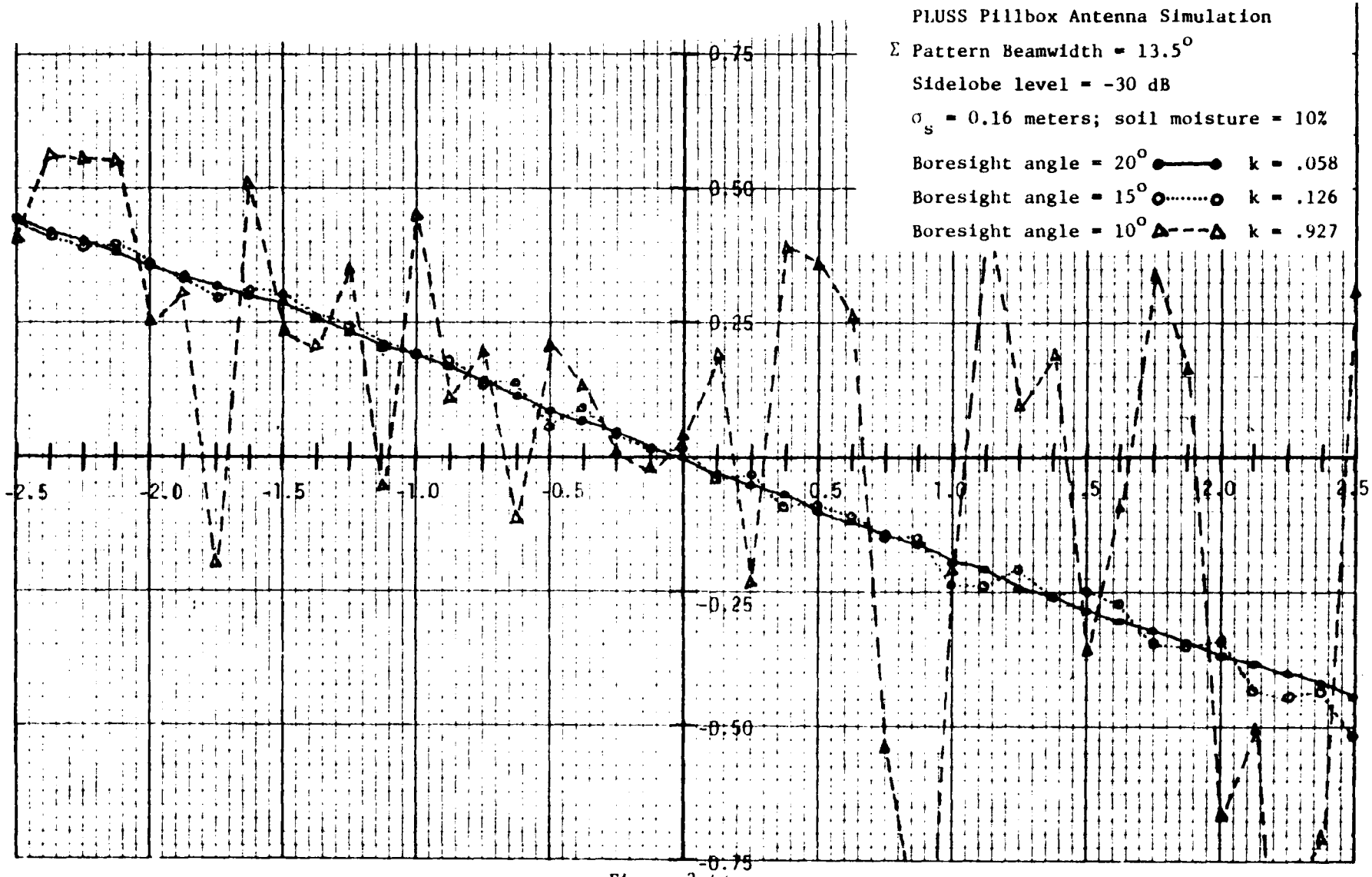

Figure 2.47

V_ε as a function of off-boresight angle for PLUSS pillbox antenna (-30 dB sidelobes) for three boresight elevation angles.

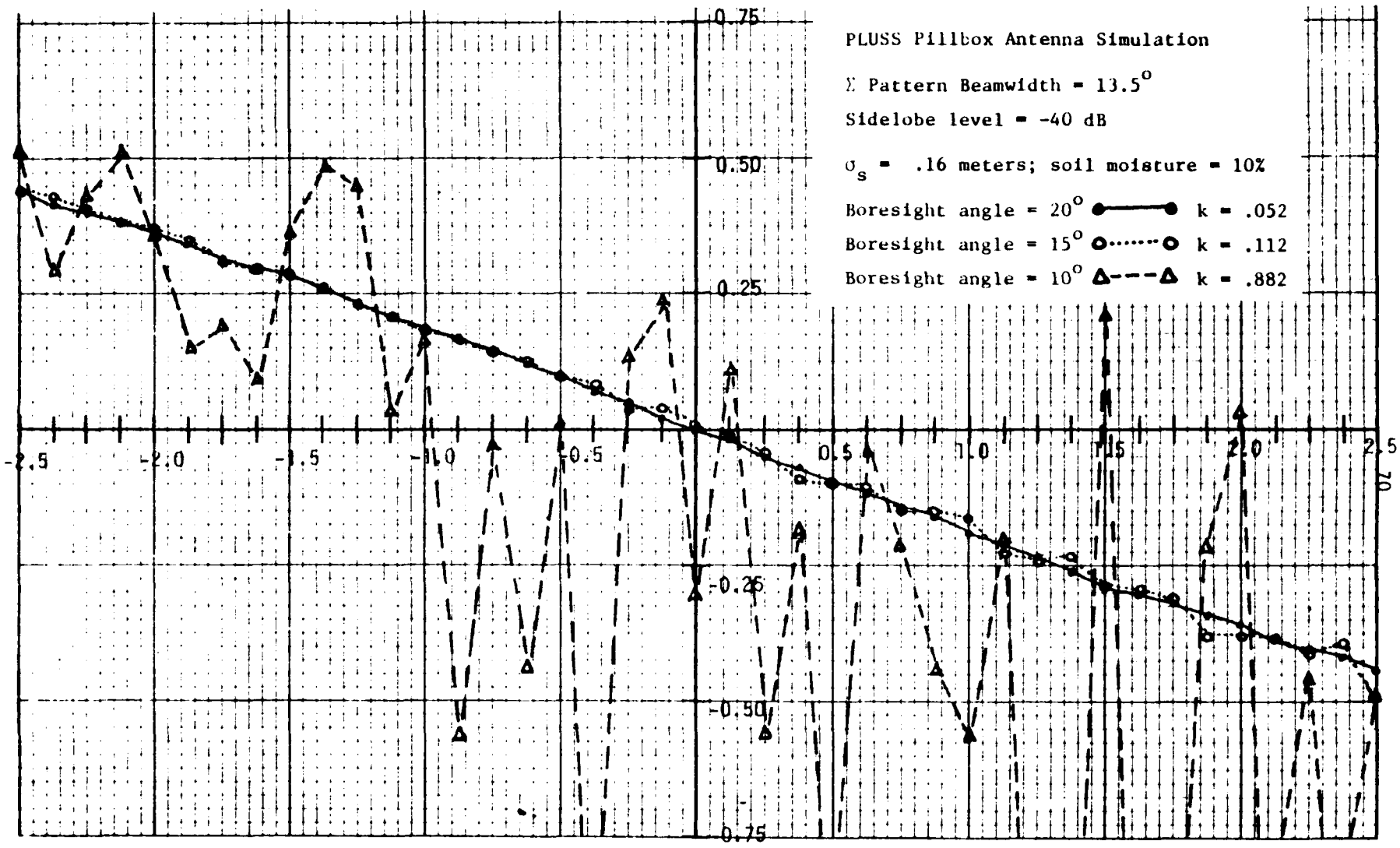

Figure 2.48

V_ε as a function of off-boresight angle for PLUSS pillbox antenna (-40 dB sidelobes) for three boresight elevation angles.

3.1 Required Antenna Performance

Although the PLUSS performance specifications call for tracking down to 6.5°, this report adopts a slightly more conservative number of 5°. From the results of the previous chapter, this will require an antenna with elevation sum pattern beamwidth of 5° and a sidelobe level of -40 dB or lower, resulting in error voltage curves of the type shown in Figures 2.43 and 2.44.

3.2 Aperture Distribution Design

A pattern with 5° beamwidth (at the -3 dB level) and a sidelobe level of -40 dB can be realized in the optimum sense using a Dolph-Tchebyscheff array with an appropriate number of elements and excitation distribution. These distributions are well-known and can be used to arrive at a projected aperture size.

A 28-element array having the excitation coefficients listed in Table 3-1 will produce a 5.1° beamwidth and a -40 dB sidelobe level, if each element is excited with the required excitation current.

In order to achieve the ideal characteristics (5.1° beamwidth and -40 dB sidelobe level), each current must be precise to four significant figures. This corresponds to a precision of 0.01 dB in delivered power to each element, which is very difficult to achieve in practice. If the tolerance on element current amplitudes is relaxed to 2 significant figures (± 0.2 dB), the pattern shape shows no important changes, as shown in Figure 3-1 for both the idealized case and the relaxed tolerance case. However, if the tolerance is relaxed even further to 1 significant figure (± 1 dB) the pattern is seriously degraded as shown in Figure 3-2, so that the peak sidelobe level is now at -32 dB.

Therefore, in order to achieve a -40 dB sidelobe level, it will be necessary to hold a tolerance of approximately ± 0.2 dB in the relative power delivered to each element.

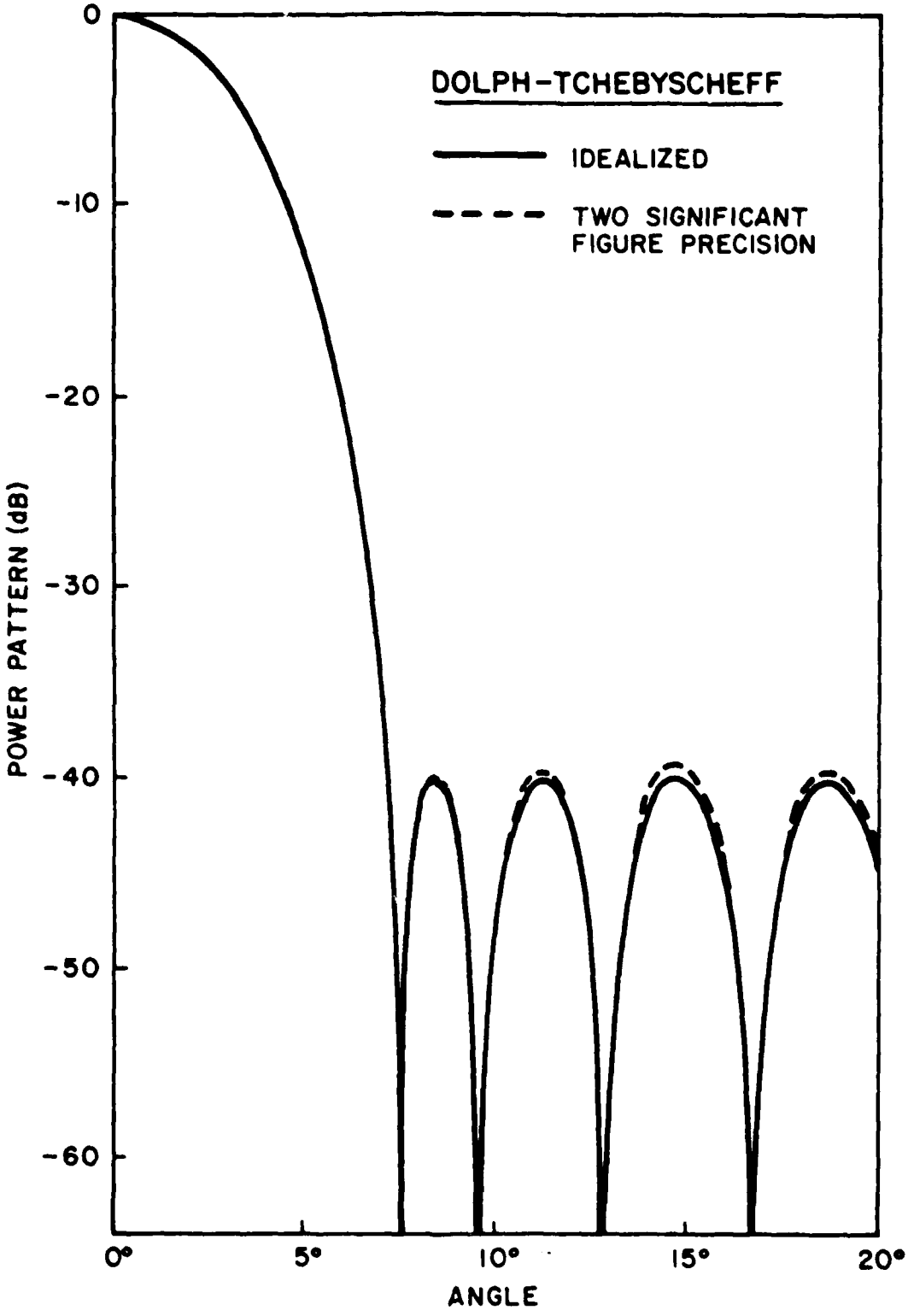

Figure 3.1 Computed elevation sum pattern for a 28-element Dolph-Tchebyscheff array, both idealized and with two significant figure precision in the element currents.

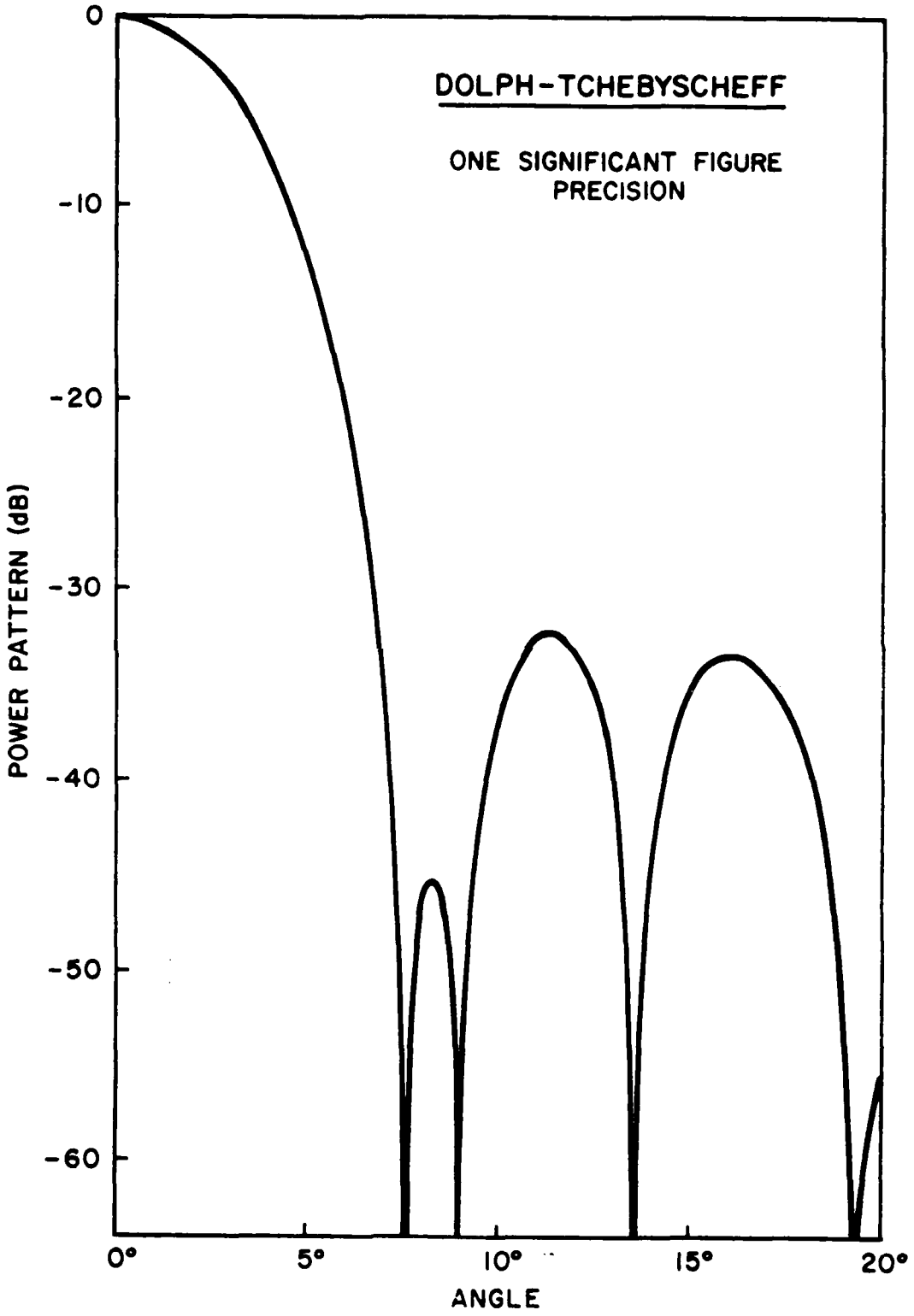

Figure 3.2 Computed elevation sum pattern for a 28-element Dolph-Tchebyscheff array, with one significant figure in the element currents.

Table 3-1

Dolph-Tchebyscheff Excitation Currents

for 5.1° beamwidth and -40 dB sidelobe level

Element No.	Current	Element No.	Current	Element No.	Current
1	.1336	10	.8065	19	.8065
2	.1358	11	.8798	20	.7219
3	.1971	12	.9383	21	.5353
4	.2696	13	.9791	22	.4413
5	.3518	14	1.0000	24	.3518
6	.4413	15	1.0000	25	.2696
7	.5353	16	.9791	26	.1971
8	.6302	17	.9383	27	.1358
9	.7219	18	.8798	28	.1336

3.3 Optimum Antenna Size

The patterns of Figures 3-1 and 3-2 are based on 28 elements with a spacing of 0.5 wavelengths. At 1680 MHz, this corresponds to an elevation aperture dimension of 9' (allowing 10" extra for the aperture edge).

If such an antenna were to be built at UHF (400 MHz), the elevation size would be 35'. However, at C-Band (5900 MHz), the elevation size would be only 30". This higher frequency antenna would also be much lighter and less susceptible to wind-induced loading. However, the present study is focused on a frequency of 1680 MHz since it seems unlikely that this will change in the near future.

The overall aperture size of such an optimum antenna would then be 9' X 4'.

3.4 Antenna Design Approaches

In this study, several specific antenna structures were examined, including:

1. Pill-box antennas (e.g., present PLUSS antenna)
2. Lundberg Lens
3. End-fire arrays
4. Dielectric-loaded structures
5. Microstrip arrays

The selection of the most promising approach was based on the findings documented in Chapter 2 that tracking accuracy at low angles is determined primarily by the beamwidth and sidelobe level. Furthermore, for tracking down to 5°, a 5° beamwidth and -40 dB sidelobe level are required.

In order to justify the cost and time required for alternative antenna design and development, it must be clearly demonstrated that a significant performance improvement can be expected.

As a rule of thumb, it can be remembered that the minimum angle for accurate tracking is roughly equal to the sum pattern -3 dB beamwidth, assuming the sidelobe level is at -30 dB or lower.

Thus, the present 3rd-generation PLUSS pillbox antenna with a 13.5° beamwidth tracks down to about 11°. The GMD dish antenna with a 6.5° beamwidth tracks down to 6.5°, etc.

Since the beamwidth is related to the aperture dimension of λ/D, it follows that diffraction limitations preclude the present pill-box antenna from accurate tracking below about 11°, regardless of electronic means (e.g., Redlien fix) used to reduce multipath interference. In other words, the elevation dimension of 4' for the pill-box antenna is a fundamental limitation on its minimum tracking angle, as seen by analogy to Figures 2.23-2.28.

The same comment holds for the Lundberg lens, which uses variable dielectric-constant concentric spheres to achieve a collimated phase front over its aperture diameter D. To achieve tracking down to 5°, it would be necessary to use a Lundberg lens of 9' diameter. This is impractical for reasons of excessive size and weight and greatly reduced portability.

An endfire array with increased directivity has a beamwidth given by:

$$-3 \text{ dB beamwidth} = \frac{52^\circ}{\sqrt{L/\lambda}}$$

where L is the array length. For a 5° beamwidth, this would require an array length of 63' at 1680 MHz. Moreover, it is difficult if not impossible to achieve -40 dB sidelobe levels with endfire arrays such as backfire arrays, Yagis, cigar antennas, etc.

Dielectric-loaded structures such as horns with dielectric plugs, etc., offer no means for easing the diffraction limitation λ/D on beamwidth, even though the wavelength in the structure may be reduced by 50% or more. Moreover, the price paid is an increase in weight.

It appears that a microstrip antenna array designs coupled with graphite-epoxy truss technology offers a means to simultaneously increase the elevation aperture to 9' while lowering the weight and increasing portability over that of the present PLUSS pill-box array. This concept is shown in Figure 3.3, for a 9' X 4' planar array of microstrip antennas in both folded or stow configuration and in opened or deployed condition.

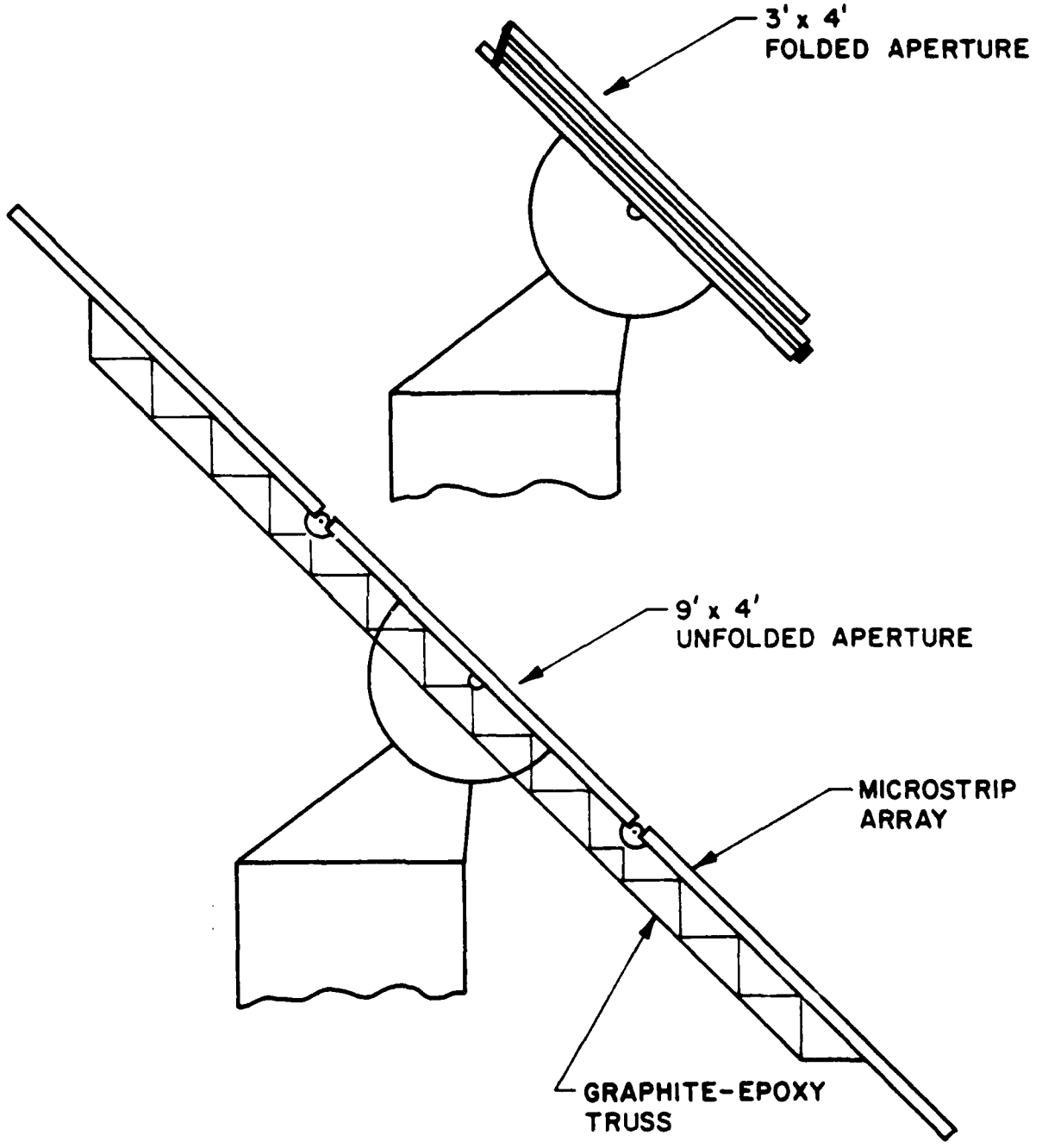

Figure 3.3 Concept drawing for a foldable portable lightweight microstrip array using graphite-epoxy truss supports.

The principal advantage of a planar array approach is that it is possible for the antenna designer to control the aperture distribution and therefore set the sidelobe level and other pattern shape features. Specifically, it should be possible to design a feed network to produce the element currents of Table 3.1 within about ±0.5 dB or better, thus enabling the desired performance specifications to be met. A separate study of the feasibility of array feed network designs to achieve the required precision should be undertaken.

The array itself can be made very lightweight by using a composite substrate formed from 1/4" Hexcell covered with 6-mil copper-clad printed circuit sheets. A 9' X 4' substrate of this material would weigh less than 10 lbs., including a printed feedline structure. Structural rigidity would be provided by a graphite-epoxy strongback truss which would be stored separately and snapped into place. The total loading on such a structure in a 70 knot wind would be 750 lbs. Graphite-epoxy tubes have a typical density of .06 lb/in^3 and an elastic modulus of 20 X 10^6 lb/in^2. Aluminum, by contrast, has a 67% greater density and a modulus half that of graphite-epoxy.

Initial estimates of the truss structure weight range from 80-140 lbs., although the exact figure would depend on a detailed mechanical design. This would mean that the antenna, without positioner, could weigh between 95 and 155 lbs, depending on design.

This planar array would have approximately 336 rectangular patch elements, each roughly $\lambda/2$ on a side. The exact size can be varied to control the input impedance and therefore the element currents. Elevation and azimuth monopulse operation would be achieved by dividing the array into four quadrants, each having 84 elements. Since the azimuth aperture dimension is the same as the pill-box antenna's, the azimuth angular tracking accuracy would be roughly the same as for the pill-box antenna.

3.5 Alternative Frequency Operation

Both UHF (400 MHz) and C-Band (5900 MHz) operation has been considered as an alternative to the present L-Band system. However, the size of a UHF antenna to achieve low-angle tracking is prohibitive (35' elevation aperture dimension),

although there is an improvement of roughly 12 dB in signal-to-noise ratio for the same transmitter power and receiver sensitivity. A UHF antenna of comparable size to the present pill-box antenna would have great difficulty in tracking below 30° elevation angle.

A C-Band system would require a much smaller tracking antenna, with an aperture size of about 30" X 14". However, at 5900 MHz, the free-space path loss is 11 dB greater than that at 1680 MHz. In order to maintain the same signal-to-noise ratio as exists at present, it would be necessary to make up this 11 dB in either (1) radiosonde transmitter power, (2) tracker receiver sensitivity, or (3) tracker antenna gain. It is not desirable to increase the antenna gain of the radiosonde since this increases the directivity and concomitant fading caused by tilting of the transmitter package.

At C-Band, the radiosonde antenna could be inexpensively fabricated using printed circuit antenna techniques designed for a bifolium pattern which would be vertically polarized. The key to expensive mass production would be to stamp out the element (avoiding any machining) and to use a very inexpensive connection to the transmitter.

4.1 Conclusions

The two major conclusions of this study are:

1. In order to track down to 5° elevation angle with minimal multipath effects, an elevation beamwidth of 5° with a sidelobe level of -40 dB is required. At 1680 MHz, this corresponds to a 9' X 4' aperture size.

2. This antenna can best be realized using a planar array of microstrip antenna elements backed by a graphite-epoxy strongback support truss. Portability would be achieved by using a folded aperture with a folded volume of 3' X 4' X 0.5', exclusive of the truss support which would be snapped on. The weight of such an array would range from 95-155 lbs., depending on design. Total wind loading at 70 knots would be 750 lbs.

Even if frequency allocation was available, UHF monopulse tracking to low angles would not be feasible because of excessive antenna size and weight. However, at C-Band a smaller antenna (30" X 14") could be used, although an 11 dB increase in the sum of transmitter power and receiver sensitivy would be required.

4.2 Recommendations

In order to determine the practical feasibility of constructing a 4th-generation PLUSS microstrip antenna having the characteristics described, it is recommended that an engineering feasibility study be undertaken. The purpose of this follow-on study would be to investigate in detail whether it is possible to achieve the desired electrical and mechanical performance necessary in a forward artillery environment.

Specifically, such a study should investigate the following:

1. The accuracy and precision which can be achieved in a practical microstrip antenna feed network to deliver the desired element currents.

2. The effect of mutual coupling between elements on the precision of excitation.

3. Optimum feed networks to achieve 4-quadrant sum and difference patterns.

4. Design of a graphite-epoxy support truss structure for use in winds to 70 knots, with emphasis on weight analysis, flexural characteristics, and structural resonant frequencies.

5. Design of a folding mechanism for use with a 9' X 4' microstrip array.

6. Estimation of the development cost for a folding monopulse array with snap-on truss structure, exclusive of positioner and servo control circuitry.

APPENDIX

This Appendix presents a listing of the FORTRAN computer code developed for calculation of the error voltage V_ε vs. off-boresight angle. The mathematical basis for the equations used has been discussed in Chapter 2 of this report.

The user specifies the following:

ANTENNA PATTERN PARAMETERS

Sum pattern - 3 dB beamwidth (degrees): THBDG
Difference pattern squint angle (degrees): THSDG
Sum pattern sidelobe level (voltage ratio): SLS
Difference pattern sidelobe level (voltage ratio: SLD
Antenna height above earth (meters): HAM

RADIOSONDE LOCATION PARAMETERS

Elevation boresight angle to sonde (degrees): THTHDG
Range to radiosonde (kilometers): RKM

TERRAIN PARAMETERS

RMS surface roughness (meters): SIGH
Gravimetric soil moisture) percent: SM

The program then calculates the dot product error voltage as a function of angle deviation from boresight. This is done at 1680 MHz, although any other frequency may be used by changing line 13 of the main program.

The output of the program is in column format, with the following calculated variables:

1. Off-boresight angle (degrees)
2. Radiosonde height (meters) at 25 km range
3. Grazing angle to specular point (degrees)

4. Voltage magnitude of sum pattern (V)
5. Voltage magnitude of difference pattern (V)
6. Voltage phase of sum pattern (radians)
7. Voltage phase of difference pattern (radians)
8. Voltage phase of product pattern (degrees)
9. Voltage magnitude of dot product pattern (V)

The principal output of interest is Column 9 vs. Column 1, i.e. the dot product error voltage vs. off-boresight angle. It is this information that has been presented in Chapter 2, Figure 3.24, et. seq.

The computer program consists of a main program (MAINPGM) with 76 statements and two subroutines (GD, GS) with 13 and 12 statements respectively. The subroutine GD calculates the voltage difference pattern based on equation (2.14). The subroutine GS calculates the voltage sum pattern based on equation (2.13). These are then passed to lines 42, 43, 56 and 57 of the main program which incorporates the multipath signals from both specularly and diffusely scattered components from the terrain with the direct ray signal to produce the composite sum, difference and dot product voltages.

From the listing of error voltage vs. angle, the coefficient of non-determination (k) is calculated from equation (2.29).

On the PSL IBM 370 Computer, the program card deck is assembled in the following order:

```
//JOB TRACK TBUSH, 4130,P,17716;AP17A
//OPTION LINK, PARTDUMP
//EXEC FFORTRAN
```

MAINPGM DECK

```
REAL LAMDA, MAGSUM, MAGDIF, ISUM, IDIF
.
.
.
.
END
```

```
                REAL FUNCTION GS(Z,THRDG,THSDG,THBDG,SLS)
                .
SUBROUTINE      .
GS              .
                .
                END

                REAL FUNCTION GD(Z,THRDG,THSDG,THBDG,SLD)
                .
SUBROUTINE      .
GD              .
                .
                END

                COMPLEX FUNCTION EPSR(SM)
                .
SUBROUTINE      .
EPSR            .
                .
                END

                /*
                INCLUDE MERF1
                INCLUDE UERTST
                //EXEC LNKEDT
                //EXEC
                DATA CARD 1
                DATA CARD 2        See text for format
                DATA CARD 3
                      .
                      .
                      .
                /*
                /&
```

The data cards are arranged in the following format by column:

Column 1:	Card No.	(e.g., 2)
Column 8-14:	THTHDG	(e.g., 5.0)
Column 15-21:	SIGH	(e.g., 0.06)
Column 22-28:	HAM	(e.g., 2.0)
Column 29-35:	THBDG	(e.g., 7.5)
Column 36-42:	THSDG	(e.g., 2.0)
Column 43-49:	SLS	(e.g., .01)
Column 50-56:	SLD	(e.g., .01)
Column 57-63:	SM	(e.g., 10.0)
Column 64-70:	RKM	(e.g., 75.0)

In this example data card No. 2 describes an antenna with a 7.5° sum beamwidth (THBDG) with a 2.0° difference pattern squint (THSDG), a sum pattern sidelobe level of 2.0 log .01 = -40 dB (SLS), a difference pattern sidelobe level of -40 dB (SLD) located 2.0 meters above ground (HAM) and 75 km in range (RKM) from the balloon. The surface roughness is .06 m rms (SIGH) and the soil moisture is 10% by weight (SM). The boresight angle is 5° above horizon (THTHDG).

```
DOS FORTRAN IV 360N-FO-479 3-9          MAINPGM          DATE   04/17/79     TIME     15.28.01      PAGE 0001

0001                REAL LAMDA,MAGSUM,MAGDIF,ISUM,IDIF
0002                COMPLEX SUMSUM,SUMDIF,RV,NUM,DENOM,RF,D3,RO
0003                PI=355.0/113.0
0004                DO 1500 K=1,9
0005                READ(1,100)       THTHDG,SIGH,HAM,THRDG,THSDG,SLS,SLD,SM,RKM
0006           100  FORMAT(7X,9F7.2)
0007                WRITE(3,103)
0008           103  FORMAT(1X,'*** INPUT PARAMETERS ***',/)
0009                WRITE(3,101)  THTHDG,SIGH,HAM,THRDG,THSDG,SLS,SLD,SM,RKM
0010           101  FORMAT(1X,'BORE SIGHT ANGLE= ',F7.2,2X,'ROUGHNESS SD= ',F7.2,2X,
                    $'HT. HT.= ',F7.2,/,1X,'BWDG= ',F7.2,14X,'SQUINT= ',F7.2,8X,
                    $'SL.S= ',F7.2,/,1X,'SL.D= ',F7.2,14X,'SM= ',F7.2,12X,'RNG= ',F7.2)
0011                WRITE(3,105) RKM
0012           105  FORMAT(//,1X,'OFF BORESIGHT ANGLE(DEG)  AT',F8.3,'KM HEIGHT',
                    $'  GRAZING ANGLE(DEG)  MAGSUM    MAGDIF     PSUM      PDIF',
                    $'      PHZDG      DOT PRD')
0013                ERSG=1680000000.0
0014                LAMDA=0.17857
0015                Z=-1.388/(THRDG**2.0)
0016                RM=RKM*1000.0
0017                THTHR=THTHDG/57.29
0018                DO 1000 I=1,41
0019                SUMSUM=CMPLX(0.0,0.0)
0020                SUMDIF=CMPLX(0.0,0.0)
0021                XI=FLOAT(I)
0022                THRDG=(XI-21.0)*0.25
0023                THRR=THRDG/57.29
0024                HR=RM*(SIN(THTHR-THRR)/COS(THTHR-THRR))+HAM
0025                PSIR=THTHR-THRR
0026                PSIDG=PSIR*57.29
0027                D1=SIN(PSIR)/COS(PSIR)
0028                C1=1+((4*HAM*HR)/(LAMDA*RM))
0029                C2=1+(((HAM+HR)**2)/(LAMDA*RM))
0030                RF=(RM/2.0)*(1.0+(2.0*HAM*(HAM+HR)/(LAMDA*RM)))/C2
0031                EL=(RM/2.0)*(SQRT(C1))/C2
0032                XF=HAM/D1
0033                DD1=COS(PSIR)**2
0034                NUM=ERSR(SM)*SIN(PSIR)-CSQRT(ERSR(SM)-CMPLX(DD1,0.0))
```

```
0035              DENOM=EPSR(SM)*SIN(PSIR)+CSQRT(EPSR(SM)-CMPLX(CD1,0.0))
0036              RV=NUM/DENOM
0037              D2=(8.0*PI*(SIGH**2.0)*(SIN(PSIR))**2.0)/LAMDA**2.0
0038              DELTA=4.0*PI*HAM*SIN(PSIR)/LAMDA
0039              D3=CMPLX(D2,DELTA)
0040              RE=CABS(RV)*CEXP(-D3)
0041              THSPDG=PSIDG+THTHDG
0042              SUMSUM=SUMSUM+GS(Z,THRDG,THSDG,THBDG,SLS)
                 $+GS(Z,THSPDG,THSDG,THBDG,SLS)*RE
0043              SUMDIF=SUMDIF+GD(Z,THRDG,THSDG,THBDG,SLD)
                 $+GD(Z,THSPDG,THSDG,THBDG,SLD)*RE
0044              DO 3000 J=1,1000
0045              XJ=FLOAT(J)
0046              XDN=(FC-FL)*(XJ-1.0)*LAMDA
0047              IF(XDN.GT.(FC+FL)) GO TO 4000
0048              PSIDR=ATAN2(HAM,XDN)
0049              PSIDEJ=(THTHR+PSIDR)*57.29
0050              DELTAL=SIGH*SIN(PSIR)/LAMDA
0051              DUMMY=0.77*(1.0-EXP(-4.0*PI*DELTAL))*EXP(-4.73*DELTAL)
0052              A=SQRT((GGNDF(851687873))**2+(GGNDF(861687873))**2)
0053              ETA=GGUBF(861687873)*2.0*PI
0054              RD=DUMMY*CABS(RV)*A*CEXP(CMPLX(0.0,-ETA))
0055              RDD=CABS(RD)
0056              SUMSUM=SUMSUM+GS(Z,PSIDEJ,THSDG,THBDG,SLS)*RD
0057              SUMDIF=SUMDIF+GD(Z,PSIDEJ,THSDG,THBDG,SLD)*RD
0058         3000 CONTINUE
0059         4000 CONTINUE
0060              MAGSUM=CABS(SUMSUM)
0061              MAGDIF=CABS(SUMDIF)
0062              RSUM=REAL(SUMSUM)
0063              ISUM=AIMAG(SUMSUM)
0064              RDIF=REAL(SUMDIF)
0065              IDIF=AIMAG(SUMDIF)
0066              PSUM=ATAN2(ISUM,RSUM)
0067              PDIF=ATAN2(IDIF,RDIF)
0068              PHSDIF=PDIF-PSUM
0069              PHZDG=PHSDIF*57.29
0070              DOTPRD=MAGSUM*MAGDIF*COS(ABS(PHSDIF))
```

```
DOS FORTRAN IV 360N-FO-479 3-9          MAINPGM          DATE   09/17/79      TIME     15.28.01       PAGE 0003

 0071                WRITE(3,400) THRDG,HR,PSIDG,MAGSUM,MAGDIF,PSUM,PDIF,PHZDG,DOTPRD
 0072            400 FORMAT(/,10X,F7.2,11X,F12.3,12X,F7.2,8X,F6.2,3(2X,F7.2),
                    $2(3X,F7.2))
 0073           1000 CONTINUE
 0074           1500 CONTINUE
 0075                STOP
 0076                END


DOS FORTRAN IV 360N-FO-479 3-9          GD               DATE   09/17/79      TIME     15.28.30       PAGE 0001

 0001                REAL FUNCTION GD(Z,THRDG,THSDG,THRDG,SLD)
 0002                A=EXP(Z*(THRDG**2+THSDG**2))
 0003                B=EXP(2.0*Z*THRDG*THSDG)
 0004                C=EXP(-(2.0*Z*THRDG*THSDG))
 0005                GD=A*(B-C)
 0006                IF(THRDG.LT.1.0) GO TO 1
 0007                F=SIN(160.22*SIN(THRDG/57.29)/THRDG)/(160.22*(SIN(THRDG/57.29)
                    $/THRDG))
 0008                IF(THRDG.EQ.0.0) GO TO 1
 0009                IF(ABS(GD).LE.SLD) GD=SLD
 0010                IF(ABS(GD).LE.SLD.AND.F.LT.0.0) GD=-SLD
 0011            1   CONTINUE
 0012                RETURN
 0013                END


DOS FORTRAN IV 360N-FO-479 3-9          GS               DATE   09/17/79      TIME     15.28.21       PAGE 0001

 0001                REAL FUNCTION GS(Z,THRDG,THSDG,THRDG,SLS)
 0002                A=EXP(Z*(THRDG**2+THSDG**2))
 0003                B=EXP(2.0*Z*THRDG*THSDG)
 0004                C=EXP(-(2.0*Z*THRDG*THSDG))
 0005                GS=A*(B+C)
 0006                IF(THRDG.LT.1.0) GO TO 1
 0007                F=SIN(160.22*SIN(THRDG/57.29)/THRDG)/(160.22*(SIN(THRDG/57.29)
                    $/THRDG))
 0008                IF(ABS(GS).LE.SLS) GS=SLS
 0009                IF(ABS(GS).LE.SLS.AND.F.LT.0.0) GS=-SLS
 0010            1   CONTINUE
 0011                RETURN
 0012                END
```

AD-A085 131 NEW MEXICO STATE UNIV LAS CRUCES PHYSICAL SCIENCE LAB F/G 17/9
ANALYSIS OF MONOPULSE TRACKER ANTENNA PERFORMANCE IN A MULTIPAT--ETC(U)
APR 80 K R CARVER, T F BUSH DAAD07-79-C-0008

UNCLASSIFIED ERADCOM/ASL -CR-80-0008-2 NL

2 OF 2

END
DATE FILMED
7 80
DTIC

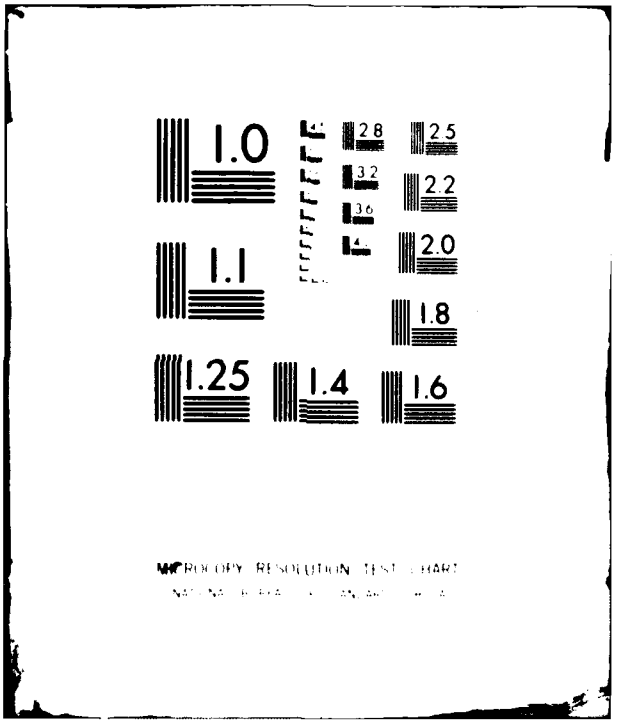
1.0
1.1
1.25
1.4
1.6
2.8
3.2
3.6
2.5
2.2
2.0
1.8
MICROCOPY RESOLUTION TEST CHART

1

SET 01
A

// EXEC

*** INPUT PARAMETERS ***

BORE SIGHT ANGLE= 10.00 ROUGHNESS SD= 0.0 ANT. HT.= 2.00
RWDG= 10.00 SOLENT= 4.00 SL.S= 0.10
SL.D= 0.10 SM= 0.0 RNG= 25.00

REF BORESIGHT ANGLE(DEG)	AT 25.000KM HEIGHT	GRAZING ANGLE(DEG)	MAGSUM	MAGDIF	PSUM	PDIF	PHZDG	DOT PRD
-5.00	6701.434	15.00	1.32	0.67	0.02	0.04	1.23	0.85
-4.75	6584.641	14.75	1.33	0.64	0.02	0.05	1.40	0.85
-4.50	6468.117	14.50	1.34	0.61	0.02	0.03	1.05	0.81
-4.25	6351.355	14.25	1.36	0.58	0.00	0.01	0.17	0.78
-4.00	6235.348	14.00	1.38	0.56	-0.01	-0.03	-0.98	0.77
-3.75	6120.098	13.75	1.42	0.55	-0.02	-0.06	-1.94	0.78
-3.50	6004.594	13.50	1.46	0.54	-0.02	-0.06	-2.28	0.79
-3.25	5889.328	13.25	1.50	0.53	-0.02	-0.05	-1.83	0.80
-3.00	5774.301	13.00	1.46	0.44	0.01	0.02	0.79	0.65
-2.75	5659.508	12.75	1.48	0.41	-0.01	-0.03	-1.27	0.61
-2.50	5544.938	12.50	1.50	0.39	-0.02	-0.08	-3.31	0.59
-2.25	5430.590	12.25	1.54	0.38	-0.02	-0.10	-4.40	0.58
-2.00	5316.461	12.00	1.57	0.36	-0.03	-0.09	-4.00	0.57
-1.75	5202.543	11.75	1.60	0.34	-0.01	-0.05	-2.04	0.54
-1.50	5088.828	11.50	1.61	0.30	0.01	0.03	1.33	0.48
-1.25	4975.320	11.25	1.61	0.25	0.02	0.12	5.91	0.40
-1.00	4862.004	11.00	1.60	0.19	0.03	0.23	11.45	0.29
-0.75	4748.883	10.75	1.58	0.12	0.03	0.33	17.51	0.18

1

68

-0.50	4635.949	10.50	1.56	0.05	0.01	0.41	23.69	0.00
-0.25	4523.155	10.25	1.56	0.00	-0.00	-1.68	-96.29	-0.00
0.0	4410.625	10.00	1.57	0.05	-0.02	-2.45	-139.35	-0.05
0.25	4298.223	9.75	1.59	0.07	-0.03	-2.47	-140.10	-0.09
0.50	4185.992	9.50	1.61	0.09	-0.03	-2.59	-146.68	-0.12
0.75	4073.924	9.25	1.63	0.10	-0.02	-2.84	-161.76	-0.15
1.00	3962.013	9.00	1.64	0.13	-0.00	-3.13	-179.29	-0.21
1.25	3850.259	8.75	1.63	0.18	0.02	2.99	170.05	-0.28
1.50	3739.655	8.50	1.59	0.25	0.03	2.94	166.99	-0.38
1.75	3627.195	8.25	1.55	0.32	0.03	2.98	169.77	-0.49
2.00	3515.877	8.00	1.51	0.38	0.02	3.05	173.14	-0.57
2.25	3404.693	7.75	1.49	0.43	0.00	3.12	178.75	-0.64
2.50	3293.644	7.50	1.48	0.46	-0.02	-3.09	-175.81	-0.68
2.75	3182.724	7.25	1.48	0.48	-0.03	-3.04	-171.96	-0.70
3.00	3071.924	7.00	1.50	0.48	-0.04	-3.02	-170.87	-0.71
3.25	2961.244	6.75	1.43	0.47	0.03	-3.05	-176.40	-0.67
3.50	2850.677	6.50	1.39	0.47	0.01	-3.11	-178.81	-0.66
3.75	2740.221	6.25	1.36	0.50	-0.02	3.09	177.99	-0.67
4.00	2629.872	6.00	1.37	0.55	-0.05	3.01	175.79	-0.75
4.25	2519.623	5.75	1.39	0.62	-0.07	2.99	175.50	-0.86
4.50	2409.469	5.50	1.43	0.70	-0.06	3.03	176.77	-0.99
4.75	2299.404	5.25	1.45	0.75	-0.03	3.10	179.82	-1.09
5.00	2189.427	5.00	1.44	0.78	0.03	-3.10	-179.88	-1.12

2

06

REFERENCES

1. Skolnik, M.I., Introduction to Radar Systems, McGraw-HIll Book Company, N.Y., pg. 180, 1962.

2. Beard, C.E., I. Katz and L.M. Spetner, "Phenomenological Vector Model of Microwave Reflection from the Ocean," IRE Transactions of Antennas and Propagation, AP-4, pp. 162-167, April, 1956.

3. Beckmann, P. and A. Spizzichino, The Scattering of Electromagnetic Waves from Rough Surfaces, Macmillan, N.Y., pg. 81, 1963.

4. Beard, C.I., "Coherent and Incoherent Scattering of Microwaves from the Ocean," IRE Transactions on Antennas and Propagation, AP-9, pp. 470-483, September, 1961.

5. Beard, C.I., "Behavior of Non-Rayleigh Statistics of Microwave Forward Scatter from a Random Water Surface," IEEE Transactions on Antennas and Propagation, AP-15, pp. 649657, September, 1967.

6. Carver, K.R., "UHF Multipath Phenomena in a Marine Environment," Final Report under NOAA Grant 04-4-158-41 to NOAA/NESS, Suitland, Md.; New Mexico State University Dept. of Electrical Engineering, Las Cruces, NM, 88003, December, 1974, pp. 149-152.

7. Jedlicka, R.P., "Saline Soil Dielectric Measurements," MS Thesis, New Mexico State University, Las Cruces, 1978.

8. AIL (Cutler-Hammer Corp.), "Analytical Study for Forward Artillery Meteorological Antenna System,: Project D437, September, 1977.